A Laboratory Workflow to Screen Fracturing Fluid Additives for Enhanced Oil Recovery

by

Maryam Eghbalvala

A thesis submitted in partial fulfillment of the requirements for the degree of

Master of science

in

Petroleum Engineering

Department of Civil & Environmental Engineering
University of Alberta

Abstract

Increasing demand for oil and gas and rapid depletion of conventional resources have shifted the focus of the industry toward hydrocarbon production from unconventional resources. Due to the extremely low permeability, complex pore structure, and mixed-wet behavior of such formations, their oil recovery factor is very low (<10%) and a considerable amount of hydrocarbon will be trapped in the sub-micron pores. Numerous enhanced oil recovery (EOR) methods have been introduced during the past decade to increase the final oil recovery from these formations. In recent years, many investigations have evaluated the application of surfactants and cosurfactants for enhancing oil recovery. These chemicals are best known for their surface activity for reducing interfacial tension (IFT) between oleic and aqueous phases and wettability alteration of the rock, both affecting capillary pressure (P_c). Water blockage at the hydraulic fracture-matrix interface is considered as formation damage in tight formations with low permeabilities, and this causes reduction of hydrocarbon recovery. Due to very small pore throats in tight formations, capillary suction is high at the interface and causes the injected fluid to enter the matrix and trap, which reduces hydrocarbon mobility. Addition of nanodroplets and surfactants reduces the capillary force which enhances water imbibition through the matrix and reduces formation damage as a result. In this study, we characterized fluid-fluid and rock-fluid properties to investigate parameters affecting oil recovery from tight rocks by the addition of nanoparticle additives to fracturing water and categorized these parameters according to their impact in enhancing oil recovery

This study presents a comprehensive laboratory workflow to investigate different parameters affecting the efficiency of enhancing oil recovery (EOR) from tight rocks using nanoparticle additives. We used core samples from the Montney (MT) Formation and nanodroplet (ND) solutions prepared by three complex nanofluid additives which include nonionic surfactants and D-Limonene solvent to conduct our experiments. This protocol is applied in the following steps: (1) Characterizing natural wettability of the core plugs by spontaneous imbibition and contact angle tests; (2) Evaluating ND-assisted imbibition oil recovery tests by conducting systematic imbibition oil recovery tests under different brine salinities; and (3) Performing bulk-phase tests to evaluate fluid properties, particle size, and stability of the ND samples to understand fluid-fluid interactions.

The experimental results show that the use of nanodroplet additives decreases the oil-water interfacial tension (IFT) and alters the rock wettability towards more water-wet conditions. However, enhanced imbibition oil recovery using ND solutions prepared by CnF additives cannot be sufficiently explained by IFT reduction and macroscopic CA measurements. Solubilization (described by Winsor type), osmosis potential, and zeta potential should also be considered to evaluate imbibition oil recovery by the ND solutions. Generally, increasing fluid salinity can reduce oil recovery by the ND solutions, which can be explained by less fluid movement through the pores, so weaker osmosis potential and the formation of larger particles in high-salinity water. The solubility results of Pipette tests indicate that the formation of middle-phase (or near middle-phase) microemulsion is favorable to increase oil recovery. As the generated microemulsion type gets closer to Winsor type III, the oil-water IFT value reaches the minimum value, which enhances the oil recovery. Measured Zeta potential values reveal that higher absolute value of oil-ND solution maintains a high net negative charge around the oil droplets. This results in higher stability and higher solubility of the oil droplets in the aqueous phase, which leads to higher final oil recovery.

Preface

This thesis is an original work by Maryam Eghbalvala.

The petrophysical analysis of the core samples, MICP data, and SEM images were conducted by commercial companies.

Part of this thesis have been published as Eghbalvala, M., Habibi, A., & Dehghanpour, H. (2020, September). "A Laboratory Protocol for Evaluating Microemulsions for Enhanced Oil Recovery while Fracturing'. In SPE Canada Unconventional Resources Conference.

This thesis has been submitted to Sustainable Energy Technologies and Assessments journal. Dr. Hassan Dehghanpour was supervisory author and reviewed the paper.

Dedication

To my dear father who supported me every step of my way.

Acknowledgment

I am heavily indebted to my supervisor Dr. Hassan Dehghanpour for giving me the opportunity to do this research. His dynamism, motivations, continuous support, and guidance have deeply inspired me. It was a great honor to work and study under his guidance. I would also like to thank him for his friendship and sense of humor. I fully acknowledge his contribution in this research.

I wish also to express my sincere appreciations to my father, Akhtar Eghbalvala, who always encouraged me to follow my dreams and never give up. He also gave me moral support and stood by me through every hardship in my life.

I am deeply thankful to Dr. Ali Habibi and Lin Yuan, without whom this dissertation could not be completed. Their valuable guidance, encouragement, suggestions, comments, and assistance on my master's research helped me throughout the entire way.

I would like to give special thanks to my colleagues: Tamer Moussa, Taregh Soleiman Asl, Mohammad Yousefi, Mohammad Sabbir Hossain, Yingkun Fu, Mohammad Hossein Doranehgard, Son Tran, Shiyu Xu, and Mahmood Reza Yassin for their valuable comments and discussions.

I would also like to thank Flotek Chemistry and Natural Sciences and Engineering Research Council (NSERC) of Canada for supporting this study.

Table of Contents

List of tables

List of figures

Nomenclature

P_c	Capillary pressure, MLT^{-2}
σ	Interfacial tension or surface tension, Mt^{-2}
θ	Contact angle, degree
r	Pore radius, L
Q	Imbibed volume,
ϕ	Effective porosity
K	Effective permeability, L^2
S	Saturation
A_c	Cross-sectional contact area, L^2
μ	Fluid viscosity, $ML^{-1}t^{-1}$
μ_o	Oil viscosity, $ML^{-1}t^{-1}$
μ_b	Brine viscosity, $ML^{-1}t^{-1}$
N_B^{-1}	Inverse bond number
Δρ	Difference between two densities, ML^{-3}
h	Length of the core, L
$P_t(h)$	Disjoining pressure, MLT^{-2}
$F_{VDW}(h)$	Van der Waals force, MLT^{-2}
$F_{DL}(h)$	Double layer force, MLT^{-2}
$F_S(h)$	Structural force, MLT^{-2}
A_H	Hamaker constant
λ_{lw}	London-wavelength, L
C_i	Concentration of component i

n_b	Ionic density of layer, CL^{-2}
k_B	Boltzman constant, $M^1\ L^2\ T^{-2}\ K^{-1}$
ψ_{ri}	Reduced surface potential, CL^{-2}
κ	Reciprocal Debye-Huckel length, L
ε_0	Vacuum dielectric constant, $A^2t^4M^{-1}L^{-3}$
ε	Dielectric constant of fluid
e	Electron charge, C
Z_i	Valency of ions
ζ_i	Zeta potential, $ML^2t^{-3}A^{-1}$
h_s	Characteristic decay length
P_o	Oil solubilization factor
P_w	Water solubilization factor
V_o	Oil volume in the microemulsion phase, L^3
V_w	Water volume in the microemulsion phase, L^3
V_s	Surfactant volume in the microemulsion phase, L^3
m	Imbibition rate, t^{-1}
m_o	Oil imbibition rate, t^{-1}
m_b	Brine imbibition rate, t^{-1}
ω	Angular spinning velocity, t^{-1}

Abbreviation

EOR	Enhanced oil recovery
IFT	Interfacial tension
MT	Montney
ND	Nanodroplet
CA	Contact angle
TW	Tap water
DI	De-ionized
PSD	Pore size distribution
SEM	Scanning electron microscope
MICP	Mercury injection capillary pressure
ITA	Imbibition transient analysis
TRA	Tight rock analysis
DLVO	Derjaguin, Landau, Verwey, and Overbeek theory
NEB	National Energy Board
BC MNGD	British Columbia Oil and Gas Commission
AER	Alberta Energy Regulator
XRD	X-ray crystallography
HLB	Hydrophilic-hydrophobic balance
DLE	Double-layer expansion
MIE	Multi-component ion exchange
RF_o	Oil recovery factor

Chapter 1: Introduction

1.1 Background

A report released on March 26, 2019, by International Energy Agency (IEA) depicts that the global energy demand in 2018 had the fastest growth in the last decade (up to 2.3%). Around 70% of this demand growth was addressed by fossil fuels. Due to the rapid depletion of conventional resources, unconventional resources such as tight formations and shales have been developed during the past decade. Although tight formations include a significant amount of resources, the oil recovery factor for these formations is very low (<10% of original oil in place) due to their complex pore structure, oil-wet behavior, low porosity, and permeability values (Manrique et al. 2010, Kathel et al. 2013). The current challenge is to find practical and economical techniques to increase the oil recovery factor from these formations by implementing different enhanced oil recovery (EOR) techniques.

Over the past decade, different EOR techniques have been used to improve the oil recovery from tight rocks (Sheng 2015, Szlendak et al. 2013, Habibi et al. 2017, Sorensen et al. 2017, Rivero et al. 2019). Among the EOR techniques, adding chemical additives such as surfactants and nanodroplets (ND) to the fracturing fluid has been considered as a practical way for displacing oil from tight rocks. Since during fracturing, a large amount of water with additives contacts with reservoir fluids and rock matrix, surface active agents are considered very effective in increasing oil recovery. This method has been the focus of many studies (Sheng 2018, Yarveicy et al. 2018, Quintero et al. 2018, Wijaya et al. 2020).

There has been growing interest in using surface-active agents in fracturing water to increase counter-current imbibition and enhance oil recovery from the Montney (MT) Formation (Shen et al 2018). The proposed main mechanisms responsible for the oil displacement from nano- and sub-micron pores are 1) interfacial tension (IFT) reduction between injected and reservoir fluids, and 2) wettability alteration of the matrix toward more water-wet conditions. (Quintero et al. 2018, Yassin et al. 2018, Soleiman Asl et al. 2019). These two mechanisms define capillary concept with Young-Laplace equation:

$$P_c = \frac{2\sigma Cos\theta}{r} \quad (1)$$

Here, σ is IFT, θ is the contact angle (CA), and r is the pore radius.

Surfactants will form microemulsions when mixed with aqueous and oleic phases. "Microemulsions are self-aggregated colloidal systems that provide a controllable system with a promising application as nanoreactors: they can act as pools within which the properties of the nanoparticles can be controlled without difficulty" this is a definition of microemulsions in nanoparticles presented by Cid (2018) in: In Microemulsion-a Chemical Nanoreactor. Microemulsions can either flow or diffuse into the sub-micron pore space with the assistance of their nano-size droplets, good solubilization capacity, and their ability to maintain low IFT. Ultra-low IFT can be achieved by the formation of middle phase (or Winsor type III) microemulsion using brine, oil, and surfactant or cosurfactant (Bera et al. 2014).

Another EOR technique is the use of low-salinity water as injection fluid. In this technique, there is an additional driving mechanism to capillary pressure called osmotic pressure. Osmotic pressure is a result of a phenomena known as chemical-osmosis and is defined as when water molecules with lower salt concentration moves through a semi-permeable membrane toward water with higher salt concentration, until salinity reaches equilibrium. In the reservoirs, clay plays the role of semi-permeable membrane, the salt in the pores plays the high concentrated medium, and the low salinity water plays the low salinity medium. Osmotic pressure will be a contribution factor in water imbibition through the pores and expelling the oil out. Capillary pressure helps water imbibition to the pores in water wet reservoirs, while in oil wet reservoirs it acts as a barrier. So, in tight formations which are oil wet in nature, when capillary pressure is lowered in addition to elevated osmotic pressure, is the best condition for enhancing the oil recovery.

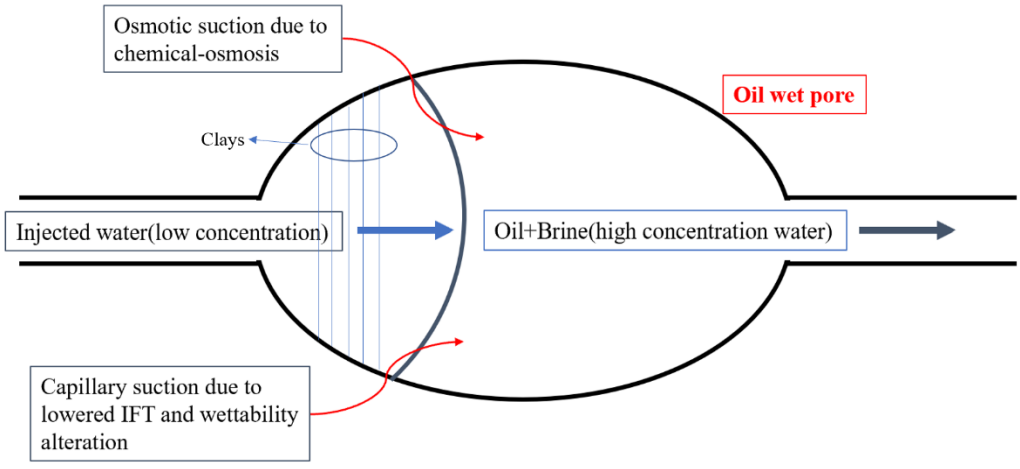

Figure 1.1: This is a schematic of contributing capillary and osmotic pressures in an oil wet pore. Water with low salinity flows to the pore with high salinity concentration through clay acting as membrane, capillary suction increased due to the addition of nanoparticles or surfactants.

From a fluid-fluid interactions point of view, IFT reduction is related to the phase behavior of the nanodroplet solutions and the type of microemulsion they make. Loads of investigators have worked on this subject (Winsor and P. A., 1954; Miller et al., 1976; Mittal and K. L., 2012; Pal et al., 2019).

In microemulsion systems, two or three phases can coexist with each other in equilibrium, while each phase preserve its structure (Bera, 2014). There are oil-in-water, water-in-oil, and bi-continuous microemulsions which are commonly referred to as Winsor type I, II, and III (Winsor and P. A., 1954), respectively. The microemulsion phase transition is controlled by the solution salinity and there is an 'optimal salinity' where the IFT between the phases reaches minimum (Chen et al. 2018, Salager et al. 1979; Winsor and P. A., 1954; Miller et al., 1976; Mittal and K. L., 2012; Pal et al., 2019). Phase behavior is the key factor in controlling the performance of microemulsion solutions in EOR processes. The nanoparticle additives form nano-sized particles in our microemulsions, therefore we name the solutions "nanodroplet (ND) solutions" in our study.

On the other hand, considering rock-fluid interactions, wettability alteration is considered the most important mechanism of surface-active agents. Contact angle measurements (Johnson and Dettre, 1969) is one of the quickest and best techniques to measure the rock's wettability. But Habibi and Dehghanpour (2018) showed that the apparent contact angle can be different from the actual contact angle because the latter is on a microscopic scale and can not be detected by eye or high-resolution camera. To calculate microscopic contact angle, we need to measure zeta-potential and determine 'disjoining pressure'.

Bera et al. (2014) used an anionic surfactant to investigate phase behavior and physicochemical properties of microemulsions in EOR operations. They also studied the effects of salinity on the structural changes of microemulsions. They concluded that salinity affects relative phase volume and solubilization parameters of microemulsion solutions. They found out that as water salinity increases, water solubilization in oil increases up to a point, called optimal salinity, and then it decreases. They also performed microemulsion flooding experiments on sand packs and observed that the microemulsion solution at the optimal salinity gives the highest oil production. However,

the performance of such microemulsion systems for oil recovery from tight rocks with complex wettability and pore structure is poorly understood and is the subject of this study.

Soleiman Asl et al. (2019) investigated the effect of microemulsion solutions prepared in tap water (TW) on oil-recovery from the Montney (MT) core plugs by performing IFT, CA, and imbibition oil-recovery tests. They found out that the imbibition of fracturing fluid containing microemulsions during the shut-in periods reduces water blockage at the fracture face and increases the post-shut-in production rate. Although Soleiman Asl et al. (2019) evaluated IFT, CA, and osmosis potential on oil recovery, they did not consider other factors such as solubilization and disjoining pressure of the microemulsion samples. Quintero et al. (2018) investigated the effects of four types of surfactants on the performance of the ND solutions for improving oil recovery from the MT core samples. Although they performed a series of experiments to evaluate fluid-fluid and rock-fluid interactions, they did not consider the salinity effect, stability of the chemical solutions, and particle size distribution of the micelles formed in the aqueous phase. The water salinity can affect the stability of the aqueous phase, and the size of particles formed in the solution. (Defined as the solution stays transparent and its droplets do not agglomerate)

1.2 Research Hypothesis

Up to this date, IFT reduction and wettability alteration have been studied and considered as the main mechanisms for EOR by ND solutions (Ali et al. 2018, Esfandyari et al. 2020). In addition, oil swelling (Kazemzadeh et al. 2015), pore channel plugging (Anganaei et al. 2014), and disjoining pressure (Aveyard et al. 2003) have been considered as factors controlling oil recovery by ND solutions. Understanding the effects of these factors along with IFT reduction and wettability alteration on imbibition oil recovery needs further investigation. This paper aims to answer the following question: In addition to capillary pressure modeled by the Young-Laplace equation, can other parameters such as solubility affect imbibition oil recovery from tight rocks by ND solutions? To achieve this objective, we investigate different parameters by conducting systematic fluid-fluid and rock-fluid experiments using different ND samples as additives and rank these parameters by their significance in the final oil recovery.

1.3 Objectives

In this study, we tried to screen and evaluate three different ND solutions, which are prepared by using three types of nanodroplet additives, through their fluid-fluid and rock-fluid interactions. Our final goals are:

1) Investigating different fluid-fluid and rock-fluid parameters on EOR when NDs are involved.
2) Ranking the most important parameters in the EOR by nanodroplet addition.
3) Determining the effect of salinity on the final oil recovery when using NDs.
4) Present a laboratory workflow to help selecting the most effective ND.

1.4 Overall Structure

In chapter 1 we briefly introduced a background about our study, explained the research gap, and overall structure of this study.

In chapter 2, we presented a literature review about each test we performed.

In chapter 3 we gave the materials and methodology of the study. Petrophysical properties of the core samples, properties of the fluids, pore size distribution, SEM images, and well logs are presented.

In chapter 4, we examined the natural wettability of the MT samples by performing two tests:

1) Air-liquid contact angle tests
2) spontaneous imbibition tests

In chapter 5, we performed spontaneous imbibition tests to compare the effect of our ND solutions. Also, we performed spontaneous imbibition oil recovery of our selected ND in different salinities to see the effect of salinity on its performance.

In chapter 6, first, we surveyed fluid-fluid interactions. These tests are summarized as:

1) Physical properties of ND solutions
2) Particle size distribution (PSD) tests
3) Interfacial tension tests (IFT)

4) Stability test
5) Solubility or Pipette test

In chapter 7, we investigated intermolecular interactions between a system consisting of oil, water, and rock by measuring zeta potentials and calculating disjoining pressures.

In the last chapter, we presented the key findings and suggested some of the studies that needs more investigations.

Chapter 2: Literature review

2.1 Dual-Wet Behavior

"Tendency of a fluid to preferentially wet a rock surface in the presence of another fluid" is the definition of wettability by Donaldson and Alam, 2008. The final oil recovery depends strongly on rock wettability (Habibi, 2016). The best condition to have more oil recovery is when the rock is preferentially water wet. The wetting affinity of the rock strongly depends on the rock mineralogy and the properties of the components that cover the surface of the pores within the rock, bitumen/pyrobitumen (Anderson, 1986). Evaluating the natural wettability of the rock samples is a prerequisite to select the best fracturing additives.

Lan et al. in two studies published in 2014 and 2015, performed contact angle and spontaneous imbibition experiments to measure and compare the wetting affinity of ten fresh core plugs from different depths of one well drilled in MT formation. He and his colleagues put core plugs vertically on a mesh in a way that only the bottom of them contact with the wetting liquid (ten cores in contact with oil and the other ten with brine). Then measured the weight of the cores periodically.

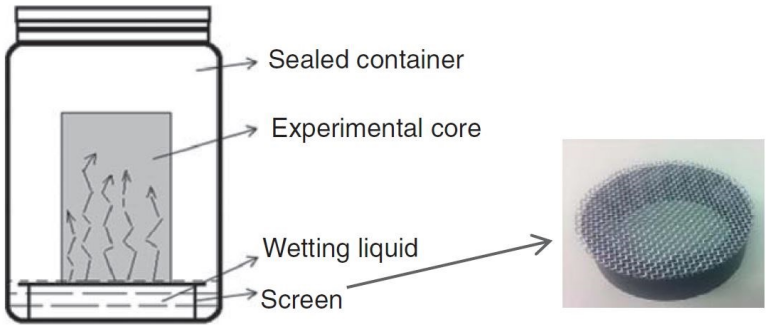

Figure 2.1: Schematic of Lan's spontaneous imbibition experiment. (Lan et al., 2015)

Their observations showed that the ratio between liquid uptake is higher than what capillary-driven imbibition models predicted. They suggested that a high oil imbibition ratio in well-connected pore network samples is the consequence of presence of degraded pyrobitumen on the surface of the pores. Then, they drew probable correlations between liquid imbibition rate and wettability, pore-size distribution, total organic matter, … and concluded that minerology of the samples in

unconventional tight rocks is a vital property to determine wettability behavior and it is an extra force in the fluid uptake.

Yassin et al., 2016 continued Lan's work furthermore by adding the analysis of FIB/SEM, MICP, and organic petrography. According to their analysis, cores from MT formation have dual-wet behavior; some nano-pores (which are the tail part of MICP profile) have oil wet affinity and they are highly water repellent. Micro-pores bordered by non-organic minerals such as quartz and calcite (bell-shaped part of MICP profile) are water wet.

Shi el at. 2019 validated previous works mentioned earlier by presenting their theory of imbibition transient analysis (ITA). In this theory "pore networks are idealized as a bundle of capillaries with different diameters." Larger capillaries represent inorganic pores, while smaller capillaries represent organic pores. Shi et al. used tight rock analysis (TRA), SEM images, and imbibition data to validate their work.

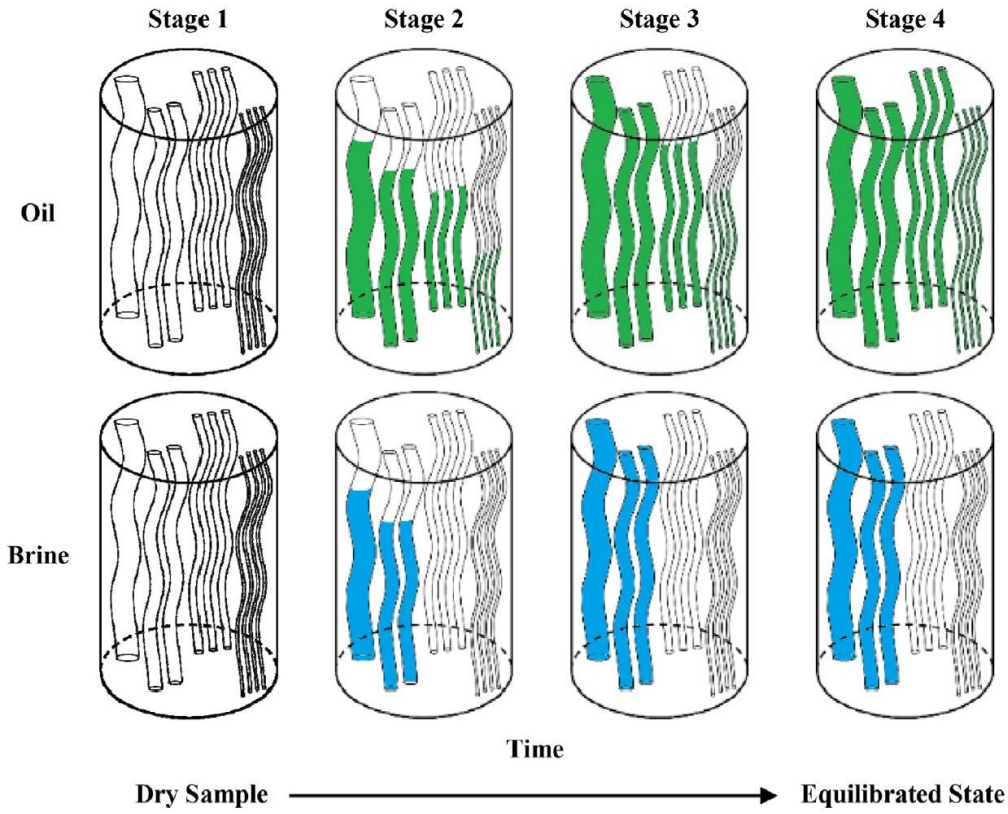

Figure 2.2: Schematic of pore networks as an idealized bundle of capillaries. Oil can imbibe into organic (small capillaries) and inorganic (large capillaries) pores, while brine can only imbibe into larger inorganic pores. (Shi et al., 2019)

Habibi et al. 2016 established a different laboratory protocol for wettability evaluation of tight oil rocks. He and his colleagues conducted systematic spontaneous imbibition tests on fresh core samples, taken from two wells drilled in MT formation. Then, they measured air-brine, air-oil, and brine-oil contact angles. In the final experiment, they performed spontaneous imbibition of brine and oil on the samples partly saturated with oil and brine. From the first experiment, they observed brine and oil spontaneously imbibe into the fresh cores and this shows an effective pore network of the samples. They calculated Young-Laplace capillary pressure for these cores, **Eq.1**, and compared it with capillary pressure which Schembre et al. 1998 calculated based on actual imbibition experimental data:

$$Q = \left(\frac{2P_c\phi KSA_c{}^2}{\mu}\right)^{0.5} t^{0.5} \quad (2)$$

Here, Q is the imbibed volume, P_c is capillary pressure, ϕ is porosity, K is effective permeability, S is saturation, A_c is contact surface area, μ is fluid viscosity, and t is time.

They observed that capillary pressure from imbibition data is much higher than that of Young-Laplace, so there must be an extra deriving mechanism besides capillary pressure. From the latter experiment, they observed brine spontaneously imbibe into the partly saturated core samples with oil and expels the oil out, but oil does not imbibe into partly saturated core samples with brine and does not expel the brine out. They also observed that oil is produced from specific layers when the core sample is layered.

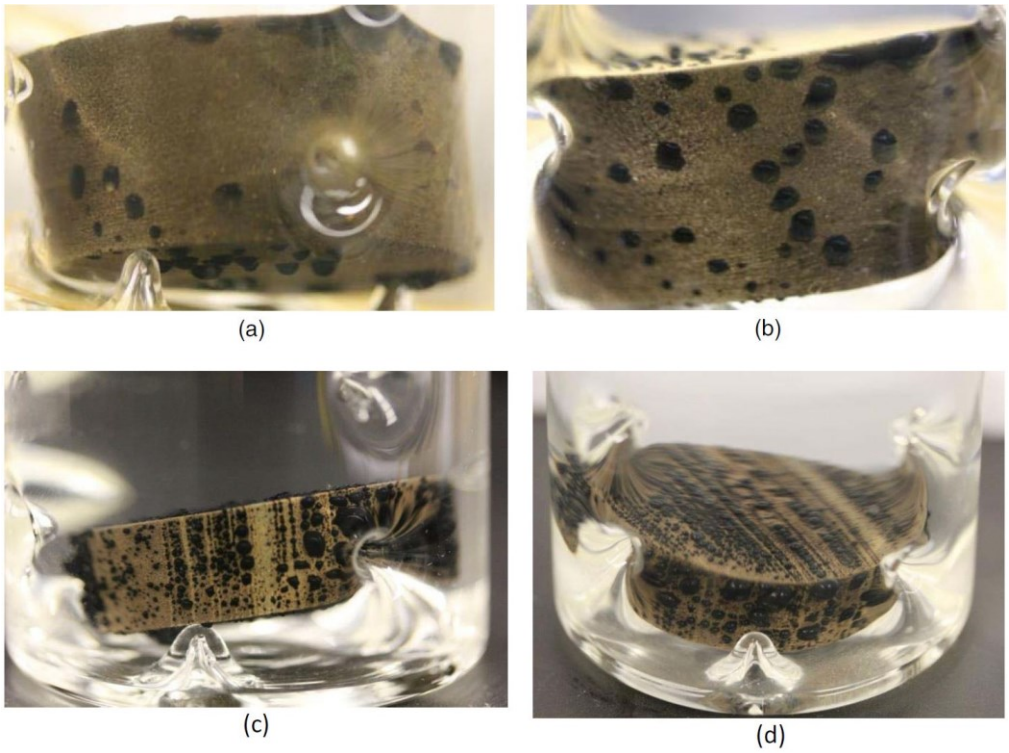

Figure 2.3: Spontaneous imbibition of brine into partly oil-saturated samples. Oil is produced from specific layers. (Habibi et al., 2016)

2.2 Spontaneous Imbibition

Several investigators performed spontaneous imbibition oil recovery on partially saturated core plugs (Habibi et al. 2016, Yassin and Dehghanpour 2016, Javaheri and Dehghanpour 2017). They all agreed on brine spontaneously imbibes into the oil-saturated core samples and expels the oil out and the produced oil is mainly from hydrophilic pores. Oil recovery is always less than the volume of brine imbibed into the fresh cores because the oil will remain in small organic or hydrophobic pores and trap in the larger, hydrophilic pores by snap-off phenomena.

As Alvarez et al., 2017 characterized three forces that lead to oil recovery from rocks: capillary, gravity, and viscous force. Schechter et al. 1994 related gravity force and capillary force by a term named Inverse bond number (N_B^{-1}):

$$N_B^{-1} = C\frac{\sigma \times \sqrt{\frac{\phi}{k}}}{\Delta\rho\, gh} \quad (3)$$

Here C is 0.4 for capillary tube model, ϕ is core porosity, k is permeability, Δρ is the difference between two densities, g is gravitational acceleration, and h is the length of the core. Schechter et al. 1994 divided N_B^{-1} into three groups:

N_B^{-1}>5 : capillary force dominates.

1<N_B^{-1}<5 : combination of capillary and gravitational forces.

N_B^{-1}<1 : gravity force dominates. (Vertical flow)

They also concluded that the fastest Inverse bond number for oil recovery is between 1 and 5, where the two forces are combined.

Habibi et al. 2016 performed a series of spontaneous imbibition tests and by calculating Young-Laplace capillary pressure (**Eq.1**) and Schembre et al. 1998 capillary pressure (**Eq.2**) and comparing them concluded that Young-Laplace capillary pressure is not the only driving mechanism.

2.3 Stability

NDs form microemulsions when in contact with water and oil. Microemulsions are composed of immiscible liquids (usually water, oil, and surfactant, sometimes a co-surfactant) which are thermodynamically stable and visually clear (Majuru and Oyewumi, 2009). The stability of NDs depends on lowering interfacial tension (IFT) between the two phases (dispersed and dispersing phases). Van der Waals attraction is the driving force for flocculation of nanoparticles, which is proportional to the particle size when the distance between particles is small (Tadros 2015); so, the nano-size particles, the large distance between particles, and the use of nonionic surfactants in NDs, act as stabilizing mechanisms. If the ND is not stable, it will lead to Ostwald ripening phenomena and result in the formation of larger droplets (Landfester 2001, Majuru 2009). Pore throat blockage can occur as a result of the larger droplets.

Multiple light scattering (MLS) method is simply defined as a technique to determine the size distribution profile of small particles in different solutions (Berne and Pecora, 2000). Particles in a solution are constantly moving and undergo Brownian motions. When the light (with wavelengths less than 250nm) hit these particles, it scatters in all directions, and due to the constant Brownian motion of the particles, its intensity changes. These changes are recorded over time, and information about the particles' movement on a time scale is gathered. Finally, a profile of the particle size over time is plotted.

2.4 Zeta Potential

When we are dealing with nano-sized particles, there is a strong van der Waals attraction between particles, which results in their aggregation and precipitation. To prevent this phenomenon, a stabilizing agent must be present which builds a repulsive force between nanoparticles. Electrical double layer force is achieved by adsorption of charged ions on the surface of the nanoparticles. This will create a strong repulsive force and prevent agglomeration of the particles. Surfactants are well-known stabilizing agents. They create a steric barrier between nanoparticles and keep them from contacting each other. Agglomeration process is as follows: 1) after nanoparticles production, electrostatic repulsion exists and is dominant, 2) due to interactions between nanoparticles and between nanoparticles with the solution, repulsive force fades, 3) as much as repulsive force decreases, van der Waals force starts to dominate and the nanoparticles starts to agglomerate. (Selvamani, 2019)

Nanoparticles have enough surface charges to prevent agglomeration in nanoparticle solutions. This electrical surface charge is quantified by a term called zeta potential and it determines the effective electric surface charge on nanoparticle surface. The closest layer to the nanoparticle surface which has the strongest bound with the surface, is called the stern layer. The outer layer is slipping plane. Zeta potential is a measurement between potentials at the slipping plane versus the bulk of the solution. The thickness of the double layer is called Debye length. We can determine zeta potential either between nanoparticles and the solution they are dispersed in, or between the nanoparticles and a charged surface (rock surface). (Gaikwad et al. 2019)

The high value of zeta potential is an indication of higher electric repulsion between particles; hence it gives information about the stability of the nanoparticle stability. Higher zeta potential, higher stability.

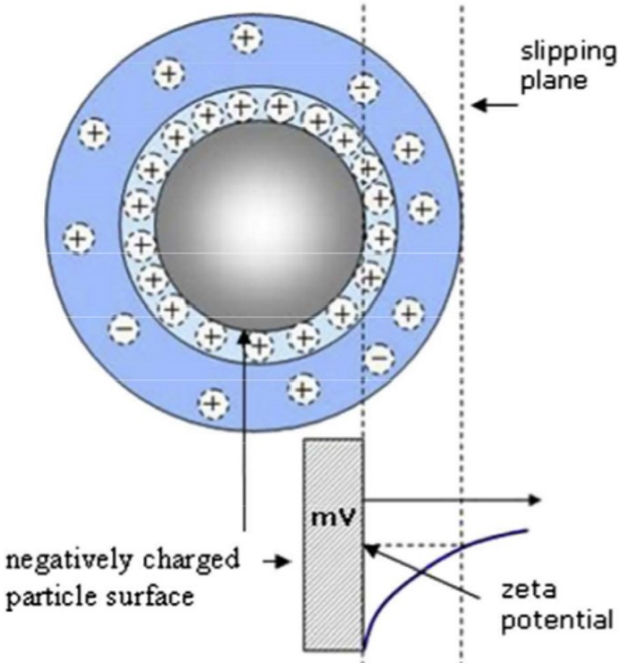

Figure 2.4: A schematic of a nanoparticle in a solution with its stern layer and slipping plane. (Selvamani, 2019)

2.5 Disjoining Pressure

The surface forces acting on liquid A and liquid B at the three-phase contact area on a microscopic scale differ from each other, which causes deformation of liquid A in its transition zone as demonstrated in **Fig.2.5**.

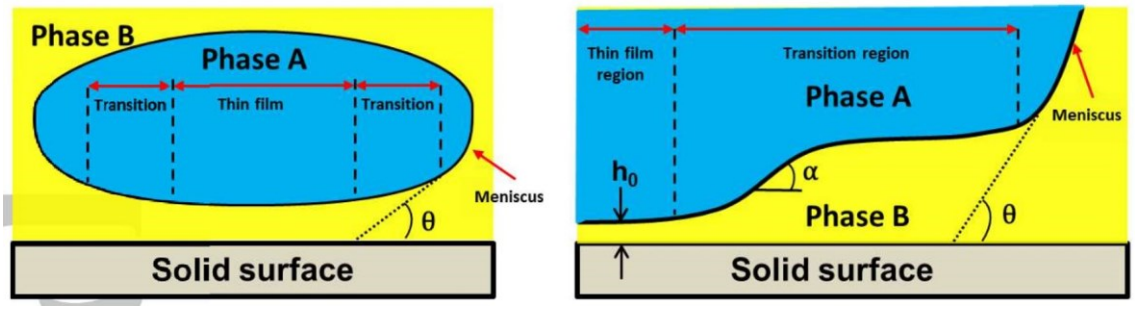

Figure 2.5: Macroscopic (left figure) and microscopic (right figure) view of the three-phase contact line. In the microscopic (right) figure, the transition zone is different. (Habibi, 2018)

Wettability alteration due to surfactant solutions has been investigated previously and the main mechanism for wettability alteration towards more water wet is ‘disjoining pressure’. The interactions between the surface of the rock and the nanoparticles will result in the nanoparticles near the surface to shape a spontaneous structural layering (stratification) which its properties like density, differs from the bulk of the solution. This layered structure will continue for a few molecular distance and decreases as the distance from the surface increases. The force which forms this layer is defined as structural force (Schön 2020).

There are both repulsive and attractive forces between nanoparticles. When these forces are balanced, the nanoparticles are stable and this results in stability of the nano dispersion. In general, the attractive force is dominant, and the nanoparticles will approach each other, until their double layer force interferes, and repulsive force starts to increase which drives the nanoparticles away from each other. By summation of these forces, we can calculate the net force existing between nanoparticles. Disjoining pressure is the sum of van der Waals (F_{VDW}), electrical double layer (F_{DL}), and structural forces (F_S). When $F_{VDW}>0$, repulsive forces are dominant and when $F_{VDW}<0$, attraction forces become dominant, and this happens when the water film is thick. $F_{DL}<0$ the attraction forces are dominant and when $F_{DL}>0$ the repulsive forces become dominant, the F_{DL} depend on the pH and salinity of the injected brine. In this study, we used DLVO (Derjaguin, Landau, Verwey, Overbeek) theory to calculate disjoining pressure (P_t) and we used a paper published by Habibi and Dehghanpour in 2018.

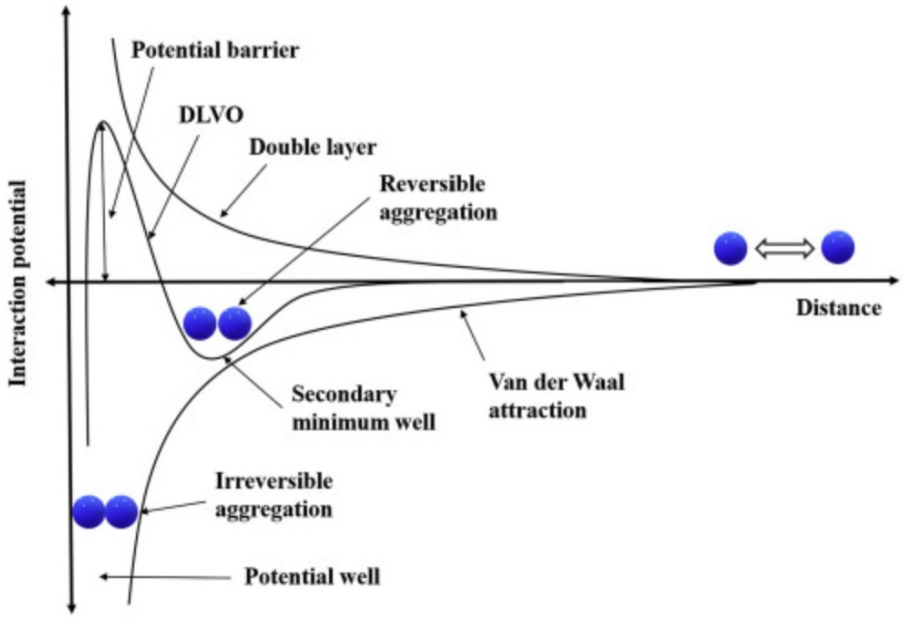

Figure 2.6: A schematic of DLVO theory. This plot shows disjoining pressure vs. particles distance. (Langford et al. 2022)

We assume three parallel films of fluid 1, fluid 2, and rock surface as is shown in **Fig.2.7**.

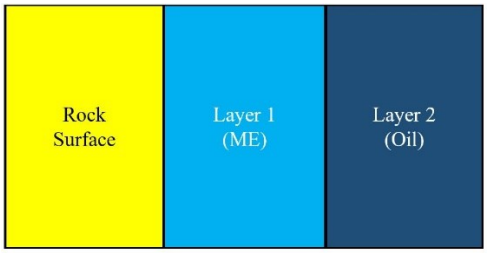

Figure 2.7: Layer 1 is the thin film between rock surface and oil droplet which is the aqueous phase with the ND. Layer 1 is stable when Pd>0 and unstable when it is Pd<0. (Habibi and Dehghanpour, 2018)

Disjoining pressure is made of three forces: van der Waals (F_{VDW}), double layer (F_{DL}), and structural (F_S):

$$P_t(h) = F_{VDW}(h) + F_{DL}(h) + F_S(h) \quad (4)$$

Here h is the distance between layer 2 and the rock surface.

Calculations of each of the parameters are presented here**,** nomenclature is from Habibi and Dehghanpour, 2018.

To calculate van der Waals force between two parallel plates, we used the following equations, **Eq.5**:

$$F_{VDW}(h) = \frac{-A_H(15.96\frac{h}{\lambda_{lw}} + 2)}{12\pi h^3(1 + 5.32\frac{h}{\lambda_{lw}})^2} \quad (5)$$

Here, $F_{VDW}(h)$ is van der Waals forces, A_H is Hamaker constant, λ_{lw} is London-wavelength which is taken 100nm according to Gregory, 1981.

For calculating Hamaker constant, we used the average Hamaker constants in the main minerals of the rock composition:

$$A_{H\,(rock)} = \frac{\sum_{i=1}^{n} C_i \times (A_H)_i}{\sum_{i=1}^{n} C_i} \quad (6)$$

C_i is Concentration of component i, $(A_H)_i$ is Hamaker constant of component i.

For double-layer force, we need to use reduced surface potentials of fluid1/fluid2 and fluid1/rock surface (Gregory, 1981).

$$F_{DL}(h) = n_b k_B T \left[\frac{2\psi_{r1}\psi_{r2}cosh(\kappa h) - {\psi_{r1}}^2 - {\psi_{r2}}^2}{(\sinh(\kappa h))^2}\right] \quad (7)$$

$$\psi_{ri} = \frac{e\zeta_i}{k_B T} \quad (8)$$

Here, $F_{DL}(h)$ is Double-layer force, n_b is ionic density of layer 1, k_B is Boltzman constant= 1.38×10^{-23} J/K, T is Absolute temperature=293.15 K, ψ_{ri} is Reduced surface potential.

The reciprocal Debye-Huckel length, κ, which is defined as the distance from where the effect of double layer fades.

$$\kappa^{-1} = \sqrt{\frac{\varepsilon_0 \varepsilon k_B T}{\sum_{i=1}^{n} C_{i,0} e^2 Z_i^2}} \quad (9)$$

ε_0 is Vacuum dielectric constant=8.85×10^{-12}F/m, ε is Dielectric constant of fluid 1=80.1 at 20°c, $C_{i,0}$ is number of ion/m3, e is Electron charge=1.6×10^{-19}C, Z_i is Valency of ions, ζ_i is Zeta potential for a pair of components.

And finally, to measure structural forces we used the following equations:

$$F_{s-water}(h) = A_s(e^{-h/h_s}) \quad (10)$$

$$F_{s-oil}(h) = C_1 \times e^{-h/\lambda_1} + C_2 \times e^{-h/\lambda_2} \quad (11)$$

Here, A_s is Structural forces coefficient= 1.5×10^{10} Pa, h_s is Characteristic decay length=0.05 nm, C_1 is Magnitude of short-range forces=8.86×10^7 Pa, λ_1 is Decay length of short-range forces= 0.1 nm, C_2 is Magnitude of long-range forces=2.87×10^6 Pa, λ_2 is Decay length of long-range forces=0.35 nm.

2.6 Interfacial Tension

Capillary pressure is the main oil trapping force which is defined by Young-Laplace, (1805) (**Eq.1**); Nonionic surfactants are best known for their ability to decrease the IFT, and as Rosano and Gebracia proposed in their work (1973): "diffusion of surface-active components across the interface could temporarily drop the dynamic interfacial tension to zero while the equilibrium IFT remained positive."

IFT reduction is one of the two most important aspects of surfactants' functions in reducing IFT and has been heavily investigated over the years (Chiang and Shah, 1980; Cash et al., 1977, etc.). As shown in a ternary diagram below, the closer we get to the plait point, the lower the IFT will be. Plait point is where two liquids at equilibrium become indistinguishable.

IFT varies with salinity, temperature, ND concentration, mixing ratio, and composition of the oil in water (O/W) or water in oil (W/O).

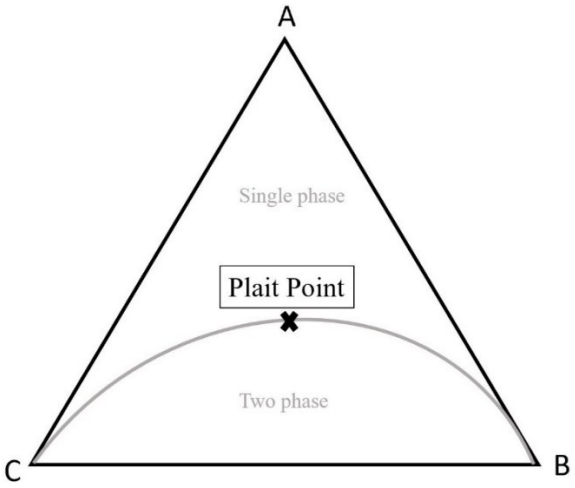

Figure 2.8: Schematic of plait point on ternary diagram. Investigations revealed that IFT between the two liquids goes down to zero at the plait point.

2.7 Solubility (Pipette)

The extent of IFT reduction depends on the type of microemulsion formed by mixing the ND (in different salinities) with the reservoir oil. In general, bi-continuous or Winsor type III microemulsion leads to more IFT reduction compared with types I and II (Winsor 1954; Chen et al. 2018, Salager et al. 1979, Wade et al. 1978). ND solubility depends on the brine salinity, type, and formulation of the surfactant, co-surfactant, the type, and the number of ions in the brine (Bera and Mandal, 2015).

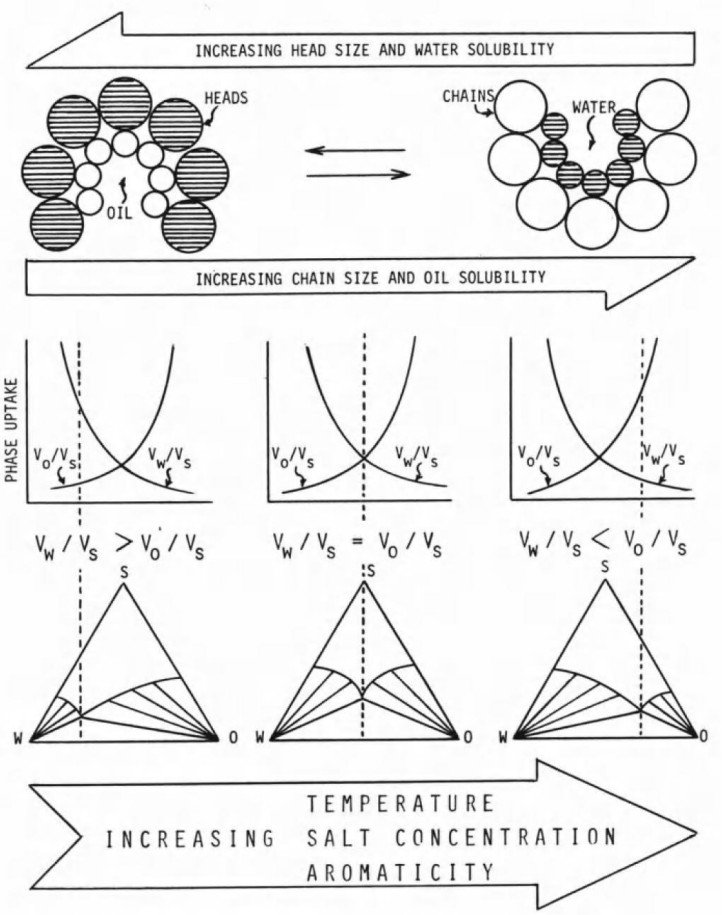

Figure 2.9: Pseudoternary diagrams presenting Winsor phase behavior of oil/brine/ND system. (a) presents Winsor type I (excess oil, meaning the ND presents in water phase), increasing salinity causes salting-out phenomenon and shifts to Winsor III (b), by further increasing salinity, the system will go through Winsor II (c) (excess water; ND presents in the oil phase). (Mittal and K.L., 2012)

Increasing salinity results in two distinctive parts in microemulsion type formation: the first part is as salinity increases, electrical double layer around polar groups shrink, so repellent force will be decreased, and more micelles will be soluble in the water (O/W microemulsion). So, as Pal et al. (2019) described, partitioning into the interface or oil phase is weak in high or low salinity (partitioning is the phenomenon of the presence of a solute between two immiscible phases like aqueous phase and an organic phase). In the second part, as salinity increases further, the salting-out effect will prevail, and water solubility decreases (W/O microemulsion). Low ion concentration in these solutions leads to the presence of more surfactant monomers/micelles in the bulk of the aqueous phase compared with higher water salinity conditions. In all these cases, there will be an optimal salinity which gives Winsor type III microemulsion and so, the lowest IFT as

is desired from microemulsions in EOR processes. Then, by measuring volume ratios of oleic and aqueous phases, the solubilization factor for oil and water was calculated and finally, we plotted them.

$$P_o = \frac{V_o}{V_s} \tag{12}$$

$$P_w = \frac{V_w}{V_s} \tag{13}$$

Here, P_o/P_w is the oil/water solubilization factor. V_o/V_w and V_s are oil/water and surfactant volumes in the microemulsion phase, respectively. All the calculations assumed that all the micelles were present in the middle phase (microemulsion), so V_s is constant.

Chapter 3: Materials and methodology

3.1 Core Samples

3.1.1 General Information

Target formation in this study is Montney (MT) formation. The conventional part of this formation containing sandstones and dolomite has been the focus of studies since the 1950s. The unconventional part of it, which is mainly siltstone, was developed by 2005 and about 80% of its wells are placed on production using horizontal wells (Ministry of Service Alberta, 2013). The eastern part of MT formation mostly contains conventional oil and gas, tight gas, and gas shale locates in the center, and black gas shale in the western part (Keneti et al., 2011).

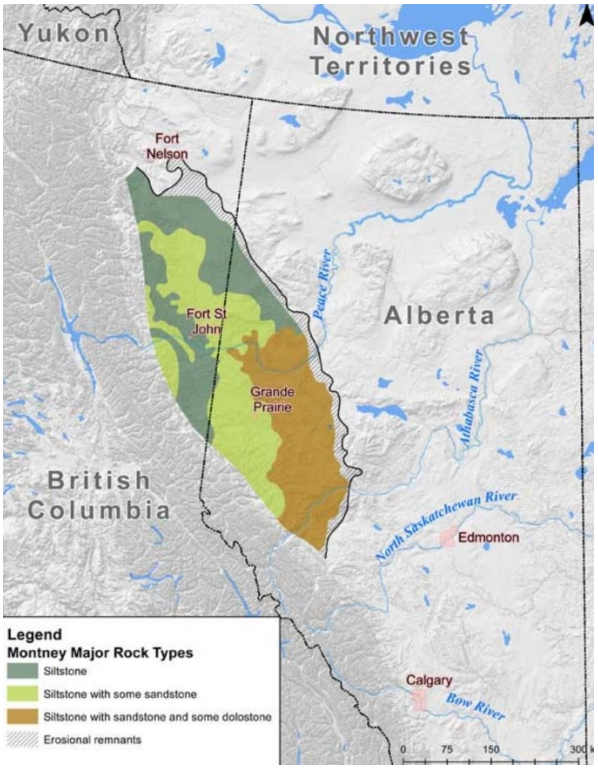

Figure 3.1: Location of Montney formation. (NEB, 2013)

The MT formation is a world-class play, located in the Western Canadian Sedimentary Basin, which is divided into Upper MT (light brown siltstone) and Lower MT (dark grey dolomitic siltstone) (Davies, 1997) with the lower MT covering an average extended area of 1.29×10^5 km^2 and its thickness ranges between 100m to 300m, which decreases to zero at the eastern and north-

eastern edges. The thickest part is its western side (assessed by CLIMA energy, https://calimaenergy.com/the-montney/). National Energy Board (NEB), the British Columbia Oil and Gas Commission (BC OGC), the Alberta Energy Regulator (AER), and the British Columbia Ministry of Natural Gas Development (BC MNGD) assessed this formation as a joint study in 2013 and presented this information: The estimated economical resources are around 30.3 million cubic meters (m^3) of oil, 333.5×10^6 m^3 of condensate, and 577.7×10^9 m^3 of gas (AER, May 2019).

3.1.2 Core Samples

We used eight core plugs collected from two wells (Well A and Well B) from two depth intervals, drilled and completed in the lower MT. Porosity, permeability, and mineralogy are evaluated by XRD analysis. SEM images, well logs, and MICP analysis are also present here. We used the cores unwashed and put them in the oven to eliminate any fluids.

3.1.2.1 Petrophysical Properties and Mineralogy

Table 3.1 summarizes the depth, permeability, and porosity of the core samples. The permeability measured by the pressure decay method is in the range of 4.50×10^{-5} to 6.04×10^{-5} mD. The porosity measured by the Helium porosimetry method ranges from 2.17 to 5.50%. **Table 3.2** lists the mineralogy of the core samples. The dominant mineral is quartz, ranging from 49 to 60 wt%. Dolomite with 8-19 wt% is the second dominant mineral. Clay contents, which are in the range of 3 to 15 wt%, are mostly mixed layers of illite/smectite, illite/mica, and chlorite.
More well log intervals are presented in **Appendix A**.

Table 3.1: Porosity and permeability of the core samples from the Montney Formation selected for this study.

Well	Sample ID	Depth (m)	Permeability (mD)	Porosity %
Well A	MT1-A	2066.20	4.50×10^{-05}	5.50
	MT2-A	2083.53	6.04×10^{-05}	3.23
	MT3-A	2091.33	4.00×10^{-05}	5.09
	MT4-A	2091.38	4.00×10^{-05}	5.09
Well B	MT5-B	2438.10	4.60×10^{-05}	5.25
	MT6-B	2438.14	4.60×10^{-05}	5.25
	MT7-B	2479.25	4.60×10^{-05}	2.17
	MT8-B	2479.29	4.60×10^{-05}	2.17

Table 3.2: Mineralogy of the core samples from the Montney Formation selected for this study.

Mineral wt%	Depth (m)							
	2066.20 MT1-A	2083.53 MT2-A	2091.33 MT3-A	2091.38 MT4-A	2438.10 MT4-A	2438.14 MT5-B	2479.25 MT6-B	2479.29 MT6-B
Quartz	59	49	49	49	60	60	52	52
K-feldspar	7	10	12	12	8	8	9	9
Plagioclase	11	11	12	12	10	10	10	10
Dolomite	19	15	8	8	13	13	12	12
Pyrite	1	3	4	4	2	2	3	3
Illite/Smectite (I/S)	0	8	10	10	4	4	10	10
Illite+Mica	3	3	4	4	3	3	5	5
Chlorite	0	1	2	2	0	0	0	0

Core samples MT5-B, MT6-B, MT7-B, and MT8-B have similar permeabilities. The first two cores and the second two cores are twin core plugs which is the reason for their similar permeabilities. But we can observe all these cores have equal permeabilities of 4.60×10^{-05} mD. There are few reasons to explain this similarity. First there might be an error in entering these numbers, or an error in measuring them in the first place. So as a suggestion, it is always better to re-measure the absolute permeabilities with water before conducting any tests. Second, when we compare permeabilities of all the cores within the intended depth, we observe a homogenous permeability trend. Also, the measurements are only within two decimal accuracies; maybe the difference would be emerged with higher accuracy due to the homogeneity between these samples.

Table 3.3: Permeabilities of the cores from well B. There is a homogenous permeability trend.

Depth (m)	Permeability (mD)
2438.1	4.60E-05
2438.14	4.60E-05
2452.5	5.10E-05
2452.54	5.10E-05
2468.04	4.30E-05
2468.09	4.30E-05
2479.25	4.60E-05
2479.29	4.60E-05

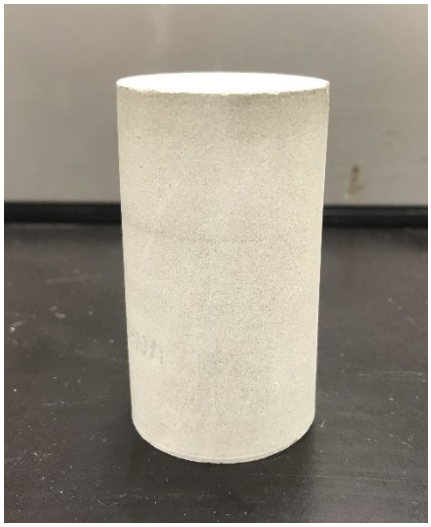

Figure 3.2: Fresh core sample from Montney formation. Dimensions are h=70.6mm and D=37.8mm.

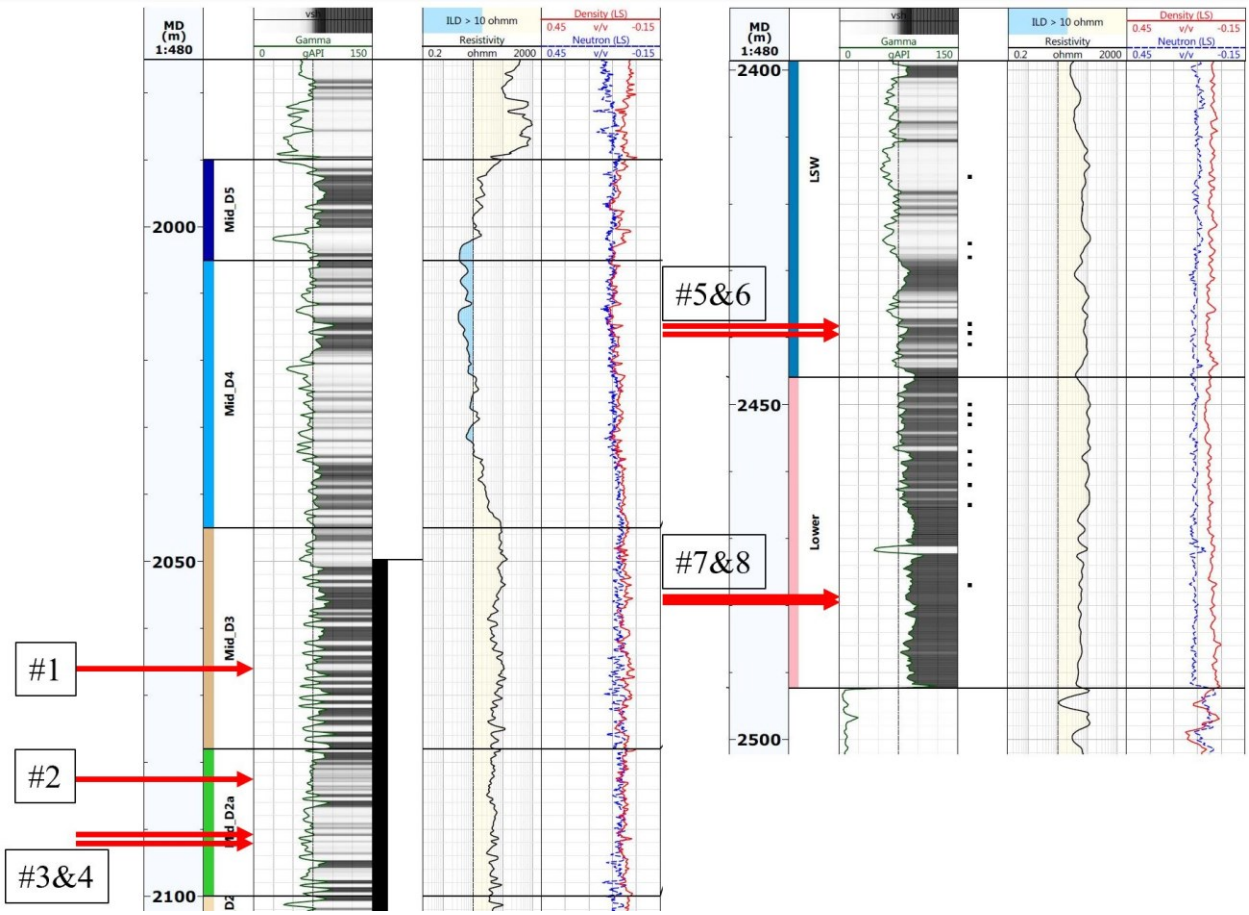

Figure 3.3: Approximate locations of the core samples on the well logs.

3.1.2.2 Pore Size Distributions (PSD)

Fig.3.4 shows the mercury injection capillary pressure (MICP) plots for four of the core plugs from the studied intervals. The porosity measured by this method is lower than helium porosity measurements, because of the very high pressure (>5800 psi) required for mercury to enter nano-size (around 3nm) pores which cause compression of the rock and as a result, a reduction in pore sizes (Labani et al. 2013). The bell-shaped part of the plot in **Fig.3.4** represents large pore-throats and the tail part represents very small pore-throats (nano-pores). **Fig.3.4(a), (b),** and **(c)** show well-developed bell-shapes ranging >240nm large pores. Tail parts of the profiles show small pores under <200nm. In **Fig.3.4(d)**, the peak is around 20 nm, but the tail is not very well developed and is extended to 4 nm. But this value does not represent the whole rock's pore distribution because the un-intruded pores are around 27% of the total pore volume. The incremental pore volume for large pores in **(a)** and **(b)** are almost twice higher than that in **(c)** and is twice as in **(d),** which are consistent with the increasing depth of the samples.

In general, we can divide the pores into two categories: 1) large pores >240nm which has an average estimation of 30-40% of intrusion volume, and 2) small pores <200nm having an estimated intrusion of 60-70%. More MICP profiles are presented in **Appendix C**.

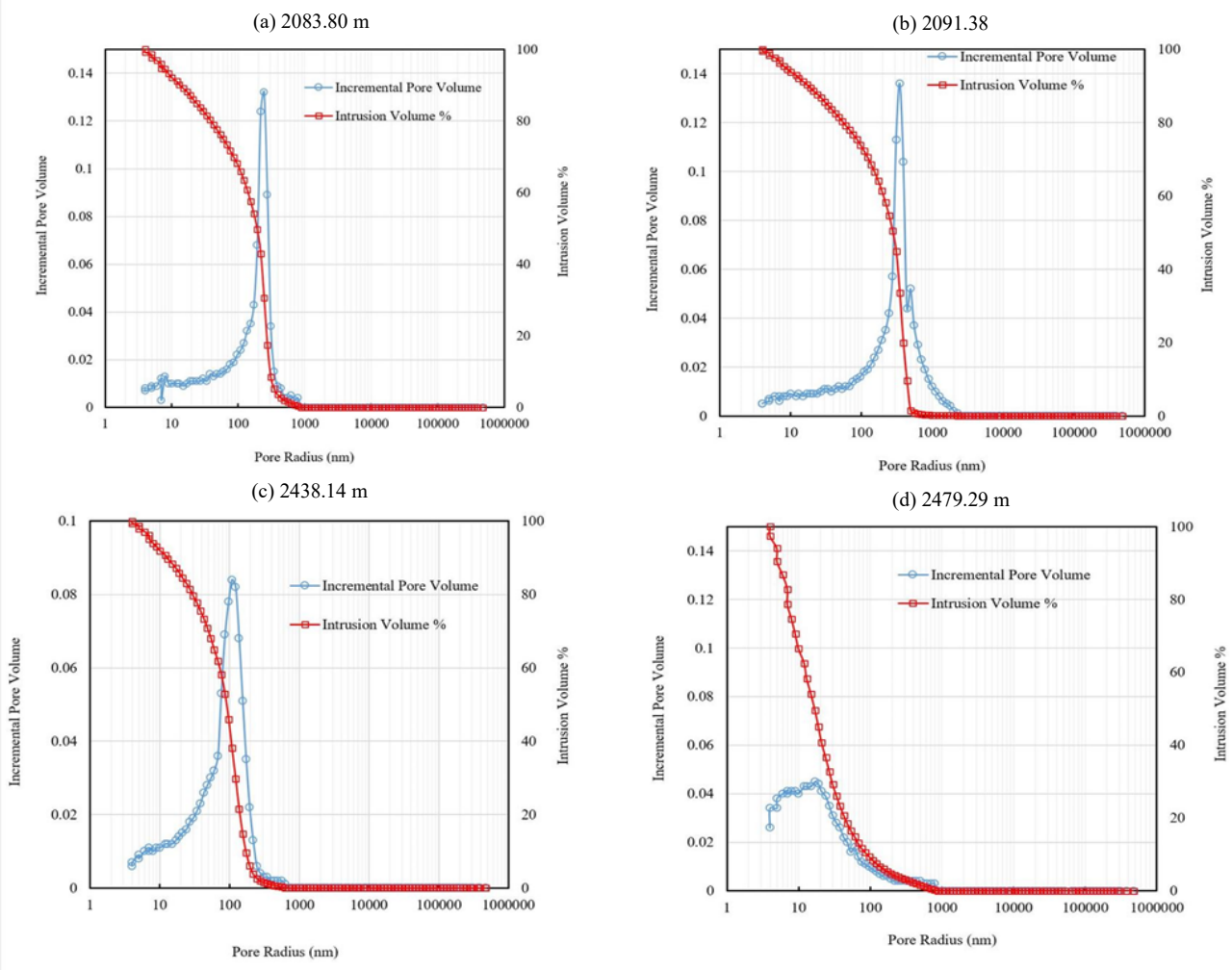

Figure 3.4: MICP profiles for four core plugs in: (a) 2083.80m, (b) 2091.38m, (c) 2438.14m and (d) 2479.29m. Cumulative intrusion percentage and incremental pore volumes on y-axes are plotted versus pore radius.

3.1.2.3 SEM Images

Fig.3.5 shows the SEM images of the samples from the candidate depth intervals. As determined by XRD, the most abundant clay mineral is illite/smectite which can be observed in **Fig.3.5(C).** Dolomite and illite are cementing agents and plug the large pores **Fig.3.5(D).** Two types of pores can be observed from **Fig.3.5**: larger pores bordered by inorganic minerals such as quartz and pyrite, and smaller pores (<1μ) within clay minerals. These results agree with MICP profiles, dividing pores into two groups.

Trace amounts of total organic carbon (TOC) are detected in these samples (<1%). The presence of quartz and carbonates (mostly dolomite) can be the reason for the mixed wettability behavior of the samples (Habibi, 2016). More SEM images are presented in **Appendix B**.

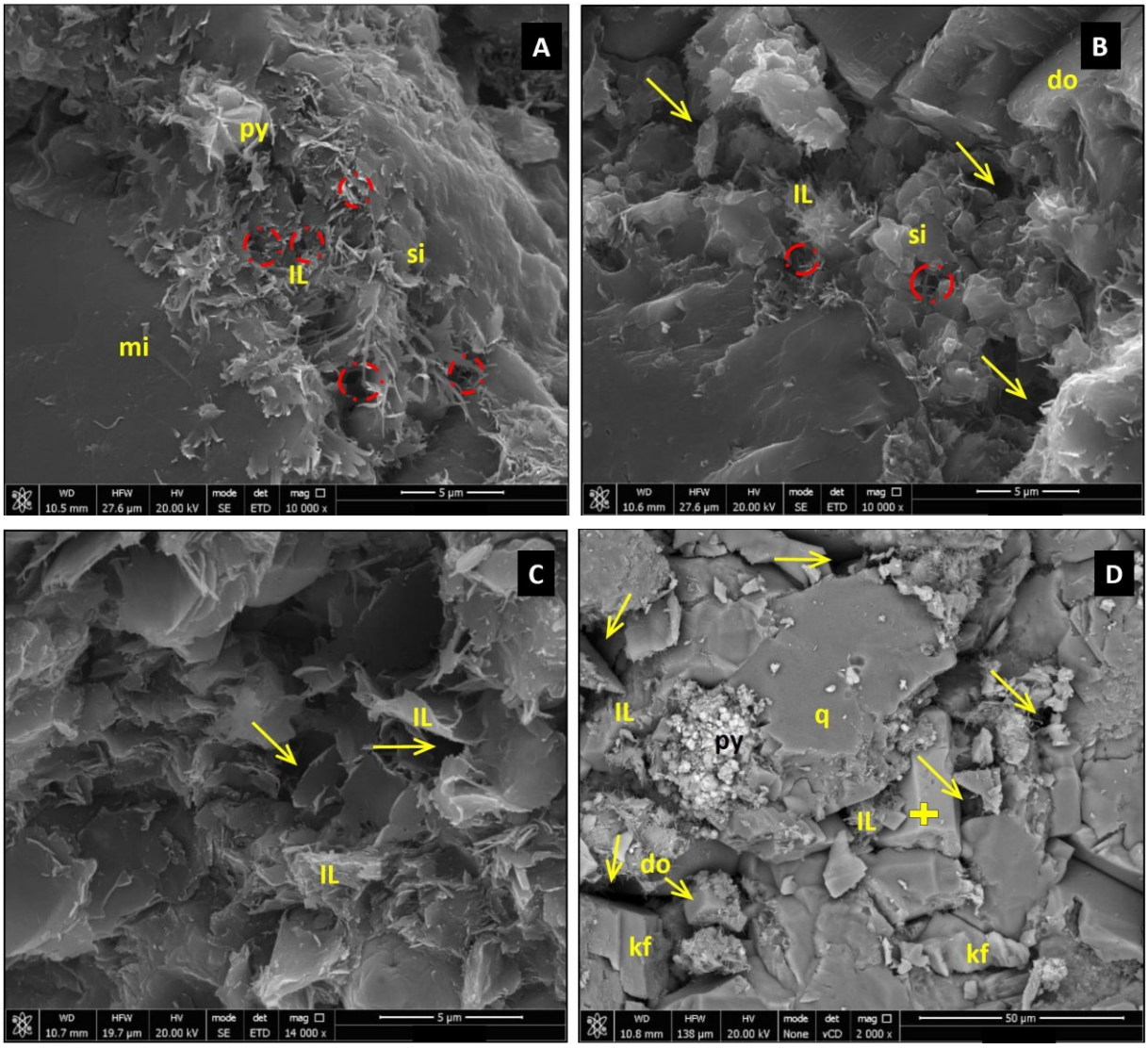

Figure 3.5: SEM images of core MT1-A. 'IL' represents illite, 'mi' is mica, 'si' is silica cement, 'q' is quartz, 'do' is dolomite and 'py' is pyrite. 'IL' and 'do' plug larger pores. Yellow arrows show larger pores and red circles mark smaller pores.

3.2 Fluid Samples

In this part, we present our fluid samples: brine, oil (collected from the MT formation), and three different ND solutions with their properties, then measured physical properties, stability, and particle size distribution (PSD) of the ND solutions. These properties are important to us because

they can describe ND solutions' flow through pores and their passing through pore throats. Finally, we discussed these results and highlight the differences between our ND solutions.

3.2.1 Oil

The core samples and fluids used in this study are taken from two wells (A and B), drilled, and completed in MT, and the oil sample is taken from well B. To eliminate the impurities from our oil sample, we filtered it twice, through filter papers; first through 6µm filter paper and then through 2.5µm. Then we centrifuged the oil samples to eliminate any possible brine.

The physical properties of the oil sample at ambient conditions are presented in **Table 3.3**.

Table 3.4: Physical properties of the oil sample.

API	Density (g/cc)	Viscosity (cp)	Surface tension (mN/m)
38.7	0.829	5.66	23.9

3.2.2 Brine

We used reservoir brine to perform our tests. We filtered the brine twice by filter papers of 6 and 2.5µm but since the produced brine is still mixed with additives used during the fracturing operation, we made a synthetic brine by using the same chemistry of the reservoir brine with total dissolved solid (TDS) of 130,000 ppm as listed in **Table 3.4.** The procedure we used to prepare synthetic brine is as follows:

1) The required mass for each salt is calculated based on the mass balance.
2) Since some salts may precipitate in the presence of other salts because of low solubility in water, the sequence of adding them is important.
3) ASTM D1141 standard is used to follow the sequence of mixing salts in water.
4) 189.3631 gr NaCl and 2.3994 gr $MgSO_4.7H_2O$ are added to 1000cc of de-ionized (DI) water in beaker 1 and stirred for 3 hours.
5) 2.5764 gr $MgCl_2$ and 6.1612 gr $CaCl_2.2H_2O$ are added to 250cc of DI water in beaker 2 and stirred for 3 hours.

6) 3.4890 gr KCl and 1.5425 gr $NaHCO_3$ are added to 250cc DI water in beaker 3 and stirred for n3 hours.

7) Solution in beaker 2 is gradually added to beaker 1 with 700rpm. Then, the solution in beaker 3 is added to beaker 1.

8) The whole solution in beaker 1 will stir for 1.5 hours.

We observe precipitations after the addition of $NaHCO_3$ in beaker 3. So, we used ASTM D1141 and substituted 190.0784 gr NaCl instead.

Table 3.5: Concentrations of the ions in the synthetic brine sample.

Ion (mg/L)	**Na^+**	**K^+**	**Ca^{2+}**	**Mg^{2+}**	**Cl^-**	**SO_4^{2-}**
Concentration in brine	49,750	1,220	1,120	596	81,379	623

To perform the bulk-phase tests at different salinities, we diluted synthetic brine with DI water, in the order shown in **Table 3.5**. The physical properties of the diluted brines are presented in **Table 3.6**.

Table 3.6: Aqueous phase salinity range.

Brine	**Reservoir brine**	**One order of magnitude diluted**	**Two orders of magnitude diluted**	**Tap water (TW)**	**DI water**
TDS (ppm)	130,000	13,000	1,300	100	0

Table 3.7: Physical properties of brines with different salinities used in this study.

Salinity (ppm)	**Surface tension (mN/m)**	**Viscosity (cp)**	**Density (g/cc)**
0	60.08	1.18	0.989
100	60.15	1.16	1.000
1300	60.01	1.18	1.008
13000	63.18	1.15	1.010
130000	63.39	1.22	1.087

3.2.3 Nanodroplet Solutions

We used three types of complex nano-fluid (CnF) additives (CnF-01, CnF-02, and CnF-03) to prepare ND solutions in this study. These CnF additives are composed of nonionic surfactants, solubilized terpene solvent, and water. More details about the CnF additives can be found elsewhere (Zelenev et al. 2011; Bui et al. 2019). CnF-01, CnF-02, and CnF-03 have 5%, 20%, and 10% terpene solvent concentrations, respectively. The ND solutions prepared by CnF additives with different physical properties are selected and used to evaluate the role of different parameters on oil recovery. A schematic of the CnF additive is presented in **Fig.3.6**. Solvents will be added to the microemulsions to dissolve oilfield deposits such as heavy crudes and paraffin and alternate wettability of the rock during EOR processes. Petroleum-based solvents such as benzene can be utilized to extract bio components conventionally. However, these solvents have low extraction efficiency, and some of the compounds might be lost. Biosolvents such as D-Limonene have been used to replace conventional petroleum solvents to reduce CO_2 and volatile organic compounds emissions and decrease the production of dangerous substances from petroleum solvents (Chemat et al. 2012). Biosolvent used in our CnFs is D-Limonene, also known as Citrus Terpene, which is an essential oil (orange oil) taken from citrus fruits. In technology, D-Limonene is the most environmentally friendly, renewable solvent these days. The solvent core targets to dissolve common oil field deposits like heavy crude, paraffins, and asphaltenes and increase hydrocarbon mobility. The surfactants around the solvent core aim to enhance fluid injectivity and mobility. Nonionic surfactants are best known for their ability in reducing IFT and good solubility capacity. The surfactants in the ND systems have a hydrophilic-hydrophobic balance (HLB) of 13 to 15, which can lead to the formation of oil-in-water droplets. Nonionic surfactants and water molecules form hydrogen bonds by using surfactants' ether groups (Myers, 2006), so they will contain an oxygen-rich portion on one end, and a big organic portion on the other end (Verkruyse and Salter, 1985). In aqueous phase, surfactants form spherical shapes in which their tails are at the center and in touch with solvent. This part will solubilize oil at the center. The head part of the surfactants are at the outer part of the spheres and in touch with the aqueous phase. These spherical formations are called micelles. These CnF samples have small droplet sizes (<200nm) to cover higher rock surface area. We diluted these CnF additives in the aqueous phase of different salinities (as presented in **Table 3.5**) with 1cc/lit ratio at room temperature to prepare ND solutions. The

physical properties of these ND solutions are measured and compared to investigate the effects of different CnF additives on fluid properties.

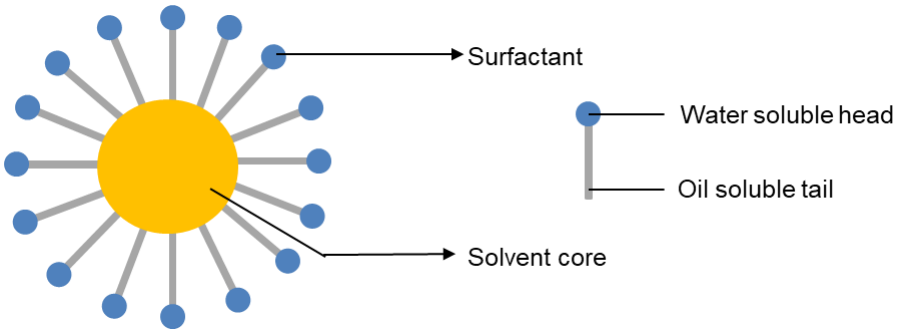

Figure 3.6: Schematic illustration of the ND samples used in this study. At the center, there is a terpene solvent core, and around it, there are multiple nonionic surfactants.

Delivery of the nanoparticles to very small pores, however, has another story which has three steps: 1) transmission of ND to the organic pores, 2) NDs break down and solvent and surfactant monomers distribute, and 3) altering the surface of the pore's properties. In this study, however, we just want to discuss the delivery of the ND droplets with different diameters to the pores with different pore throats.

Some of the particles have a larger diameter than the pore throats. As Bui et al. (2017) explained by simulating the penetration of ND solutions into the shale nanopores, the solvent at the core of ND will be adsorbed by the oil-wet surface of the rock, then breaks-down (which is the second step and we do not discuss it in this study) and turn into surfactant monomers and terpene molecules which are much smaller than micelles and can penetrate to the pores. A schematic of this process is presented in **Fig.3.7(a)** through **(d)**.

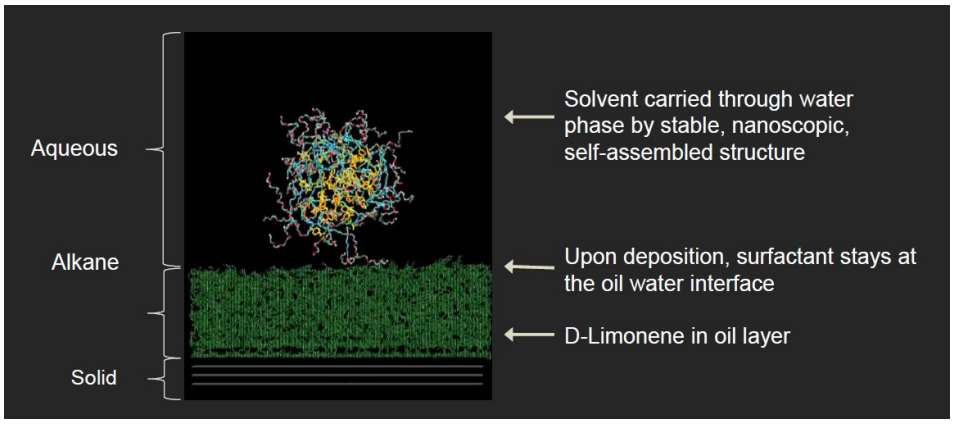

(a)

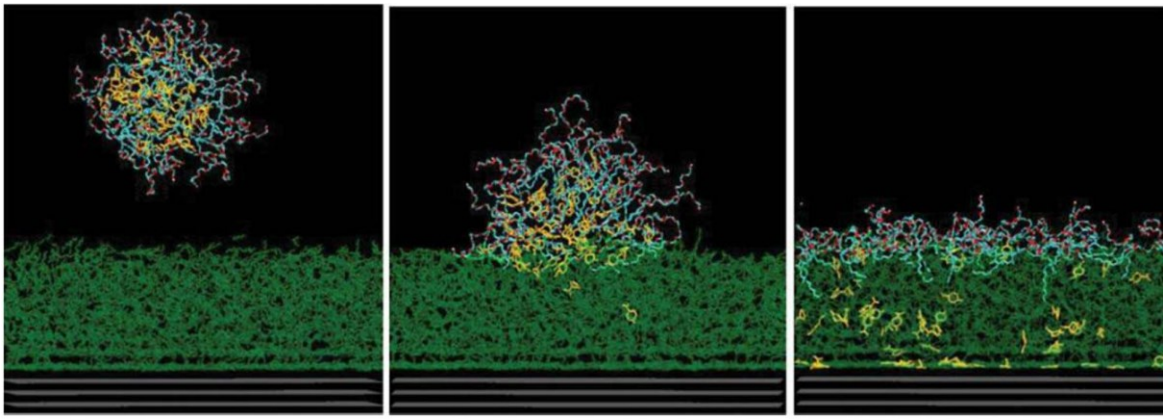

(b) (c) (d)

Figure 3.7: Schematic of ND break down steps into surfactant monomers and solvent molecules (Bui et al. 2015).

3.3 Methodology

Our experiments are divided into four parts, and we presented its flowchart in **Fig.3.8** below:

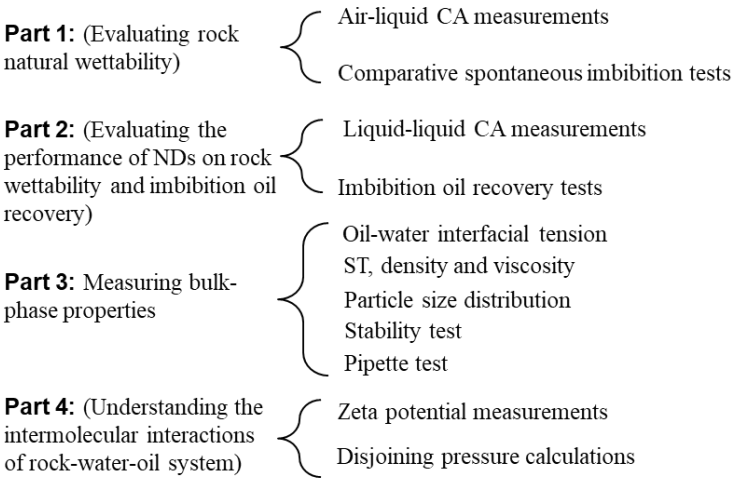

Figure 3.8: The flowchart of the laboratory protocol presented in this study.

Chapter 4: Wettability of the Montney Rock Samples

4.1 Air-Liquid CA Measurements

In this part, we evaluate the natural wettability of the rock samples under air-liquid conditions by conducting air-liquid CA measurements and spontaneous imbibition tests using reservoir oil and brine. Summary of the main goals in this chapter will be:

1. High imbibed volume of oil suggests that oil can imbibe into most of the pores, including both large and very small pores.
2. Low imbibed volume of brine suggests that brine can only imbibe into the larger pores.

4.1.1 Materials

We used two end pieces from cores MT2-A and MT4-A. We used CnF-01, CnF-02, and CnF-03 mixed with synthetic brine and TW.

4.1.2 Methodology

We polished end-pieces by using 400- and 600-grit sandpapers. Then, we aged them in the oil sample for a week. We visualized and recorded CA of equilibrated droplets of aqueous (TW and brine) and oil phases on the rock surface by the high-resolution camera of Biolin OneAttension theta instrument (accuracy of ±0.1 degree). We measured the CA of each droplet three times for 15 minutes, and the average value was reported.

4.2.2 Results

Fig. 4.1 shows the air-liquid CA of TW and brine droplet on oil-saturated end-pieces. TW and brine form droplets with CAs of 63.0±2.1 and 73.0±0.8 degrees, respectively. However, oil completely spreads on the rock surface immediately after being released. This suggests relatively strong oil-wetting characteristics of the dry rock samples in the presence of air.

The difference between brine (130,000 ppm) and TW CA can be explained by three mechanisms which were proposed and commonly referred to after years of investigations (Snosy et al., 2020):

1) Double-layer expansion (DLE): The ionic double layer thickness between clay and oil interface will increase as the water salinity decreases (Ligthelm et al., 2009).

2) Multi-component ion exchange (MIE): This phenomenon happens due to the different affinities of the rock surface towards distinct cations (Pouryousefy et al. 2016).
3) Chemical mechanism: pH in the aqueous phase increases when the salinity is low. This will desorb ions and some of the organic matters (Austad et al., 2010).

Table 4.1 presents air-liquid CA.

Table 4.1: Air-liquid CA of two extreme aqueous cases without any additives.

Fluid	Angle (degrees)
Oil	Complete spreading
TW – Base Case	63.0±2.1
Brine – Base Case	73.0±0.8

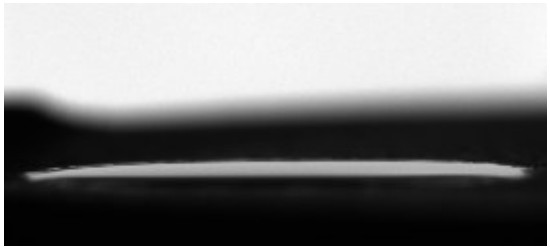

(a)

(b)

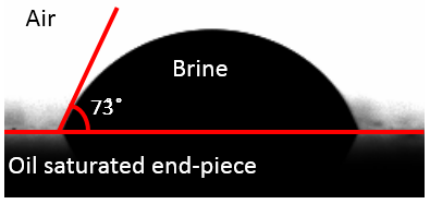

(c)

Figure 4.1: Air-liquid CA of a) oil, b) TW and c) brine droplet on oil-saturated end-pieces; oil droplet spreads completely, this suggests strong affinity of the rock samples to oil in the presence of air.

4.2 Spontaneous Imbibition Tests

4.2.1 Materials

We used two cores MT2-A and MT4-A. For fluid samples, we used TW and reservoir oil to conduct comparative spontaneous imbibition.

4.2.2 Methodology

We dried core plugs in an oven at 90°C and measured the weight loss every 24 hours until no further weight loss is observed to ensure evaporation of free fluids in the rock samples. The plugs were drilled using dry-cut technology, and we used them under as-received conditions without washing them. Then, we measured co-current imbibition of the brine and oil into MT2-A and MT4-A respectively, by weighing the core plugs periodically. More details about the procedure are presented in previous publications (Javaheri et. al 2017, Dehghanpour et al. 2013; Lan et al., 2015).

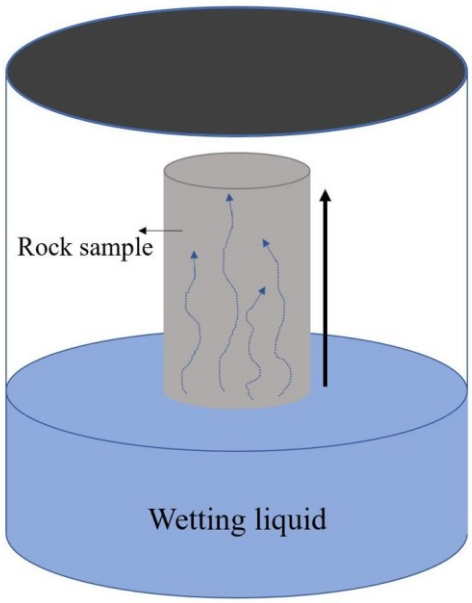

Figure 4.2: Schematic of comparative spontaneous imbibition test. Wetting fluid can be either oil or brine without any additives.

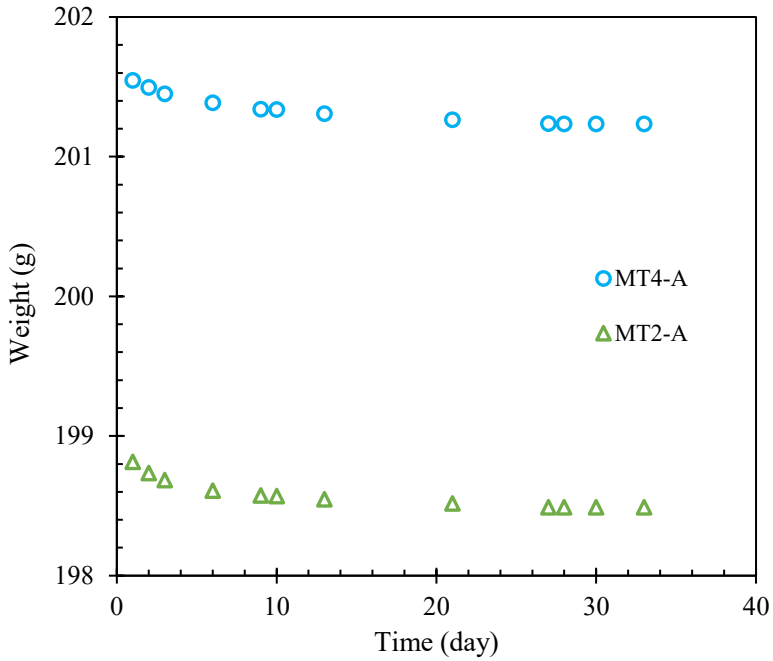

Figure 4.3: Drying process of the cores. At the beginning of the process weight loss is high, then by the time, it decreases until it is flattened.

4.2.3 Results

Fig.4.4 shows normalized imbibed volume of oil and TW into the dry cores versus time. TW gradually imbibes into the sample and fills 34.5% of its pore volume after 2 days. Oil imbibition has two parts: First oil quickly imbibes into the rock sample and fills 40% of its pore volume, then it continues imbibing with a lower rate and fills up to a final value of 52.5% of its pore volume. This suggests that water can only imbibe into the large hydrophilic pores, while oil can imbibe into both large and small pores. Lan et al. 2015 performed comparative spontaneous imbibition tests on nine twin-core plugs from the MT Formation. They observed that the equilibrium imbibed volume of oil is much higher than that of water and concluded that only a small fraction of pores is hydrophilic and most of the pore network can be invaded by the oleic phase.

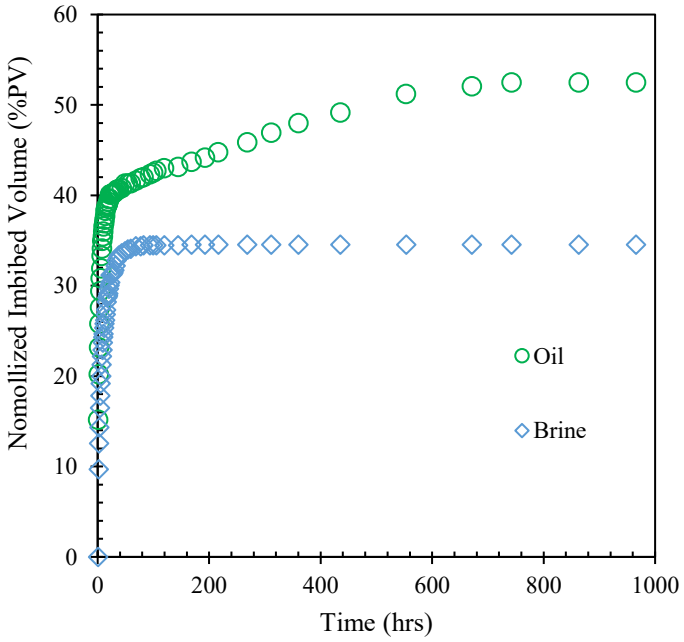

Figure 4.4: Normalized imbibed volume of brine and oil into the dry core plugs MT2-A and MT4-A versus (a) time and (b) square root of time.

4.3 Discussions

Schembre et al. 1998, derived an equation for the imbibed volume of the fluid (Q) as a function of capillary pressure (P_c):

$$Q = \left(\frac{2P_c\phi KSA_c{}^2}{\mu}\right)^{0.5} t^{0.5} \tag{14}$$

Where Q is the imbibed volume, P_c is capillary pressure, ϕ is porosity, K is effective permeability, S is saturation, A_c is contact surface area, μ is fluid viscosity, and t is time.
If we plot Q versus square root of time, the imbibition rate (slope) will be:

$$m = \left(\frac{2P_c\phi KSA_c{}^2}{\mu}\right)^{0.5} \tag{15}$$

If we assume ϕ, K, S, and A_c constant for our twin core plugs, then the ratio between imbibition rate of oil to brine will be:

$$\frac{m_o}{m_b} = \frac{\frac{2P_{co}\phi KSA_c{}^2}{\mu_o}}{\frac{2P_{cb}\phi KSA_c^2}{\mu_b}} \tag{16}$$

and by rearranging **Eq.16** we will have:

$$\left(\frac{P_{co}}{P_{cb}}\right)_{imbibition} = \left(\frac{m_o}{m_b}\right)^2 \frac{\mu_o}{\mu_b} \tag{17}$$

On the other hand, we can estimate capillary pressure ratio between oil and brine by using the Young-Laplace equation:

$$\left(\frac{P_{co}}{P_{cb}}\right)_{Young-Laplace} = \frac{\sigma_o Cos\theta_o}{\sigma_b Cos\theta_b} \tag{18}$$

Where σ is surface tension and θ is the contact angle between fluid and rock surface.
We calculated and compared these two capillary pressure ratios for the first part of the oil and brine imbibition.

$$\left(\frac{P_{co}}{P_{cb}}\right)_{imbibition} = 7.4135$$

$$\left(\frac{P_{co}}{P_{cb}}\right)_{Young-Laplace} = 0.7312$$

The capillary pressure ratio of imbibition data is 10 times bigger than the Young-Laplace ratio. This gap means that capillary pressure is not the only driving mechanism for fluid imbibition, otherwise these two ratios would be the same. The extra driving mechanism can be attributed to the presence of connected pore networks, covered with organic matters in which case oil will imbibe faster into these pore networks.

4.4 Results

Considering results of XRD, SEM images, and MICP profile, they all suggest MT rock samples have a mixed-wettability behavior. Quartz, with water-wet characteristics and dolomite, with mixed-wettability, create complex pore structures which result in mixed behavior of these samples. Spontaneous imbibition results suggest that brine reaches equilibrium faster than oil which is due

to brine imbibing into larger hydrophilic pores. From MICP profiles it can be observed that larger hydrophilic pores occupy less incremental pore volume of the cores (30-38% PV). Relatively lower initial imbibition rate of brine compared with oil, suggest that water preferentially imbibes into the large hydrophilic pores. On the other hand, smaller pores (nano-size) mostly exist in carbonates and clays with oil-wet nature. Also, there are connected pore networks, covered with organic matters which oil can imbibe into them as well as smaller pores (**Fig.4.5**). These nano-pores form higher incremental pore volume of the cores according to MICP profile (around 50-60% of intrusion volume). As mentioned earlier, the work of Lan et al. 2014 suggested that extra oil uptake is due to presence of materials such as pyrobitumen on the surface of the pores.

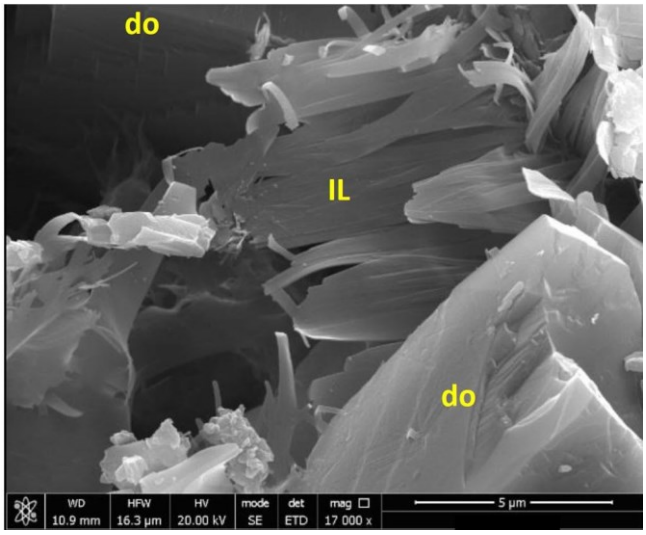

Figure 4.5: SEM image of the core sample with 5µm resolution. In this picture, 'IL' represents illite, 'do' represents dolomite.

CA results suggest more tendency of the rock towards oil wet. Water forms an angle of 63 while oil spreads completely immediately after the droplet is released.

The results indicate dual-wet behavior of the pore network, as discussed in previous studies (Javaheri et al. 2017 and Shi et al. 2019). Finally, the wettability evaluation tests suggest our rock samples have more tendency toward oil wet. More investigations on this part can be found in previous work done by Yuan, 2019.

Chapter 5: Imbibition Oil Recovery Tests

We have tried to answer this question in this study: is capillary pressure the most important mechanism working in the oil recovery by ND solutions? Can other mechanisms, such as solubility, also be used as selecting factors while using ND solutions?

Many papers have been published and have discussed wettability alteration and IFT reduction of the ND solutions as main mechanisms in the EOR applications (Ali et al. 2018, Esfandyari et al. 2020, Ayirala et al. 2019, Jiang et al. 2017). These two, affect capillary pressure defined by the Young equation (**Eq.1**). In addition, some also discussed oil swelling (Kazemzadeh et al. 2015), pore channel plugging (Anganaei et al. 2014), and disjoining pressure (Aveyard et al. 2003) factors. However, none of them mentioned any of these factors are equally important as capillary pressure in the final oil recovery.

In this chapter, we performed two sets of soaking tests: firstly, to investigate and compare our ND solutions performance. We conducted soaking tests by using TW as the base aqueous phase. Secondly, to investigate the effect of salinity on the final oil recovery, we performed soaking tests by using the ND solution with the highest oil recovery from part 1, TW, and brine as aqueous phases.

5.1 Imbibition Oil Recovery by Different ND Solutions

5.1.1 Materials

We used three core samples MT5-B, MT6-B, and MT7-B. We made three ND solutions (CnF-01, CnF-02, CnF03) by using TW as their aqueous phase. We selected TW as the base fluid since it is commonly used in field operations.

5.1.2 Methodology

We performed spontaneous imbibition oil recovery tests on the oil-saturated core plugs soaked in different ND solutions to evaluate controlling factors on oil recovery. Firstly, we dried three core plugs using an oven at 90^{o}C until no weight loss is observed. Then, we vacuumed the plugs in a core holder for five days. Next, we injected the oil at 1200 psig into the plugs under the overburden pressure of 1800 psig. After the oil injection, we measured the weight of the plugs to calculate the final oil saturation. We placed the oil-saturated core plugs in the imbibition cells, filled with

different ND solutions in the sequence presented in **Table 5.1** to measure and compare their RF_o profiles.

Table 5.1: List of core plugs used for the imbibition oil recovery tests.

Core number	Soaking fluid
MT5-B	CnF-02+TW
MT6-B	CnF-01+TW
MT7-B	CnF-03+TW

Figure 5.1: Core plugs in Amott cells, from left to right: CnF-01+TW, CnF-03+TW, and CnF-02+TW.

5.1.3 Results

ND Solution Prepared by CnF-03 Gives the Highest Imbibition Oil Recovery.

Fig.5.2 presents normalized imbibition oil recovery versus time for 65 days. The oil recovery factor (RF_o) is calculated by dividing the final produced oil volume by the oil volume initially in the core plugs. RF_o for the core plugs immersed in the three ND solutions ranges from 31.4% to

52%, which is much higher than RF_o of the core plug soaked in TW (11.3%), as the base case. This indicates that the presence of CnF samples can efficiently enhance the rate of oil production. Among the three ND solutions, CnF-03+TW shows the highest RF_o (52%).

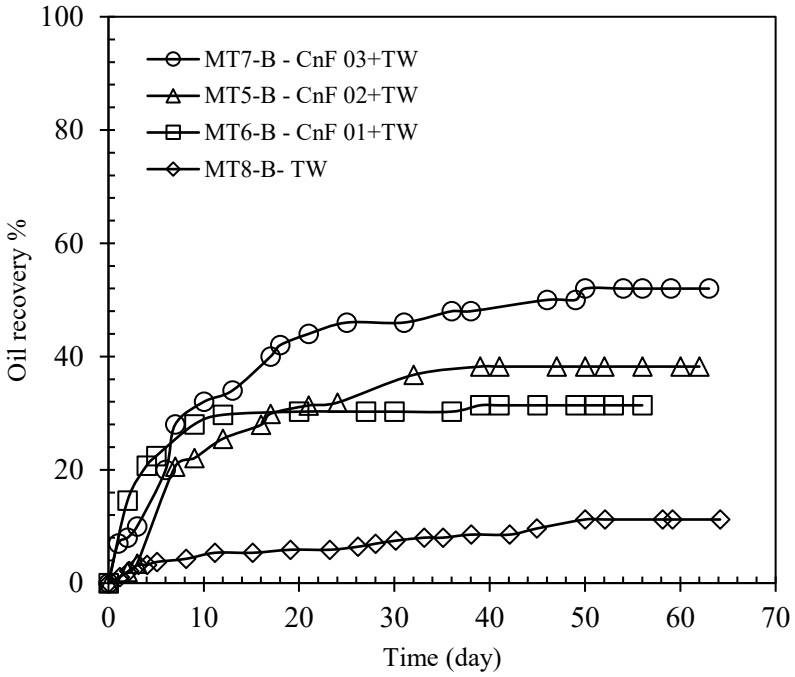

Figure 5.2: The measured RF_o profiles for oil-saturated MT7-B in CnF-03+TW, MT5-B in CnF-02+TW, MT6-B in CnF-01+TW, and MT8-B in TW. CnF-03+TW gives the highest RF_o while TW gives the lowest RF_o.

5.2 Imbibition Oil Recovery by the ND Solutions Under Different Salinities

5.2.1 Materials

We used four core samples MT1-A, MT3-A, MT7-B, and MT8-B. as our fluids, we made two ND solutions by using CnF-03; in brine and in TW.

5.2.2 Methodology

To investigate how osmosis potential affects imbibition oil recovery, we placed four of the oil-saturated core plugs in the imbibition cells, filled with the aqueous solutions under different salinities. **Table 5.2** lists the core plugs and the corresponding soaking fluids. The processes for drying and saturating the core plugs were described in **section 5.1**. We periodically measured the produced oil volume by a graduated tube (with an accuracy of ±0.1 cc) on the top part of the cell.

Table 5.2: List of the core plugs for the imbibition oil recovery tests.

Core number	Soaking fluid
MT1-A	brine
MT3-A	TW
MT7-B	CnF-03+TW
MT8-B	CnF-03+brine

5.2.3 Results

Fig. 5.3 shows the imbibition oil recovery results for the core plugs soaked in brine, TW, CnF-03+brine, and CnF-03+TW solutions, leading to the following key observations:

1) RF_o by brine and TW without CnF-03 are relatively low (11.3% by TW and 7.5% by brine).
2) RF_o by CnF-03+TW (52%) is 35.4% higher than by CnF-03+brine (16.6%).

Based on these results, high salinity is detrimental to imbibition oil recovery by CnF-03 that can be explained by the following hypotheses:

1) Higher possibility of middle-phase microemulsion formation in low-salinity water.
2) Higher osmotic pressure due to the difference in salt concentration of pore water and imbibing fluid (Fakcharoenphol et al. 2014). The higher salt concentration in the pores and lower salt concentration in the imbibition water, also the presence of clay working as semi-permeable membrane increases the osmotic suction in TW case and as a result, expelling more oil out. In the brine case, osmotic suction decreases, and brine imbibition to the pores decreases.

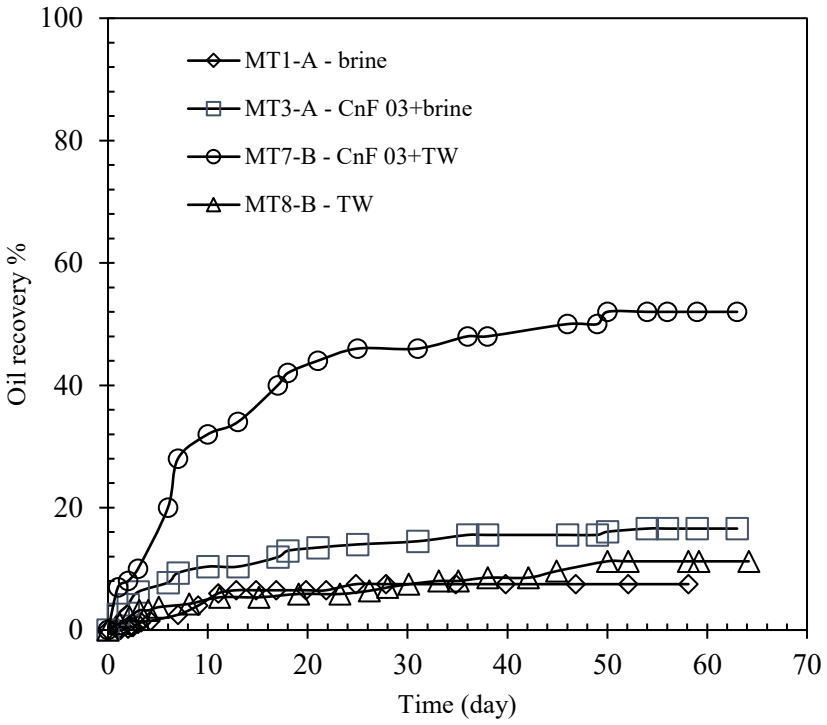

Figure 5.3: The measured RF_o versus time for the oil-saturated core plugs of MT1-A in brine, MT3-A in CnF-03+brine, MT7-B in CnF03+TW, and MT8-B in TW.

5.3 Liquid-liquid CA

We performed this test through visual estimation of the angle that wetting and non-wetting phase form with the solid surface (rock). The Young equation is using interfacial tension between phases to calculate CA:

$$\cos\theta = \frac{\sigma_{sv} - \sigma_{sl}}{\sigma_{lv}} \tag{19}$$

Here θ is the CA, σ_{sv} , σ_{sl} and σ_{lv} are the interfacial tensions between solid/vapor, solid/liquid, and liquid/vapor. In liquid-liquid condition, vapor is considered as the lower density liquid, liquid as the higher density liquid, and solid is considered as the rock sample.

5.3.1 Materials

We used end pieces from core samples MT5-B, MT6-B, MT7-B, MT1-A, MT2-A, MT3-A, and MT8-B. CnF-01, CnF-02, CnF-03 in brine as high salinity, and CnF-01, CnF-02, CnF-03 in TW as low salinity set of ND solutions.

5.3.2 Methodology

We measured the equilibrated water CAs for oil-saturated end-pieces immersed in the selected ND solutions by injecting oil from the bottom of the cell, using a J-shape needle. The end-piece preparation was described in **section 4.2.1**. We selected TW and brine as the base cases to investigate the effects of salinity on the wettability alteration of the rock samples. After releasing the oil droplet, we waited 20 minutes to let the droplet and aqueous phase reach equilibrium. Then, by using the instrument's high-resolution camera, we measured and compared water CAs in TW, brine, and ND solutions prepared in TW or brine. Each measurement was repeated three times and the average values are reported.

5.3.3 Results

Table 5.3 lists the measured CAs for equilibrated oil droplets in brine, TW, and ND solutions prepared in brine and TW. The observed CAs are based on visual observations of the oil droplets. The measured water CAs in brine (133.0±0.7) and TW (150.5±0.9) suggest that the rock samples are strongly oil wet. Higher water CA in TW compared to that in brine is explained in **section 4.2.1**.

The results listed in **Table 5.3** show that adding three CnF additives in TW significantly reduces the water CA. For example, as shown in **Fig. 5.4**, the presence of CnF-01 in TW reduces the water CA from 150.5^{o} to 80.6^{o}, altering the rock wettability toward water wet conditions. More CA figures in different ND solutions are presented in **Appendix D.** The wettability alteration by CnF additives can explain the higher imbibition oil recovery of ND solutions compared with that of base cases (brine and TW). The observed changes in CAs are minimal when the CnF additives are added in brine due to the reaction of the salt ions with the polar head of the surfactants, which limits the performance of the CnF additives. This indicates that salinity works as a barrier in wettability alteration. CnF-02 solution prepared in the brine is cloudy, and thus, the CA could not

be detected by the instrument. This solution has large particle sizes according to **section 6.1.2**, so this will put it in the emulsion category and referring to emulsion definition, they have cloudy appearance due to formation of different phases. Water CA in CnF-02+TW is 68.3°, which gives the highest wettability alteration and indicates the most water wet condition. Water CA in CnF-03+TW is 108.0 °, which is the least CA reduction and indicates a more oil wet condition. However, the RF_o of CnF-03+TW is higher than those of CnF-01+TW and CnF-02+TW, as shown in **Fig. 5.2**. Therefore, the macroscopic CA measurements cannot fully explain the oil recovery results. CnF-03 has the lowest IFT and the shape of oil droplet in CnF-03 is more elongated than the shape of oil droplets in the other ND solutions. Oil droplet in CnF-02 with the highest IFT has a more spherical shape with higher CA.

Table 5.3: Liquid-liquid CA of oil droplets in the ND solutions prepared in TW and brine. Oil droplets in CnF-02+brine could not be detected by the instrument because of their cloudy appearance.

Aqueous phase	Base case (No ND)	CnF-01	CnF-02	CnF-03
TW	150.5±0.9	80.6±3.7	68.3±4.4	108.0±5.1
Brine	133.0±0.7	112.0±2.4	-	133.5±5.3

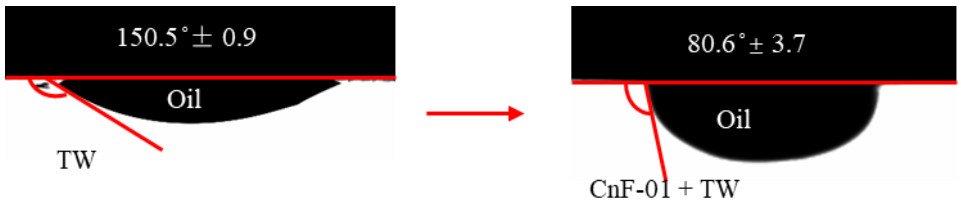

(a) (b)

Figure 5.4: Comparing liquid-liquid water CA of oil in a) TW and in b) CnF-01+TW shows the significant change in the CA by CnF-01.

Chapter 6: Properties Characterization of ND Solutions

Two aspects must be investigated about ND solutions: first, the interactions between fluids, and second, interactions between rock and fluids. We conducted bulk-phase tests to measure physical properties, particle size, IFT, stability, zeta potential, disjoining pressure, and solubility of the ND solutions. The results of bulk-phase tests can be correlated with imbibition oil recovery to study the role of other parameters such as particle size distribution, fluid stability, and microemulsion type on imbibition oil recovery from tight rocks.

6.1 Physical Properties (Density, Viscosity, and Surface tension)

6.1.1 Materials

We mixed CnF-01, CnF-02, and CnF-03 in our salinity range.

6.1.2 Methodology

We measured the density and surface tension of the ND solutions, using the glass ball probe and Wilhelmy plate of the OneAttension instrument. Wilhelmy plate is a square platinum plate, which is roughened to ensure complete wetting.

$$\sigma = \frac{F}{LCos\theta} \tag{20}$$

In which σ is the surface tension, L is the plate's perimeter, and θ is the contact angle between the fluid and the plate.

We also used Brookfield Viscometer to measure the viscosity of the samples. This viscometer is a *rotational viscometer* which analyzes the torque which is required to rotate a spindle immersed in the desired fluid at a constant speed. This viscometer gives us a good understanding about the flow behavior of the fluid we are using. Each measurement was repeated three times at ambient conditions and the mean values are reported.

6.1.3 Results

Here, we present the results of bulk-phase tests to investigate the phase behavior and fluid-fluid interactions in presence of the CnF additives under different salinities. Since the macroscopic CA measurements results were not sufficient to explain the oil recovery results, we also analyze the bulk-phase results to study other parameters affecting the imbibition oil recovery.

Surface tension: **Fig. 6.1a** shows surface tension of ND solutions with different salinities. The ND solutions prepared by CnF-03 have the lowest surface tension values through the whole salinity range. In general, in this plot, the correlation between ST and salinity of ND solutions is not clear. Previous studies show that water salinity can strongly affect the interfacial properties of surfactant solutions (Standal et al. 1999; Seedher and Kanojia 2008; L. Zhang et al. 1996). In general, increasing salinity decreases surface tension (or IFT) until reaching a minimum value (Li et al. 2007). This can be explained by electrostatic interactions between salt ions and the polar head of surfactants in the water and the salting-out effect. The salting-out effect is defined as the condition where the surfactant monomers move toward the interface when salinity increases, promoting surface tension (or IFT) reduction (Santos et al. 2009, Kumar and Mandal 2016). However, there are no strong interactions between the hydrophilic head of nonionic surfactants and the ions in the water. Therefore, surface tension reduction by this mechanism may not be significant for ND solutions with nonionic surfactants. The surface tension values versus water salinity, observed in **Fig. 10a,** may be due to the hydrogen bonding between the hydrophilic head of the surfactants and water molecules (Kumar and Mandal 2016), leading to the increase in surface tension values. However, due to the presence of nonionic surfactants, this attraction is small for the ND solutions studied here.

Viscosity: Viscosity values of all the solutions are very close, in the range of 0.7-1.17±0.04 cp, as shown in **Fig. 6.1b**, except for CnF-02+ brine with 130,000 ppm salinity which is 1.99 cP.

Density: **Fig. 6.1c** shows that the density of all the solutions has the same increasing trend.

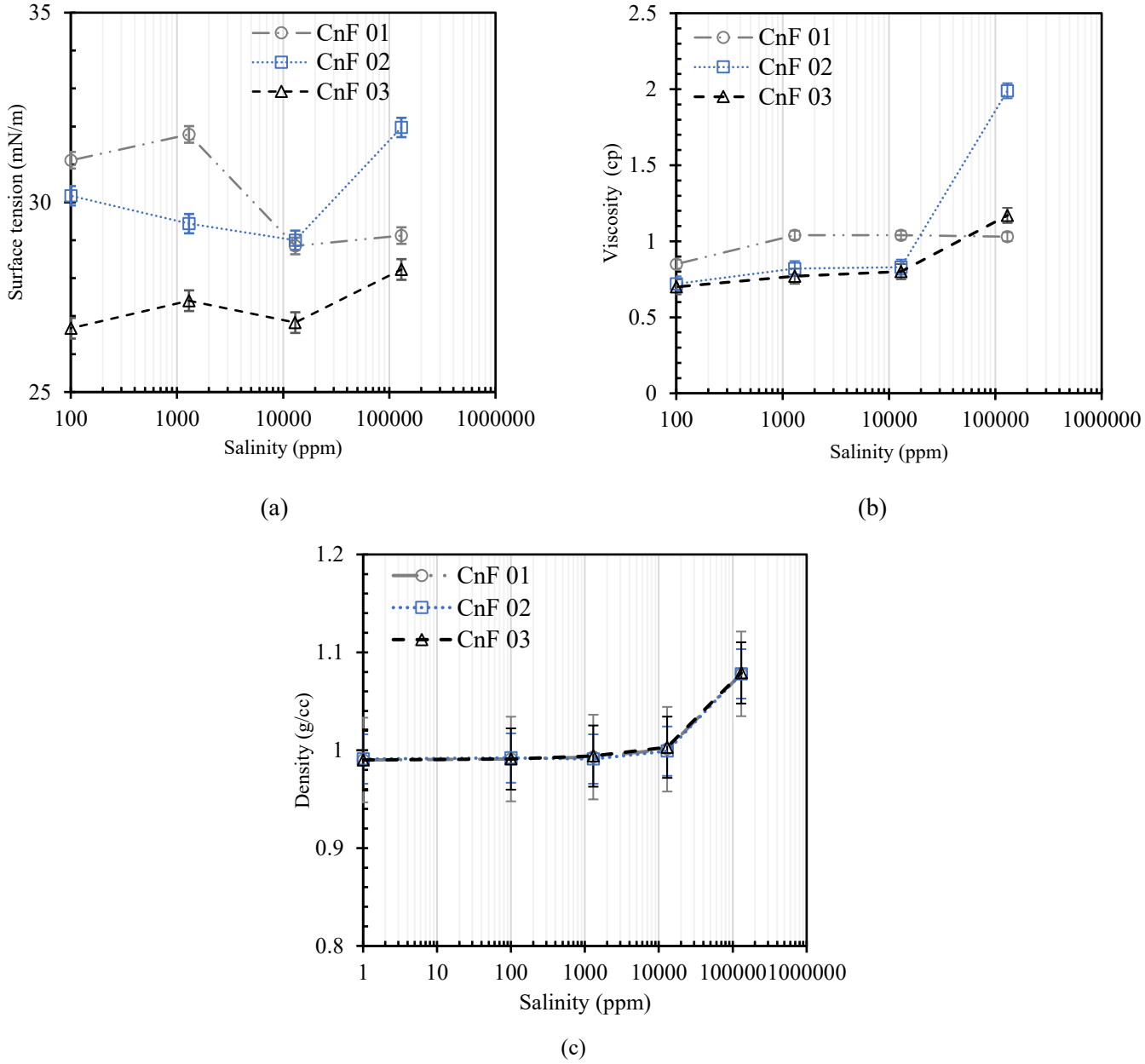

Figure 6.1: Effect of three CnF additives on aqueous phase physical properties at different salinities: a) there no clear trend for surface tension with salinity, b) viscosity increases as salinity increases, c) density remains almost constant until 10000 ppm, and then sharply increases by increasing the salinity.

6.2 Particle Size Distribution (PSD)

As mentioned in **section 3.2.3**, ND solutions are prepared by CnF additives. CnF additives include a nonionic surfactant package with terpene solvent cores and water. This package is also known

as ‘swollen micelles’. Particle size distribution is important because it will affect the interactions between ND particles, the stability of the solutions, and pore accessibility for the particles.

6.2.1 Materials

We mixed CnF-01, CnF-02, and CnF-03 in our salinity range.

6.2.2 Methodology

We used Malvern Zetasizer Nano ZS that works based on the dynamic light scattering (DLS) technique (Berne, 2000) and it can measure the size of particles ranging from 0.3 nm to 1 µm. We put 20 cc of each of the ND solutions (in different salinities) in specific vials and put them in the instrument. Each measurement was repeated three times at room conditions and the mean values are reported.

6.2.3 Results

Fig. 6.2 shows the mean size of nanodroplets formed in the ND solutions versus water salinity. Generally, the average size of nanodroplets increases by increasing the water salinity. For ND solutions prepared by CnF-01 and CnF-02, the particle size reaches the highest when salinity is 13,000 ppm. Although the surfactants in the solutions are nonionic, the hydrogen bonding between ions in the high-salinity brine (130,000 ppm) and the hydrophilic head of the surfactant molecules can form larger particles. Also, the ionic interactions between water molecules and salt ions form larger brine particles, which will expand the CnF micelles to create hydrogen bonding that we mentioned.

The mean particle size of ND solutions prepared by the three types of CnF additive is less than 120 nm when the water salinity is less than 13,000 ppm. However, the CnF additives show different behavior when the water salinity increases to 130,000 ppm. The mean size of droplets formed in the CnF-02 solution significantly increases from 48.49 nm to 1123nm when the water salinity increases from 13,000 to 130,000 ppm. This indicates that the CnF-02 solution is not stable at high salinities, leading to the formation of large and agglomerated particles which excludes the solution from microemulsion category according to their definition. The high viscosity of CnF-02 in brine, reported above, could be a result of its relatively larger particles. The mean particle size of CnF-01 and CnF-03 solutions with 130,000 ppm salinity is 153.7 and 113.4 nm respectively,

indicating that CnF-01 and CnF-03 can tolerate a wide range of water salinities. In general, core plugs are more accessible to ND solutions in low-salinity water compared with that in high-salinity brine. This is due to the formation of larger particles by the CnF additives in high-salinity conditions which reduces their accessibility to the rock pores. Therefore, the ND solutions in low-salinity conditions can imbibe more in core plugs and are more efficient for increasing oil recovery compared with that in high-salinity conditions, which is consistent with the imbibition oil-recovery results.

Comparing **Fig.6.3** and **Fig.3.4** (MICP), shows all the ND solutions except for CnF-02 in brine, can easily enter the most portion of the pores, just with the aid of capillary force. But the part of the pores with nano-sizes can also be invaded by the mechanism of micelles break down.

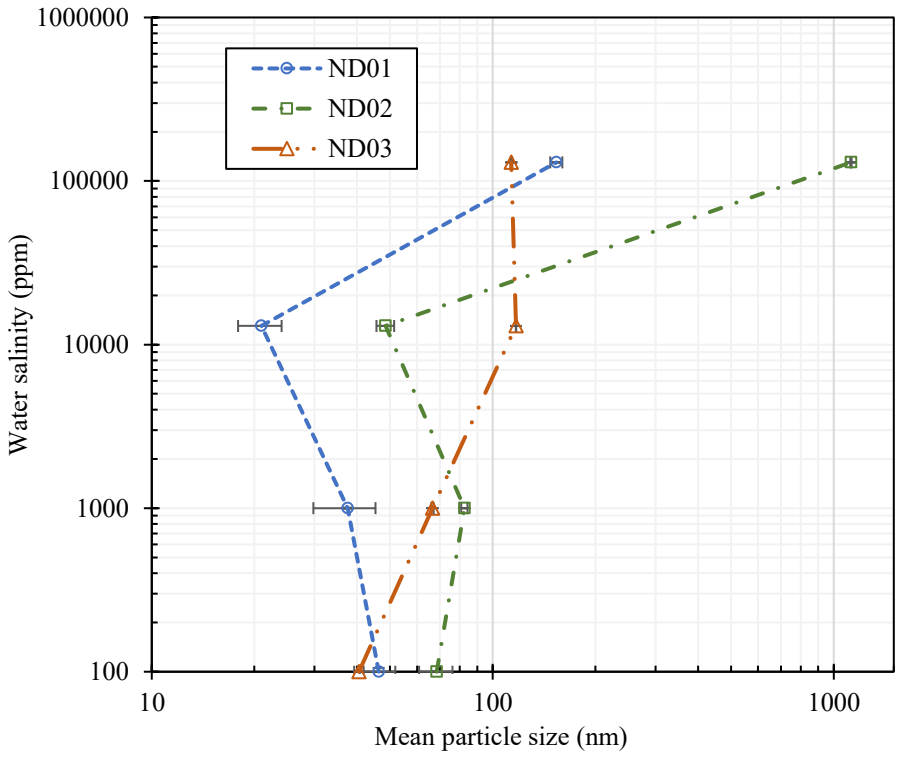

Figure 6.2: Plots of the mean particle size versus water salinity for ND solutions prepared by three CnF additives. CnF-03 forms the smallest particles when the water salinity is low. The particle size follows a general increasing trend by increasing the water salinity. CnF-02+brine forms the largest particles. All the ND solutions form microemulsions except for CnF-02+brine.

6.3 Interfacial Tension (IFT)

We measured IFTs between the oil and the ND solutions with different salinities using Tensiometer KRUSS Spinning Drop instrument with the spinning drop method.

6.3.1 Materials

We mixed CnF-01, CnF-02, and CnF-03 in our salinity range as aqueous phase and reservoir oil as our oleic phase.

6.3.2 Methodology

We measured IFTs between the oil and ND solutions prepared in different salinities using the Spinning drop method. The instrument we used, includes a capillary tube filled with the ND solution, and an end plug filled with the oil sample. The end plug caps the capillary tube, then placed in the tensiometer with the rotational speed of 2000rpm. The shape of the oil droplet was analyzed and IFT between the oil and ND solution was calculated using the Vonnegut equation (Joseph, D.D. 1994):

$$\sigma = \frac{(\rho_1 - \rho_2)\omega^2 R^2}{4} \tag{21}$$

Here, ρ is fluid density, ω is angular spinning velocity, and R is droplet radius. Each test was repeated three times at ambient conditions and the mean values are reported.

6.3.3 Results

All the studied ND solutions decrease the IFT compared with the base cases without CnF additives, and CnF-03 leads to the maximum IFT reduction. **Fig. 6.3** shows IFT values between the oil and the ND solutions in different salinities.

None of the ND solutions show a consistent decreasing or increasing trend of IFT change with salinity. This can be due to the existence of nonionic surfactants which do not create a strong ionic bond with salt ions. IFT values of CnF-02 and CnF-01 are very close for the whole salinity range, which are between 0.306-0.378 mN/m, but CnF-03 has lower values ranging from 0.092 to 0.175 mN/m.

Decreasing IFT by increasing salinity is the result of two phenomena: lowering double layer and salting-out effect. As described by Sayyouh (1994), the IFT will decrease by increasing salinity until a specific salinity, which is called the 'optimal salinity', after that, the IFT increases. In our ND solutions, the optimal salinity can not be observed due to the small salinity range and the non-ionic nature of our surfactants (weak interactions between salt ions and polar groups of the surfactants).

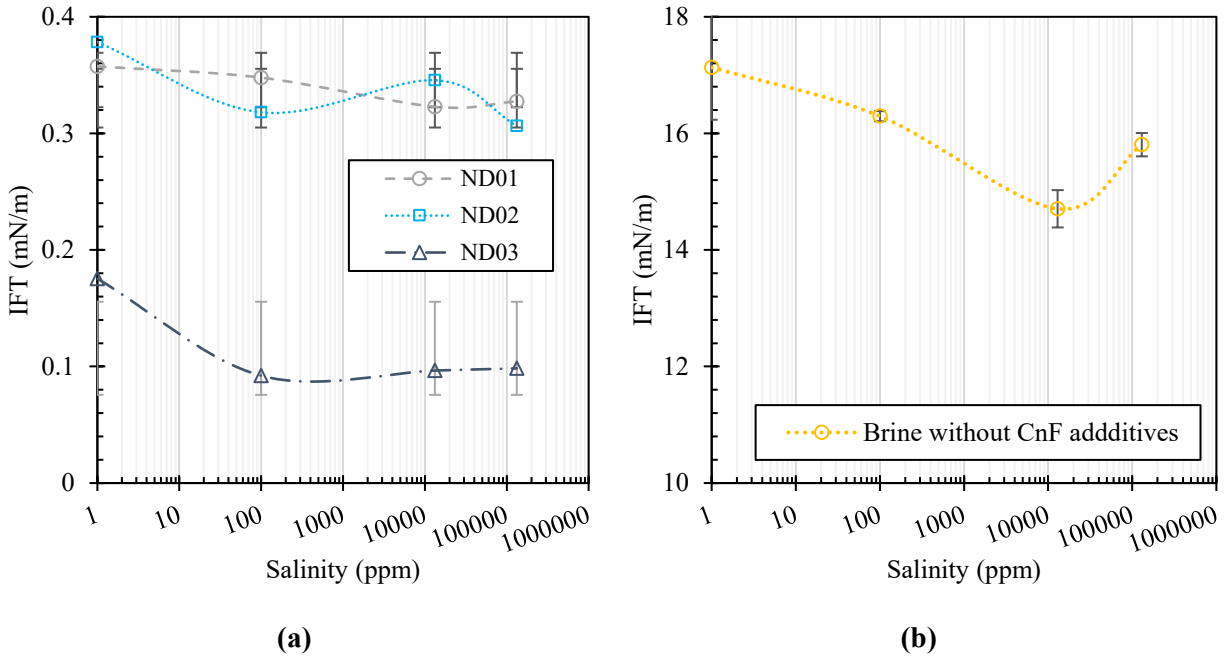

Figure 6.3: (a) IFT change with salinity on IFT for different ND solutions; and (b) IFT values of the brine with different salinities without the presence of CnF additives.

6.4 Stability Test

Microemulsions are composed of immiscible liquids which are thermodynamically stable and visually clear (Majuru and Oyewumi, 2009). The solution is stable if it can stay integrated and phase separation does not occur over time. Van der Waals attraction is the driving force for flocculation of particles, which is proportional to the particle size when the distance between particles is small (Tadros 2015). Therefore, the nano-sized particles, large distances between the particles, and the existence of nonionic surfactants in ND solutions act as stabilizing mechanisms. If the ND solution is not stable, it will lead to Ostwald ripening phenomena leading to the formation of larger droplets (Landfester 2001, Majuru 2009) which may lead to pore-throat blockage. In this part we performed both visual and measuring the stability test.

6.4.1 Visual investigation methodology

6.4.2.1 Materials

We mixed CnF-01, CnF-02, and CnF-03 in different water salinities.

6.4.2.2 Methodology

We added equal volumes of the ND solutions in different vials and after stirring them for 24 hours, left them for 10 days at room temperature. We visualized the ND solutions in different salinities to see if any phase separation occurs.

6.4.2.3 Results

By visualization, as shown in **Fig. 6.4**, most of the ND solutions are translucent in the whole salinity range (0 to 130,000 ppm), except for CnF-01 and CnF-02 in brine (130,000 ppm) which have a cloudy appearance. Comparing these results with the results in **section 6.2**, we can observe that CnF-02 in brine with 130,000 ppm forms relatively larger particles (1123 nm). This particle size value is off the range of the nano-sized category, which is between 10-200 nm. CnF-02 in high-salinity brine is then categorized as emulsions that have droplet sizes larger than 1μm (Tadros, 2015). This can result in instability and finally phase separation of the solution (Friberg, 1992). We can conclude that the cloudy appearance of CnF-02+brine can be a result of phase separation.

For CnF-01+brine with an average particle size of 153.7 nm, the cloudy appearance of the solution cannot be explained by phase separation. Here, we consider that CnF additives adsorb more ions and form larger droplets due to the abundance of ions in brine, which causes its cloudy appearance.

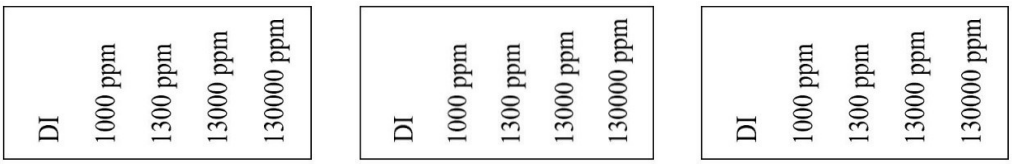

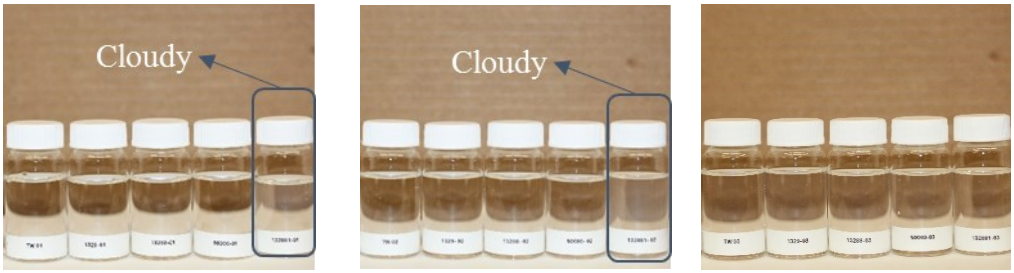

CnF-01 **CnF-02** **CnF-03**

Figure 6.4: The visual appearance of the ND solutions in the studied salinity range, from left to right: DI, TW. 1300 ppm, 13000 ppm, and 130,000 ppm brine. CnF-02 in brine is the cloudiest followed by CnF-01 in brine.

6.4.2 Multiple light scattering (MLS) methodology

We used a Turbiscan instrument to quantify the physical stability of the ND solutions over time (Kang et al. 2011). This instrument works based on the mentioned MLS technique (Mengual et al. 1999; Bru et al. 2004). A unitless Turbiscan Stability Index (TSI) was calculated based on the readings for a solution to quantify its stability (Ren et al. 2018):

$$TSI = \frac{\sum_h |scan_i(h) - scan_{i-1}(h)|}{H} \quad (2)$$

Here, H is the total height of the sample, and $scan_i(h)$ is the reading for height of h at time interval of i. The higher the TSI value, the less stable the sample is. **Table 9** lists the range of TSI defined for evaluating solution stability (Yang et al. 2017).

Table 6.1: TSI range for evaluating ND solutions stability (Yang et al. 2017).

TSI	Meaning
<0.5	No significant variation, not visible, stable
0.5-2.0	Emerging destabilization, not visible
2.0-4.0	Weak destabilization, potentially visible
4.0-10	Significant destabilization, visible
>10	High destabilization, visible

6.4.2.1 Materials

Same as **section 6.4.2.1**.

6.4.2.2 Methodology

We filled a specific vial with 20cc of each ND solution and placed it in the instrument. The light emitted from a light source was transmitted through the sample, and the transmitted light was detected by two optical sensors (180º and 45º from the light source). This instrument works in scanning mode acquiring transmitted light every 40µm along the length of the sample. The measurements were repeated every minute for 30 minutes to dynamically monitor the change in stability of an ND solution. The stability analysis was performed under ambient conditions and repeated three times for each sample. Mean values for each test were reported.

6.4.2.3 Results

Fig.6.5 shows that TSI values for all the ND solutions increase over time, suggesting the formation of larger particles. In these plots, solid lines represent the measured values until the 1500s. Then we extrapolated the lines up to the 3000s, represented by dashed lines in the plots. The increase of TSI is less than 2 for all the cases, indicating good stability of ND solutions over time. Although CnF-01+brine and CnF-02+brine are cloudy as shown in the previous section, their TSI values are less than 2. In general, transparent appearance and low TSIs (<2) for all the ND solutions suggest that large particles in the range of significant destabilization (TSI>4) are not formed over time.

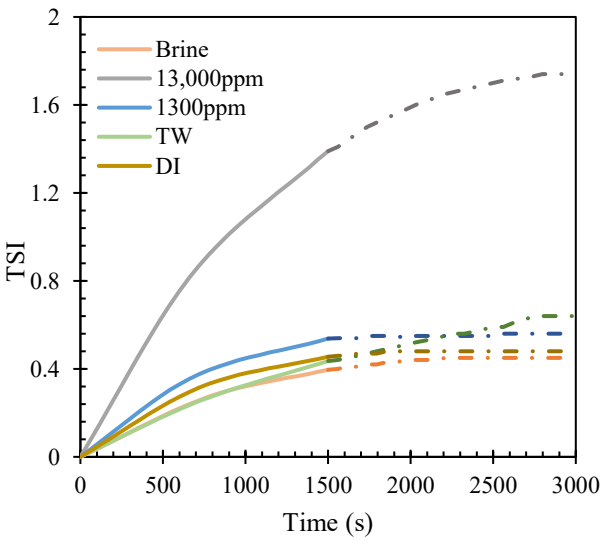

(a)

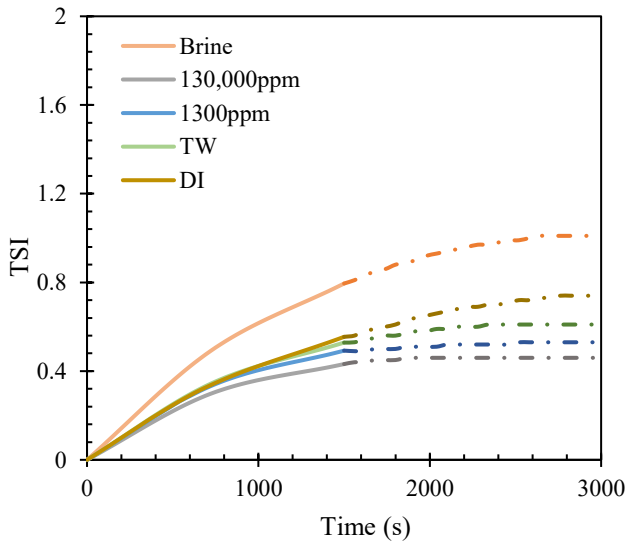

(b)

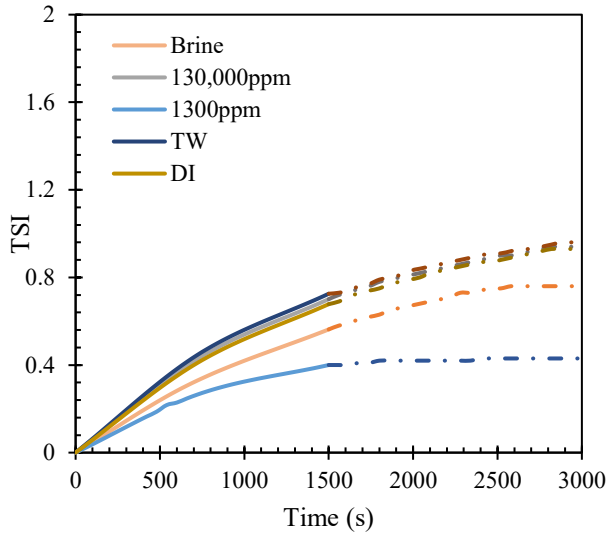

(c)

Figure 6.5: TSI values versus time for the ND solutions prepared with: a) CnF-01, b) CnF-02, c) CnF-03 at different salinities. Lines represent measured values for the 1500s, and dashed lines represent extrapolated values up to the 3000s.

6.5 Solubility (Pipette test)

The goal of this test is to characterize the type of microemulsions formed by mixing the ND solutions (prepared in different salinities) with the oil sample. This can be achieved by determining oil and aqueous phase solubilization parameters using the Pipette Test. The effect of formed microemulsion type on imbibition oil recovery can be investigated.

The oil and ND solutions (with different salinities) were mixed in graduated tubes (by volume ratio of 1:1) by rotating the mixtures for 24 hours at 1 rpm to simulate slow mixing under reservoir conditions. Then, the solution was left at stationary conditions for seven days at ambient temperature and pressure. We determined volumes of oleic and aqueous phases by:

$$V_o = V_{oi} - V_{of} \tag{22}$$

$$V_w = V_{wi} - V_{wf} \tag{23}$$

Here, V_o is the volume of oil solubilized in the microemulsion, V_{oi} is the initial volume of oil in the solution, V_{of} is the volume of the upper oil phase after equilibrium, V_w is the volume of aqueous phase solubilized in the microemulsion, V_{wi} is the initial volume of the aqueous phase in the

solution, V_{wf} is the volume of the lower aqueous phase after equilibrium. Solubilization factors for oil and water were calculated by (Abalkhail et al., 2020):

$$P_o = \frac{V_o}{V_s} \tag{24}$$

$$P_w = \frac{V_w}{V_s} \tag{25}$$

Here, P_o and P_w are oil and water solubilization factors. V_o, V_w, and V_s are oil, water, and surfactant volumes in the microemulsion phase, respectively. All the calculations assumed that all the surfactants present in the microemulsion, and thus V_s is constant. After calculating solubilization parameters and plotting them, the intersection will determine middle phase microemulsion.

Microemulsions are classified by Winsor type definition: Winsor type I occurs when oil is solubilized in water and forms oil-in-water microemulsion. Winsor type II is when water and ND solutions are solubilized in the oil and form a water-in-oil microemulsion. Winsor type III occurs when a third phase with equal volumes of solubilized water and oil forms. The extent of IFT reduction depends on the type of microemulsion formed by mixing the ND solutions with oil and water. In general, bi-continuous or Winsor III microemulsion leads to more IFT reduction compared with types I and II (Winsor 1954; Chen et al. 2018, Salager et al. 1979, Wade et al. 1978). Oil/water solubility in ND solutions depends on the brine salinity, the type of brine ions, and formulation of the surfactant and/or cosurfactant (Bera and Mandal, 2015).

6.5.1 Materials

Reservoir oil as oleic phase. We mixed CnF-01, CnF-02, and CnF-03 in twoe sets of salinities: high salinity brine, and TW.

6.5.2 Methodology

We added equal volumes of the ND solutions in different vials and after stirring them for 24 hours, left them for 10 days at room temperature. We visualized the ND solutions in different salinities to see if any phase separation occurs.

6.5.3 Results

Fig.6.6 shows the mixtures of oil and CnF-03, before and after mixing them at 1 rpm for 24 hours. The ND solution prepared in DI changes from colorless to faint yellowish, suggesting the dissolution of oil components into the aqueous phase. **Fig.6.7** shows the calculated water and oil solubilization ratios for all the mixtures versus salinity for a three-phase system consisting of oil, brine, and ND solutions. The calculation results can be used to classify the microemulsions (Winsor type) and determine the optimum salinities. The details of the calculation method are described in the methodology section. It should be noted that the exact volume of oil could not be determined for solutions prepared in DI since oil droplets were trapped in the narrower part of the graduated tube.

Based on **Fig.6.7,** in general, as salinity increases oil solubility (V_o/V_s) increases, while water solubility (V_w/V_s) decreases. At low salinities, most of the ND remains in the aqueous phase. However, as the salinity increases, ND particles move toward the oil-water interface and finally into the oil phase (Pal et al., 2019). There is a point where the water and oil solubility curves cross each other, indicating the conditions for the formation of middle-phase or Winsor type III microemulsion (Bera et al., 2011). This point occurs at a salinity referred to as “optimal salinity” leading to the lowest IFT value. As we get closer to this point, the volume of the aqueous phase and oil phase in the middle phase increase. The optimal salinity for CnF-01, CnF-02, and CnF-03 are at 13800, 2500, and 1380ppm, respectively. CnF-03+TW is the closest to optimal salinity, and CnF-01+TW is the furthest.

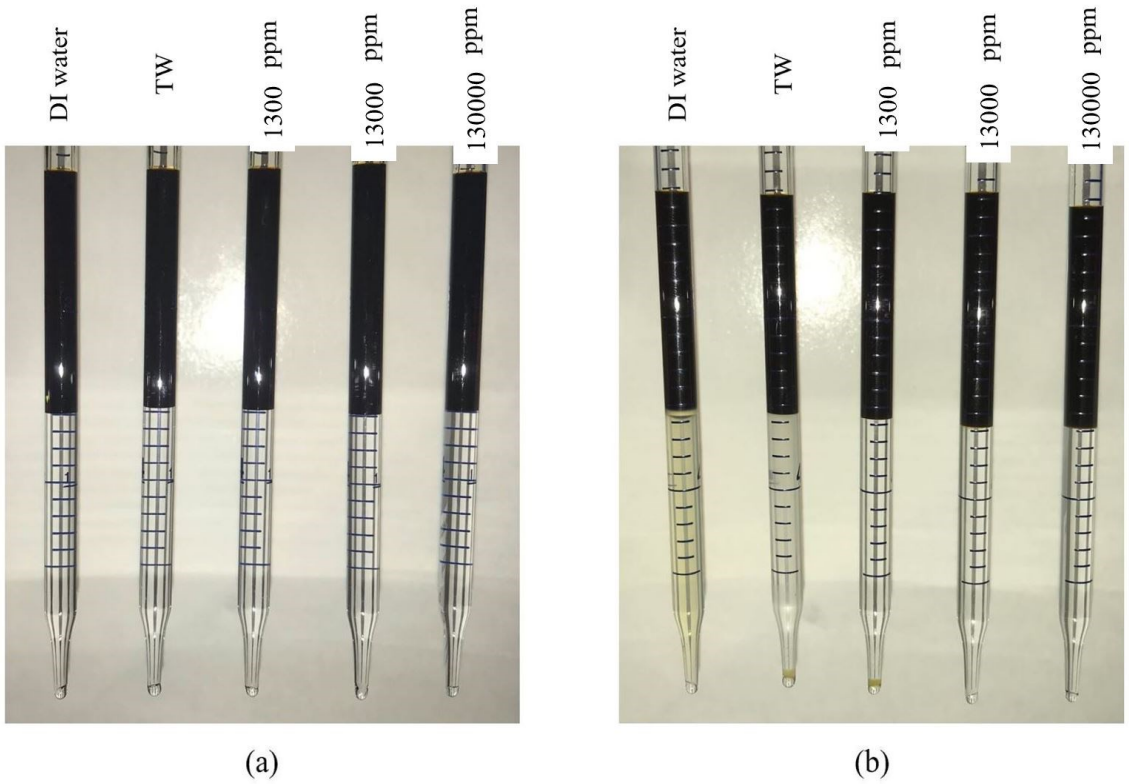

Figure 6.6: Pipette tests for CnF-03 with different salinities from left to right in both pictures: DI, TW, 1300 ppm, 13000 ppm, and brine a) before rotation, b) after rotation and equilibrium. The color of the aqueous phase is changed due to the solubilization of oil in water.

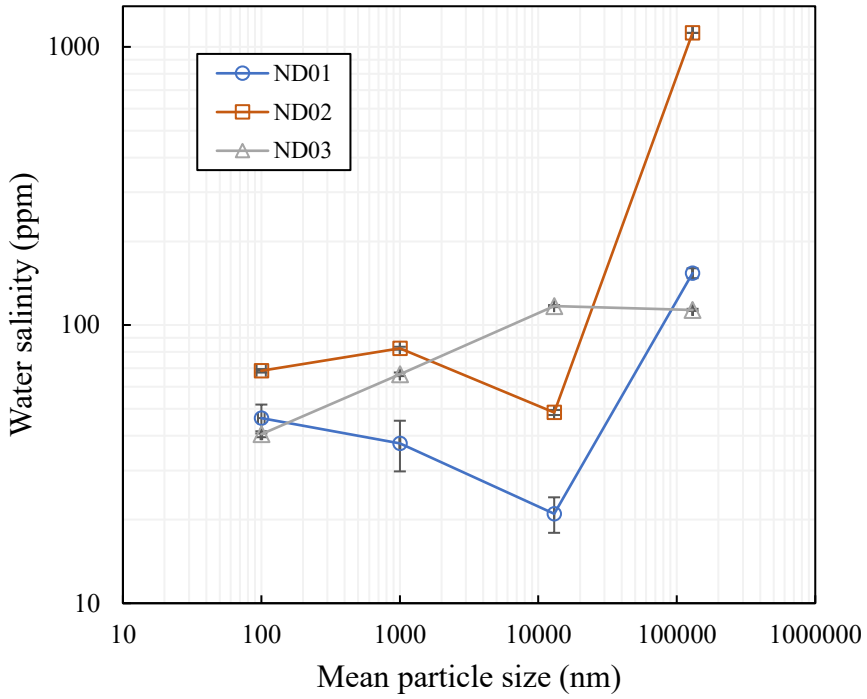

Figure 6.7: Water/oil solubility of the ND solutions at different salinities. Subscripts W and O mean oil and water solubilization ratio respectively. CnF-03+TW forms middle phase microemulsion. For DI, some oil was trapped in the aqueous phase and the exact volume of oil could not be determined leading to overestimation of the oil solubility.

6.6 Discussions

Capillary pressure calculation based on measured IFT and CA. Based on the conventional theories, P_c is the most important parameter affecting imbibition oil recovery. The ND solutions prepared by CnF-01 and CnF-02 have very close IFT values (CnF-01=0.347mN/m, CnF-02=0.318mN/m) in low salinity water, but their oil recoveries are significantly different. The liquid-liquid CA results show that CnF-03+TW does not change CA significantly while CnF-01+TW and CnF-02+TW change CA to less than 90° and leads to more water-wet conditions. Although CnF-03 does not alter the rock wettability as significantly as CnF-01 and CnF-02, it gives the highest imbibition oil recovery. Therefore, to explain the imbibition oil recovery results properly, we used the measured IFT and CA results to calculate and compare the P_c of different cases during the imbibition process.

We used the IFT results from and liquid-liquid CA measurements from **section 5.3** to do a rough estimation of P_c during the imbibition process for different ND solutions in TW and TW without

any CnF additives. Three core plugs that we used for liquid-liquid CA are MT5-B, MT6-B, and MT7-B. These core plugs are taken from the deep section of the same well and their pore radius is in the same range. Here we assume an average pore radius value of 90 nm to calculate P_c.

Table 7.1 lists the calculated P_c values during the counter-current imbibition process for ND solutions in TW. Negative P_c hinders the soaking fluid entering oil-saturated rock while positive P_c promotes the suction of soaking fluid into the rock (Sharma and Mohanty, 2013). Here we observe that TW without CnF additives has a negative P_c value, explaining the lower imbibition oil recovery of TW compared with ND solutions. By adding CnF additives into TW, P_c increases and leads to higher suction of water into rock. Comparing the effects of different CnF additives, we found CnF-01+TW and CnF-02+TW gave positive values of P_c, explaining their high imbibition oil recovery. However, CnF-3+TW with P_c close to zero gives the maximum oil recovery. Therefore, the P_c model cannot fully explain the observed oil recovery values. In addition to wettability alteration and IFT reduction, there are other parameters affecting oil recovery.

Table 6.2: Rough Pc values of the ND solutions.

	TW	**CnF-01+TW**	**CnF-02+TW**	**CnF-03+TW**
IFT (mN/m)	16.295	0.348	0.318	0.0921
CA (degree)	150.5	80.6	68.3	108
P_c (psi)	-0.3151	0.0013	0.0026	-0.0006

Effects of oil/water solubilization on imbibition oil recovery. The solubility results (**section 6.1.5**) are used to determine optimal salinity for the formation of a middle-phase microemulsion. The optimal salinity for CnF-01, CnF-02, and CnF-03 are 13800, 2500, and 1380 ppm respectively. When we use ND solutions in TW to conduct imbibition oil recovery tests, the salinity is at 100 ppm. CnF-03+TW, which gives the highest oil recovery, is the closest to its optimal salinity. While CnF-01+TW, which has the lowest oil recovery, is the furthest from its optimal salinity. Therefore, the ND solution will have a higher imbibition oil recovery when its salinity is closer to the optimal salinity to form a middle-phase microemulsion. Here, we can conclude that solubilization is an important factor affecting imbibition oil recovery. The formation of middle-phase (or near middle-phase) microemulsion is favorable to increase oil recovery.

Chapter 7: Understanding Intermolecular Interactions in Water-Oil-Rock System

7.1 Zeta Potential Measurement

Here, we present the results of zeta potential measurements of rock powders and oil emulsions in ND solutions. The disjoining pressure of the rock-fluid-fluid system is calculated in the next section to investigate the effect of intermolecular interactions on wettability and oil recovery when using different ND solutions.

7.1.1 Materials

We mixed CnF-01, CnF-02, and CnF-03 in TW for our ND solutions. MT rock powder for rock sample, reservoir oil for our oleic phase.

7.1.2 Methodology

We used a Malvern Zetasizer Nano ZS to measure the zeta potential of rock-ND solutions and ND solutions-oil pairs. Measured zeta potential values are used to calculate reduced surface potential parameter which is needed to calculate F_{DL}. To measure the zeta potential value, the following steps were followed:

1) Crushed a rock sample to prepare rock powder with a mean size of less than 2 μm;

2) Mixed the rock powder with the ND solution prepared in different salinities for five minutes by a vortex mixer to ensure the formation of a stable suspension.

3) Mixed 2 cc of oil in 10 cc of the ND solution to prepare oil in water emulsion by a vortex mixer for five minutes.

4) Mixed rock powders with the water to prepare rock powder-water suspension with 0.03 wt% concentration for zeta potential using the Malvern Zetasizer machine.

7.1.3 Results

The zeta-potential value defines the degree of electrostatic repulsion between particles in a solution and it is a good indicator of colloidal solution stability (Hanaor et al., 2012). A high absolute value

of zeta potential means that the repulsive forces between particles dominate, and these particles will not agglomerate. The measured zeta potentials for TW-oil and TW-rock pairs with and without CnF additives are presented in **Table 6.1.** The measured zeta potentials for rock-ND and oil-ND pairs show moderate stability, meaning that the ND particles will not agglomerate (Bassioni and Taqvi 2015). The zeta-potential values for TW-rock and TW-oil pairs are -48.20 and 15.70 mV respectively. The higher values of zeta-potentials for TW-oil and TW-rock pairs are due to the interaction of ionic groups (H^+ and OH^- of water) present in the aqueous phase with the surface of the rock/oil phase (Sis et al. 2009). The addition of CnF additives in TW decreases the absolute values of zeta-potential for TW-rock and TW-oil pairs. This is due to the strong adsorption of the hydrophobic parts of the surfactants in the ND solutions (nonionic surfactants) on the hydrophobic surface of the oil/rock surface. Therefore, their zeta-potential is lower than that of TW without any ND (Geng et al. 2017). The change in the zeta-potential by surfactants can be used to predict the stability of the particles (oil droplets in our study), and morphology of the surface (Sis et al. 2009). Oil-CnF-03 has the highest value (-32 mV). This can be interpreted as CnF-03 can maintain higher negative charges around the oil droplets so it can solubilize a higher volume of oil in it (Malhotra et al. 2004). After CnF-03, CnF-02 and CnF-01 have the highest values of zeta-potential, respectively.

Table 7.1: Measured zeta potentials for TW-rock and TW-oil pairs with and without CnF additives.

	ND sample	Zeta potential (mV)
Rock-Aqueous phase	CnF-01+TW	-11.10
	CnF-02+TW	-10.53
	CnF-03+TW	-15.57
	TW	-15.70
Oil-Aqueous phase	CnF-01+TW	-29.73
	CnF-02+TW	-30.57
	CnF-03+TW	-32.00
	TW	-48.20

7.2 Disjoining Pressure Calculations

7.2.1 Materials

We measured zeta potential in **section 7.1**. the materials are mentioned in the **section 7.1.1**.

7.2.2 Methodology

Here, we calculated disjoining pressure to understand the intermolecular interactions of a rock-fluid-fluid system and to explain the enhanced imbibition oil recovery of ND solutions. The rock-fluid-fluid system is defined as nano-size particles (micelles), which form a spontaneous structural layering (stratification) in a restricted film between the oil phase and the solid surface (Habibi and Dehghanpour, 2018). The force which is needed to conquer the attraction between this film and the rock surface is defined as disjoining pressure, and it affects the equilibrium CA (Hirasaki and G. J., 1991). The condition where F_{VDW} between oil and the rock surface dominates, the water film will become unstable, and oil will rupture the water film and attach to the rock surface.

In the considered rock-water-oil system, water exists between oil and rock. h is the thickness of the water layer between oil and rock. P_t is the disjoining pressure between rock and oil layer. $P_t>0$ indicate presence of a very stable water film on the rock surface and $P_t<0$ indicate an unstable water film.

7.2.3 Results

In **Fig.6.8,** we plotted disjoining pressure (P_t) versus distance (h_w). When $h_w<0.5$nm, we have very strong repulsive structural forces between oil and rock surface, indicate that water layer completely coats the rock surface. At $h_w=0.5$nm, we have a minimum P_t ($P_{t\text{-}min}$), indicating that attractive forces between oil and rock surfaces become dominant. The attraction between rock and oil leads to an unstable water film and oil can replace the water film. The disjoining pressure for the CnF-02 solution has the lowest value indicating that oil can replace the water film easier than that for the other two CnF additives. When $h_w>0.5$nm, repulsive forces increase, and the attraction between water film and rock surface increases, indicating that with increasing h_w, the water film becomes more stable (Habibi and Dehghanpour 2018, Yuan et al. 2021).

Disjoining pressure can be discussed from spontaneous imbibition point of view. From **Fig.6.8**, CnF-03 with the lowest disjoining pressure is expected to have the lowest oil film stability, leading to more water imbibition and a higher oil recovery rate. Since zeta potentials between brine-oil and brine-rock were very low, they could not be measured.

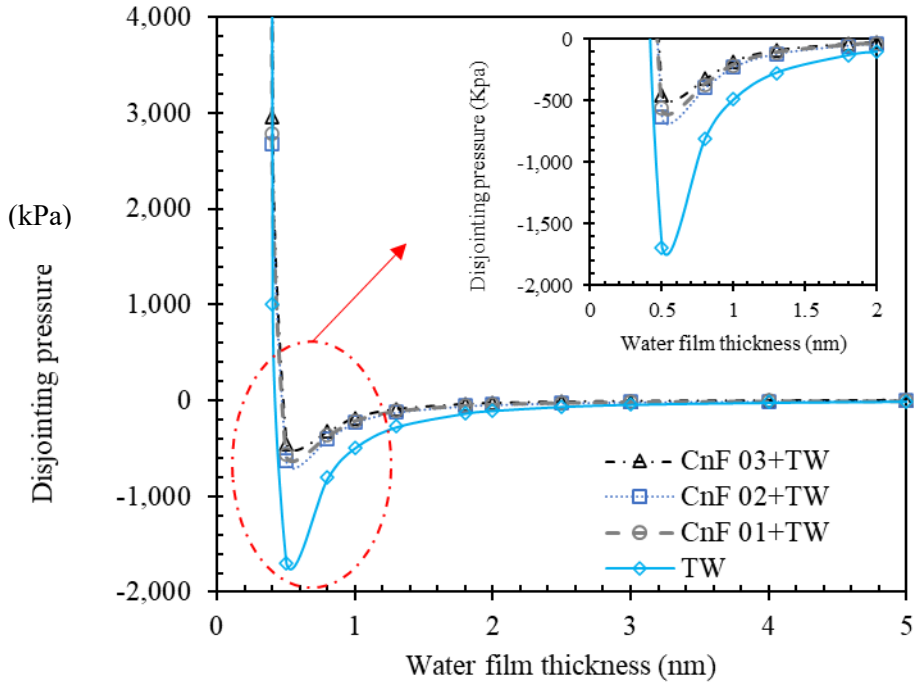

Figure 7.1: Plot of disjoining pressure versus distance, showing that CnF-03+TW has the highest disjoining pressure among the ND solutions.

7.3 Discussions

Effect of zeta potential on imbibition oil recovery. Zeta-potential measurements for the oil-ND and rock-ND pairs, and the results of **section 6.1.6** indicate that the sequence of absolute values for the oil-ND pairs matches with the sequence of the oil recovery results. These results also match with solubility results from **section 6.1.5**.

Three consecutive stages happen in the dispersion of oleic phase into aqueous phase: 1) passing of the oleic droplets into the aqueous phase and becoming wet, 2) breaking the oleic droplets by stirring (mechanical force), and 3) stabilization of small oil droplets by the aid of surfactants. According to a study performed by Sis et al. 2009, nonionic surfactants act better in dispersion and stabilization of the oleic phase. Their results also reveal that in the absence of surfactant, the size of the dispersed phase droplets does not reduce enough, due to their strong hydrophobicity. This overcomes the high net negative charge around the particles, measured by zeta potential. This can be related to the ability of CnF additives with their ability to solubilize oil. Malhotra et al. (2004) studied the effects of surfactants on the solubility and zeta potential of the proteins. They concluded that insolubility of the protein molecules is related to charge insufficiency around the particles.

This will result in rapid aggregation of the particles and finally their sedimentation. According to Hayakawa et al. 1985, an important factor affecting solubility manifests as a function of pH. Due to difficulties in comparing the charge effect as a function of pH, it is more functional to use zeta potential as a variable. In their work, protein which is an insoluble molecule showed the maximum insolubility when zeta potential reached zero.

In our results, we can conclude that a higher absolute value of zeta potentials in ND solutions will cause higher stability and solubility of oil-ND solutions which can lead to higher oil recovery.

Effect of disjoining pressure on imbibition oil recovery. **Fig.6.7** shows that $P_{t\text{-}min}$ for TW case is the lowest, indicating the relatively stronger repulsive forces for the rock-TW-oil system. When adding CnF additives in TW, $P_{t\text{-}min}$ for the system increases, suggesting less attractive forces between oil and rock across the ND film. Therefore, the ND film becomes more stable on the rock surface compared to the TW film in the absence of CnF additives. The results suggest that the addition of the CnF additives can reduce the attractive forces between rock and oil, increasing the water film stability. This is consistent with our imbibition oil recovery results that show higher oil recovery by CnF03+TW. Comparing different CnF additives, the profile for CnF-03+TW gives the highest $P_{t\text{-}min}$, indicating the most stable water film. CnF-01 and CnF-02 have less stable water films on the rock surface compared with CnF-03. The relatively more stable water film for the CnF-03+TW case is favorable for water imbibition and results in higher oil recovery, which is supported by our imbibition oil recovery results. However, the sequence of CnF-02 and CnF-01 in **Fig.6.7** does not support our oil recovery results.

Chapter 8: Discussions, Conclusions, and Future studies

8.1 Key Findings

In this study, we developed and applied a systematic laboratory protocol to study the parameters affecting the performance of complex nanofluid additives on imbibition oil recovery from tight rocks. In addition to wettability alteration and IFT reduction by surfactant solutions, the effects of other factors such as solubility, viscosity, salinity, and disjoining pressure on imbibition oil recovery using surfactant solutions are also investigated. Here is the summary of our conclusions:

- IFT reduction and wettability alteration cannot fully explain the enhanced imbibition oil recovery by ND solutions, other parameters including particle size, solubility, microemulsion type, and osmosis potential should be considered for evaluating the performance of the ND solutions to enhance imbibition oil recovery.
- Based on the spontaneous imbibition oil-recovery results, increasing salinity reduces oil recovery by the ND solutions. Increasing salinity decreases the osmotic effect (due to the presence of precipitated salts in the pores) and increases viscosity and the average particle size of the ND solutions. In some cases, the ND solutions become unstable and form a cloudy solution at high salinities.
- Oil/water solubilization ratio (described by Winsor type) is one important parameter to predict imbibition oil recovery by ND solutions. By increasing salinity, oil solubility in microemulsion increases, while water solubility in microemulsion decreases. The point where water solubility is equal to oil solubility represents the formation of middle-phase or Winsor type III microemulsion. At this salinity, the oil-water IFT reaches the lowest value. As the generated microemulsion type gets closer to Winsor type III, the oil recovery increases.
- Absolute value of zeta potential for the oil-ND pairs can be an indicator of stability and solubility, and thus, it can be used as a confirmation of the solubility tests.
- Adding CnF additives to water increases the disjoining pressure between the rock surface and the aqueous phase. This leads to a more stable aqueous film between rock and oil and alters the wettability of the rock surface towards more water-wet conditions, leading to higher imbibition oil recovery.

8.2 Future studies

In future studies, we should analyze the brine in the Amott cell at the end of the imbibition oil recovery test for salinity and CnF concentration. Comparing before and after amounts of CnF concentration and salinity give us a better view of CnF adsorption in the rock and the role of osmosis mechanism in the oil recovery.

In the PSD part, each CnF with different salinities can be simulated with software to compare the penetration of brine and TW then, use these results to find a relation with salinity effect of oil recovery results.

In the IFT test and zeta-potential, we need to let the oil-ND solution mixture reach to an equilibrium for at least one week and then investigate their effect.

References

Anganaei, H., Pourabdollah, K., & Rostami, A. (2014). Experimental improvement of nano-enhanced oil recovery using nano-emulsions. Arabian Journal for Science and Engineering, 39(8), 6453-6461.

Aveyard, R., Binks, B. P., & Clint, J. H. (2003). Emulsions stabilised solely by colloidal particles. Advances in Colloid and Interface Science, 100, 503-546.

Ayirala, S., Boqmi, A., Alghamdi, A., & AlSofi, A. (2019, April). Dilute surfactants for wettability alteration and enhanced oil recovery in carbonates. In IOR 2019–20th European Symposium on Improved Oil Recovery (Vol. 2019, No. 1, pp. 1-15). European Association of Geoscientists & Engineers.

Barriol, J. P., Coste, J. F., & Grangette, H. (1981). U.S. Patent No. 4,252,657. Washington, DC: U.S. Patent and Trademark Office.

Bera, A., Mandal, A., & Guha, B. B. (2013). Synergistic effect of surfactant and salt mixture on interfacial tension reduction between crude oil and water in enhanced oil recovery. *Journal of Chemical & Engineering Data*, *59*(1), 89-96.

Bera, A., Ojha, K., Mandal, A., & Kumar, T. (2011). Interfacial tension and phase behavior of surfactant-brine–oil system. *Colloids and surfaces a: physicochemical and engineering aspects*, *383*(1-3), 114-119.

Bera, A., Kumar, T., Ojha, K., & Mandal, A. (2014). Screening of microemulsion properties for application in enhanced oil recovery. Fuel, 121, 198-207.

Berne, B. J., & Pecora, R. (2000). *Dynamic light scattering: with applications to chemistry, biology, and physics*. Courier Corporation.

Binazadeh, M., Xu, M., Zolfaghari, A., & Dehghanpour, H. (2016). Effect of electrostatic interactions on water uptake of gas shales: the interplay of solution ionic strength and electrostatic double layer. *Energy & Fuels*, *30*(2), 992-1001.

Boles, M. A., Engel, M., & Talapin, D. V. (2016). Self-assembly of colloidal nanocrystals: From intricate structures to functional materials. *Chemical reviews*, *116*(18), 11220-11289.

Bru, P., Brunel, L., Buron, H., Cayré, I., Ducarre, X., Fraux, A., Mengual, O., Meunier, G., de Sainte Marie, A. and Snabre, P., 2004. Particle size and rapid stability analyses of concentrated dispersions: use of multiple light scattering technique.

Bui, K., Akkutlu, I. Y., Zelenev, A., Saboowala, H., Gillis, J. R., & Silas, J. A. (2016). Insights into mobilization of shale oil by use of microemulsion. *SPE Journal*, *21*(02), 613-620.

Bui, K., Akkutlu, I. Y., Zelenev, A. S., Hill, W. A., Griman, C., Boudreaux, T. C., & Silas, J. A. (2019). Microemulsion Effects on Oil Recovery From Kerogen Using Molecular-Dynamics Simulation. *SPE Journal*.

Burke, L. H., Nevison, G. W., & Peters, W. E. (2011, January). Improved Unconventional Gas Recovery With Energized Fracturing Fluids: Montney Example. In *SPE Eastern Regional Meeting*. Society of Petroleum Engineers.

Cash, L., Cayias, J. L., Fournier, G., Macallister, D., Schares, T., Schechter, R., & Wade, W. H. (1977). The application of low interfacial tension scaling rules to binary hydrocarbon mixtures. Journal of Colloid and Interface Science, 59(1), 39-44.

Chai, J. L., Zhao, J. R., Gao, Y. H., Yang, X. D., & Wu, C. J. (2007). Studies on the phase behavior of the microemulsions formed by sodium dodecyl sulfonate, sodium dodecyl sulfate and sodium dodecyl benzene sulfonate with a novel fishlike phase diagram. Colloids and Surfaces A: Physicochemical and Engineering Aspects, 302(1-3), 31-35.

Chen, Z., Han, X., Kurnia, I., Yu, J., Zhang, G., & Li, L. (2018). Adoption of phase behavior tests and negative salinity gradient concept to optimize Daqing oilfield alkaline-surfactant-polymer flooding. *Fuel*, *232*, 71-80.

Chiang, J. C., Sanyal, S. K., Castanier, L. M., Brigham, W. E., & Shah, D. O. (1980). Foam as an agent to reduce gravity override effect during gas injection in oil reservoirs. Final report (No. DOE/ET/12056-T1). Stanford Univ., CA (USA). Petroleum Research Inst..

Cid, A. (2018). Synthesis of NPs by microemulsion method. In *Microemulsion-a Chemical Nanoreactor*. IntechOpen.

Davies, G. R., Moslow, T. F., & Sherwin, M. D. (1997). The lower Triassic Montney formation, west-central Alberta. Bulletin of Canadian Petroleum Geology, 45(4), 474-505.

Deglint, H. J., Ghanizadeh, A., DeBuhr, C., Clarkson, C. R., & Wood, J. M. (2017, September). Comparison of Micro-and Macro-Wettability Measurements for Unconventional Reservoirs: The Devil is in the Detail. In *Unconventional Resources Technology Conference, Austin, Texas, 24-26 July 2017* (pp. 2544-2552). Society of Exploration Geophysicists, American Association of Petroleum Geologists, Society of Petroleum Engineers.

Dehghanpour, H., Lan, Q., Saeed, Y., Fei, H., & Qi, Z. (2013). Spontaneous imbibition of brine and oil in gas shales: Effect of water adsorption and resulting microfractures. *Energy & Fuels*, *27*(6), 3039-3049.

Derjaguin, B. V. (1989). Theory of stability of colloids and thin films (pp. 30-30). New York: Consultants Bureau.

Esfandyari, H., Shadizadeh, S. R., Esmaeilzadeh, F., & Davarpanah, A. (2020). Implications of anionic and natural surfactants to measure wettability alteration in EOR processes. Fuel, 278, 118392.

Fakcharoenphol, P., Kurtoglu, B., Kazemi, H., Charoenwongsa, S., & Wu, Y. S. (2014, April). The effect of osmotic pressure on improve oil recovery from fractured shale formations. In *SPE unconventional resources conference*. Society of Petroleum Engineers.

Gaikwad, V. L., Choudhari, P. B., Bhatia, N. M., & Bhatia, M. S. (2019). Characterization of pharmaceutical nanocarriers: in vitro and in vivo studies. In *Nanomaterials for drug delivery and therapy* (pp. 33-58). William Andrew Publishing.

Gerbacia, W., & Rosano, H. L. (1973). Microemulsions: formation and stabilization. *Journal of Colloid and Interface Science*, *44*(2), 242-248.

Ghanbari, E., & Dehghanpour, H. (2016). The fate of fracturing water: A field and simulation study. *Fuel*, *163*, 282-294.

Ghanizadeh, A., Clarkson, C. R., Song, C., Vahedian, A., DeBuhr, C., Deglint, H. J., & Wood, J. M. (2018, September). Controls on liquid hydrocarbon permeability of tight oil and liquid-rich gas reservoirs: Examples from Bakken and Montney formations (Canada). In *Unconventional Resources Technology Conference, Houston, Texas, 23-25 July 2018* (pp. 3316-3341). Society of Exploration Geophysicists, American Association of Petroleum Geologists, Society of Petroleum Engineers.

Gruener, S., Hermes, H. E., Schillinger, B., Egelhaaf, S. U., & Huber, P. (2016). Capillary rise dynamics of liquid hydrocarbons in mesoporous silica as explored by gravimetry, optical and neutron imaging: Nano-rheology and determination of pore size distributions from the shape of imbibition fronts. *Colloids and Surfaces A: Physicochemical and Engineering Aspects*, *496*, 13-27.

Habibi, A., & Dehghanpour, H. (2018). Wetting behavior of tight rocks: From core scale to pore scale. *Water Resources Research*, *54*(11), 9162-9186.

Habibi, A., Dehghanpour, H., Binazadeh, M., Bryan, D., & Uswak, G. (2016). Advances in understanding wettability of tight oil formations: a Montney case study. SPE Reservoir Evaluation & Engineering, 19(04), 583-603.

Habibi, A., Yassin, M. R., Dehghanpour, H., & Bryan, D. (2017). Experimental investigation of CO2-oil interactions in tight rocks: A Montney case study. *Fuel*, *203*, 853-867.

Habibi, A., & Dehghanpour, H. (2018). Wetting Behavior of Tight Rocks: From Core Scale to Pore Scale. *Water Resources Research*, *54*(11), 9162-9186.

Hayes, M. E., Bourrel, M., El-Emary, M. M., Schechter, R. S., & Wade, W. H. (1979). Interfacial tension and behavior of nonionic surfactants. *Society of Petroleum Engineers Journal*, *19*(06), 349-356.

Huh, C. (1979). Interfacial tensions and solubilizing ability of a microemulsion phase that coexists with oil and brine. *Journal of Colloid and Interface Science*, *71*(2), 408-426.

Javaheri, A., Dehghanpour, H., & Wood, J. (2017, February). Imbibition oil recovery from tight rocks with dual-wettability pore-network a Montney case study. In SPE Unconventional Resources Conference. Society of Petroleum Engineers.

Jiang, R., Li, K., & Horne, R. (2017, October). A mechanism study of wettability and interfacial tension for EOR using silica nanoparticles. In SPE Annual Technical Conference and Exhibition. OnePetro.

Johnson, R. E. (1969). Wettability Contact Angles. *Surface Colloid Sci.*, *2*, 85-153.

Joseph, D. D. (1994). Evolution of a liquid drop in a spinning drop tensiometer. *Journal of Colloid and Interface Science*, *162*, 331-339.

Kang, W., Xu, B., Wang, Y., Li, Y., Shan, X., An, F., & Liu, J. (2011). Stability mechanism of W/O crude oil emulsion stabilized by polymer and surfactant. *Colloids and surfaces A: Physicochemical and engineering aspects*, *384*(1-3), 555-560.

Kathel, P., & Mohanty, K. K. (2013). Wettability alteration in a tight oil reservoir. *Energy & Fuels*, 27(11), 6460-6468.

Kazemzadeh, Y., Eshraghi, S. E., Sourani, S., & Reyhani, M. (2015). An interface-analyzing technique to evaluate the heavy oil swelling in presence of nickel oxide nanoparticles. Journal of Molecular Liquids, 211, 553-559.

Keneti, S. A. R., & Wong, R. C. K. (2011, January). Investigation of bimodularity in the Montney shale using the Brazilian test. In *45th US Rock Mechanics/Geomechanics Symposium*. American Rock Mechanics Association.

Kumar, S., & Mandal, A. (2016). Studies on interfacial behavior and wettability change phenomena by ionic and nonionic surfactants in presence of alkalis and salt for enhanced oil recovery. *Applied Surface Science*, *372*, 42-51.

Labani, M. M., Rezaee, R., Saeedi, A., & Al Hinai, A. (2013). Evaluation of pore size spectrum of gas shale reservoirs using low pressure nitrogen adsorption, gas expansion and mercury

porosimetry: A case study from the Perth and Canning Basins, Western Australia. *Journal of Petroleum Science and Engineering*, *112*, 7-16.

Lan, Q., Xu, M., Dehghanpour, H., & Wood, J. (2014, October). Advances in understanding wettability of tight and shale gas formations. In *SPE Annual Technical Conference and Exhibition*. OnePetro.

Lan, Q., Dehghanpour, H., Wood, J., & Sanei, H. (2015). Wettability of the Montney tight gas formation. *SPE Reservoir Evaluation & Engineering*, *18*(03), 417-431.

Landfester, K. (2001). The generation of nanoparticles in miniemulsions. Advanced Materials, 13(10), 765-768.

Langford, A., Bruchsaler, M., & Gupta, M. (2022). Suspension properties and characterization of aluminum-adjuvanted vaccines. In *Practical Aspects of Vaccine Development* (pp. 225-266). Academic Press.

Li, Y., He, X., Cao, X., Zhao, G., Tian, X., & Cui, X. (2007). Molecular behavior and synergistic effects between sodium dodecylbenzene sulfonate and Triton X-100 at oil/water interface. *Journal of colloid and interface science*, *307*(1), 215-220.

Li, X., Abass, H., Teklu, T. W., & Cui, Q. (2016, September). A shale matrix imbibition model–interplay between capillary pressure and osmotic pressure. In *SPE annual technical conference and exhibition*. Society of Petroleum Engineers.

Longoria, R. A., Liang, T., Huynh, U. T., Nguyen, Q. P., & DiCarlo, D. A. (2017). Water blocks in tight formations: the role of matrix/fracture interaction in hydrocarbon-permeability reduction and its implications in the use of enhanced oil recovery techniques. *SPE Journal*, *22*(05), 1-393.

Majuru, S., & Oyewumi, M. O. (2009). Nanotechnology in drug development and life cycle management. In Nanotechnology in drug delivery (pp. 597-619). Springer, New York, NY.

Makhanov, K., Habibi, A., Dehghanpour, H., & Kuru, E. (2014). Liquid uptake of gas shales: A workflow to estimate water loss during shut-in periods after fracturing operations. *Journal of Unconventional Oil and Gas Resources*, *7*, 22-32.

Manrique, E. J., Thomas, C. P., Ravikiran, R., Izadi Kamouei, M., Lantz, M., Romero, J. L., & Alvarado, V. (2010, January). EOR: current status and opportunities. In *SPE improved oil recovery symposium*. Society of Petroleum Engineers.

Mengual, O., Meunier, G., Cayre, I., Puech, K., & Snabre, P. (1999). Characterisation of instability of concentrated dispersions by a new optical analyser: the TURBISCAN MA 1000. *Colloids and Surfaces A: Physicochemical and Engineering Aspects*, *152*(1-2), 111-123.

Miller, C. A., Hwan, R. N., Benton, W. J., & Fort Jr, T. (1977). Ultralow interfacial tensions and their relation to phase separation in micellar solutions. Journal of Colloid and Interface Science, 61(3), 554-568.

Mittal, K. L. (2012). Micellization*, solubilization, and microemulsions* (Vol. 2). Springer Science & Business Media.

Montgomery, C. (2013, May). Fracturing fluids. In *ISRM International Conference for Effective and Sustainable Hydraulic Fracturing*. International Society for Rock Mechanics and Rock Engineering.

Myers, D. (2005). Surfactant science and technology. John Wiley & Sons.

NEB, A., OGC, B., & MNGD, B. (2013). The Ultimate Potential for Unconventional Petroleum from the Montney Formation of British Columbia and Alberta. *Energy Briefing Note*.

Nikolov, A., Kondiparty, K., & Wasan, D. (2010). Nanoparticle self-structuring in a nanofluid film spreading on a solid surface. Langmuir, 26(11), 7665-7670.

Pal, N., Kumar, S., Bera, A., & Mandal, A. (2019). Phase behaviour and characterization of microemulsion stabilized by a novel synthesized surfactant: Implications for enhanced oil recovery. Fuel, 235, 995-1009.

Quintero, H., Mattucci, M., Hawkes, R., Zhang, K., & O'Neil, B. (2018, March). Nano-Particle Surfactant in Hydraulic Fracturing Fluids for Enhanced Post Frac Oil Recovery. In *SPE Canada Unconventional Resources Conference*. Society of Petroleum Engineers.

Ren, Y., Zheng, J., Xu, Z., Zhang, Y., & Zheng, J. (2018). Application of Turbiscan LAB to study the influence of lignite on the static stability of PCLWS. *Fuel*, *214*, 446-456.

Rivero*, J. A., Faskhoodi, M. M., Ferrer, G. G., Mukisa, H., & Zhmodik, A. (2019, October). Huff-and-Puff Enhanced Oil Recovery in the Liquids-Rich Portion of the Montney: Applications for Gas Condensates. In *Unconventional Resources Technology Conference, Denver, Colorado, 22-24 July 2019* (pp. 3461-3479). Unconventional Resources Technology Conference (URTeC); Society of Exploration Geophysicists.

Rostami, A., & Nasr-El-Din, H. A. (2014, April). Microemulsion vs. surfactant assisted gas recovery in low permeability formations with water blockage. In *SPE Western North American and Rocky Mountain Joint Meeting*. Society of Petroleum Engineers.

Sadatshojaei, E., Jamialahmadi, M., Esmaeilzadeh, F., & Ghazanfari, M. H. (2016). Effects of low-salinity water coupled with silica nanoparticles on wettability alteration of dolomite at reservoir temperature. *Petroleum Science and Technology*, *34*(15), 1345-1351.

Salager, J. L., Morgan, J. C., Schechter, R. S., Wade, W. H., & Vasquez, E. (1979). Optimum formulation of surfactant/water/oil systems for minimum interfacial tension or phase behavior. *Society of Petroleum Engineers Journal*, *19*(02), 107-115.

Santos, F. K. G., Neto, E. L. B., Moura, M. C. P., Dantas, T. N. C., & Neto, A. A. D. (2009). Molecular behavior of ionic and nonionic surfactants in saline medium. *Colloids and Surfaces A: Physicochemical and Engineering Aspects*, *333*(1-3), 156-162.

Seedher, N., & Kanojia, M. (2008). Micellar solubilization of some poorly soluble antidiabetic drugs: a technical note. *Aaps Pharmscitech*, *9*(2), 431-436.

Selvamani, V. (2019). Stability studies on nanomaterials used in drugs. In *Characterization and biology of nanomaterials for drug delivery* (pp. 425-444). Elsevier.

Schön, S. (2020). Oscillatory structural forces.

Schembre, J. M., Akin, S., Castanier, L. M., & Kovscek, A. R. (1998, January). Spontaneous water imbibition into diatomite. In *SPE Western Regional Meeting*. Society of Petroleum Engineers.

Sheng, J. J. (2015). Enhanced oil recovery in shale reservoirs by gas injection. *Journal of Natural Gas Science and Engineering*, *22*, 252-259.

Sheng, J. J. (2018). Performance analysis of chemical flooding in fractured shale and tight reservoirs. *Asia-Pacific Journal of Chemical Engineering*, *13*(1), e2147.

Shen, A., Liu, Y., Bai, M., Liang, S., Wang, F., Cai, B., & Gao, Y. (2018). Surfactant Effects of Wettability Alteration and Low IFT on Countercurrent Imbibition for Tight Oil Formation. *Energy & fuels*, *32*(12), 12365-12372.Shi, Y., Yassin, M. R., & Dehghanpour, H. (2018). A modified model for spontaneous imbibition of wetting phase into fractal porous media. *Colloids and Surfaces A: Physicochemical and Engineering Aspects*, *543*, 64-75.

Shi, Y., Yassin, M. R., Yuan, L., & Dehghanpour, H. (2019). Modelling imbibition data for determining size distribution of organic and inorganic pores in unconventional rocks. *International Journal of Coal Geology*, *201*, 26-43.

Siddiqui, M. A. Q., Ali, S., Fei, H., & Roshan, H. (2018). Current understanding of shale wettability: A review on contact angle measurements. *Earth-Science Reviews*, *181*, 1-11.

Standal, S. H., Blokhus, A. M., Haavik, J., Skauge, A., & Barth, T. (1999). Partition coefficients and interfacial activity for polar components in oil/water model systems. *Journal of colloid and interface science*, *212*(1), 33-41.

Tadros, T. F. (2009). *Emulsion science and technology: a general introduction* (pp. 1-56). Wiley-VCH: Weinheim.

Tadros, T. F. (2015). Nanodispersions. Walter de Gruyter GmbH & Co KG.

Unsal, E., Broens, M., Buijse, M., Boersma, D., Makurat, A., & Armstrong, R. T. (2015, August). Visualization of Microemulsion Phase. In *SPE Asia Pacific Enhanced Oil Recovery Conference*. Society of Petroleum Engineers

Verkruyse, L. A., & Salter, S. J. (1985, January). Potential use of nonionic surfactants in micellar flooding. In SPE Oilfield and Geothermal Chemistry Symposium. Society of Petroleum Engineers.

Wade, W. H., Morgan, J. C., Schechter, R. S., Jacobson, J. K., & Salager, J. L. (1978). Interfacial tension and phase behavior of surfactant systems. *Society of Petroleum Engineers Journal*, *18*(04), 242-252.

Walstra, P. (1993). Principles of emulsion formation. *Chemical Engineering Science*, *48*(2), 333-349.

Wasan, D., Nikolov, A., & Kondiparty, K. (2011). The wetting and spreading of nanofluids on solids: Role of the structural disjoining pressure. Current Opinion in Colloid & Interface Science, 16(4), 344-349.

Winsor, P. A. (1954). *Solvent properties of amphiphilic compounds*. Butterworths Scientific Publications.

Wijaya, N., & Sheng, J. J. (2020). Optimum surfactant criteria for controlling invasion-induced water blockage in tight water-wet cores. *Journal of Petroleum Science and Engineering*, 106931.

Yan, Q., Lemanski, C., Karpyn, Z. T., & Ayala, L. F. (2015). Experimental investigation of shale gas production impairment due to fracturing fluid migration during shut-in time. *Journal of Natural Gas Science and Engineering*, *24*, 99-105.

Yang, L., Ge, H., Shi, X., Cheng, Y., Zhang, K., Chen, H., ... & Qu, X. (2016). The effect of microstructure and rock mineralogy on water imbibition characteristics in tight reservoirs. *Journal of Natural Gas Science and Engineering*, *34*, 1461-1471.

Yang, H., Kang, W., Yu, Y., Yin, X., Wang, P., & Zhang, X. (2017). A new approach to evaluate the particle growth and sedimentation of dispersed polymer microsphere profile control system based on multiple light scattering. *Powder technology*, *315*, 477-485.

Yao, J., Han, H., Hou, Y., Gong, E., & Yin, W. (2016). A method of calculating the interaction energy between particles in minerals flotation. *Mathematical Problems in Engineering*, *2016*.

Yarveicy, H., Habibi, A., Pegov, S., Zolfaghari, A., & Dehghanpour, H. (2018, March). Enhancing oil recovery by adding surfactants in fracturing water: A Montney case study. In *SPE Canada Unconventional Resources Conference*. Society of Petroleum Engineers.

Yassin, M. R., Begum, M., & Dehghanpour, H. (2016, August). Source rock wettability: A Duvernay case study. In *Unconventional Resources Technology Conference, San Antonio, Texas, 1-3 August 2016* (pp. 3039-3057). Society of Exploration Geophysicists, American Association of Petroleum Geologists, Society of Petroleum Engineers.

Yassin, M. R., Begum, M., & Dehghanpour, H. (2017). Organic shale wettability and its relationship to other petrophysical properties: A Duvernay case study. *International Journal of Coal Geology*, *169*, 74-91.

Yassin, M. R., Habibi, A., Zolfaghari, A., Eghbali, S., & Dehghanpour, H. (2018). An experimental study of nonequilibrium carbon dioxide/oil interactions. *SPE Journal*.

Yuan, L. (2019). Imbibition Oil Recovery from Montney Core Plugs: The Interplay of Surfactants, Osmotic Potential, and Wettability.

Zelenev, A. S., Champagne, L. M., & Hamilton, M. (2011). Investigation of interactions of diluted microemulsions with shale rock and sand by adsorption and wettability measurements. *Colloids and Surfaces A: Physicochemical and Engineering Aspects*, *391*(1-3), 201-207.

Zhang, L., Somasundaran, P., & Maltesh, C. (1996). Electrolyte effects on the surface tension and micellization of n-dodecyl β-d-maltoside solutions. *Langmuir*, *12*(10), 2371-2373.

Zhang, J., Wang, Z., Wang, Q., Ma, J., Cao, J., Hu, W., & Wu, Z. (2017). Relationship between polymers compatibility and casting solution stability in fabricating PVDF/PVA membranes. *Journal of membrane science*, *537*, 263-271.

Zhang, Y., Di, Y., Yu, W., & Sepehrnoori, K. (2019). A comprehensive model for investigation of carbon dioxide enhanced oil recovery with nanopore confinement in the Bakken tight oil reservoir. *SPE Reservoir Evaluation & Engineering*, *22*(01), 122-136.

Appendix

A. Montney core intervals

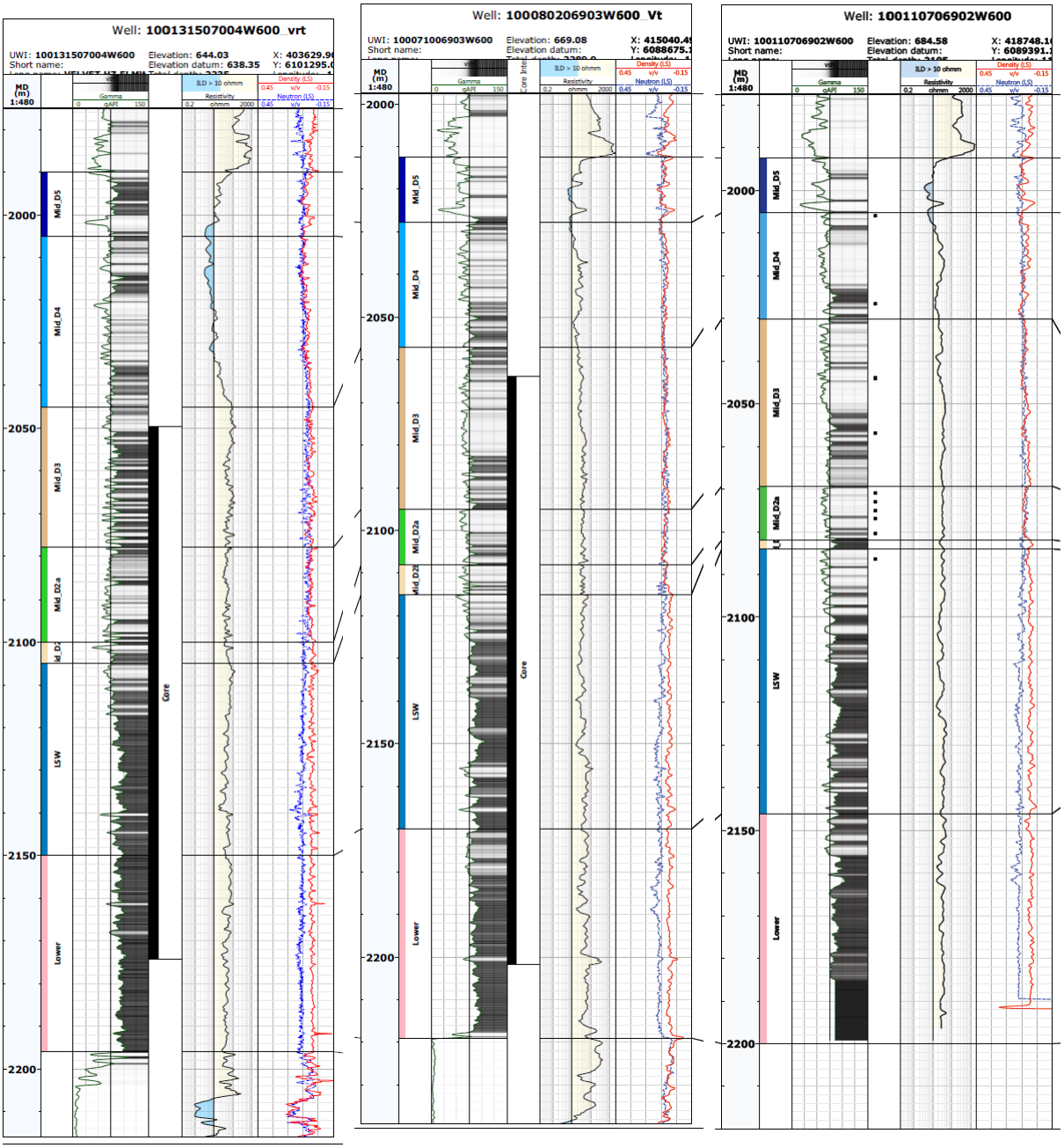

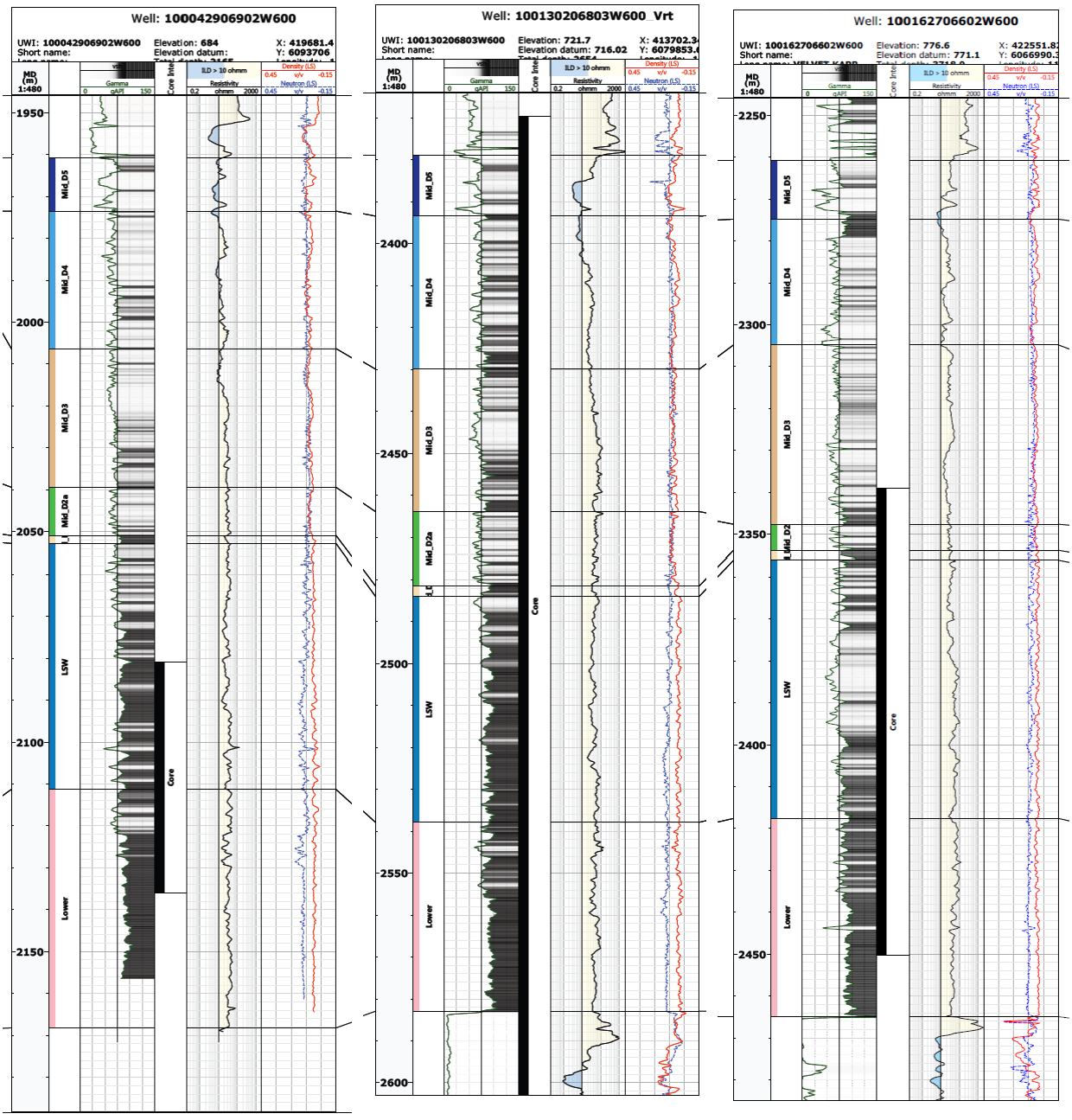
Well: 100042906902W600
UWI: 100042906902W600
Short name:
Elevation: 684
Elevation datum:
X: 419681.4
Y: 6093706
Well: 100130206803W600_Vrt
UWI: 100130206803W600
Short name:
Elevation: 721.7
Elevation datum: 716.02
Well: 100162706602W600
UWI: 100162706602W600
Short name:
Elevation: 776.6
Elevation datum: 771.1
MD (m) 1:480
Gamma
gAPI
Resistivity
ohmm
Density (LS)
Neutron (LS)
Mid_D5
Mid_D4
Mid_D3
Mid_D2a
LSW
Lower
Core

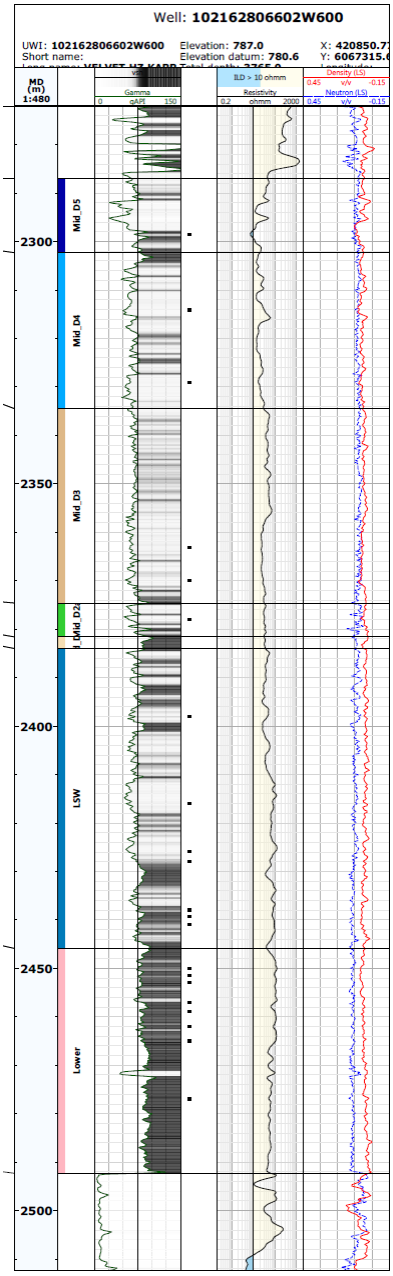
Well: 102162806602W600
UWI: 102162806602W600
Short name:
Elevation: 787.0
Elevation datum: 780.6
X: 420850.7
Y: 6067315.6
MD (m) 1:480
Gamma
0 gAPI 150
ILD > 10 ohmm
Resistivity
0.2 ohmm 2000
Density (LS)
0.45 v/v 0.15
Neutron (LS)
0.45 v/v 0.15
Mid_D5
Mid_D4
Mid_D3
Mid_D2
LSW
Lower
2300
2350
2400
2450
2500

B. SEM images

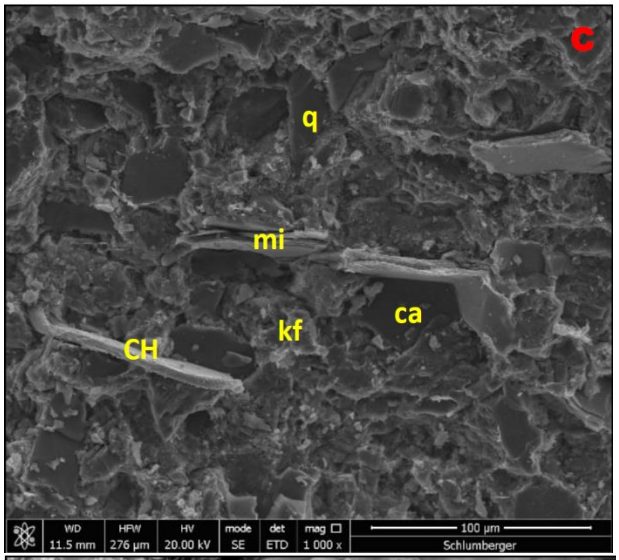
C
q
mi
ca
kf
CH
WD 11.5 mm
HFW 276 µm
HV 20.00 kV
mode SE
det ETD
mag 1 000 x
100 µm
Schlumberger

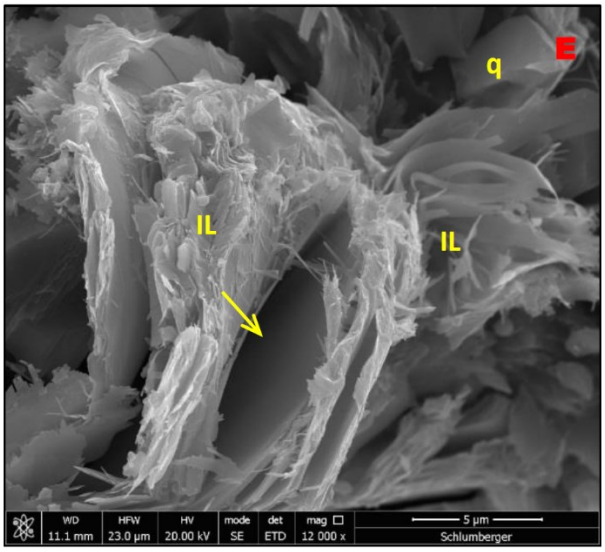
E
q
IL
IL
WD 11.1 mm
HFW 23.0 µm
HV 20.00 kV
mode SE
det ETD
mag 12 000 x
5 µm
Schlumberger

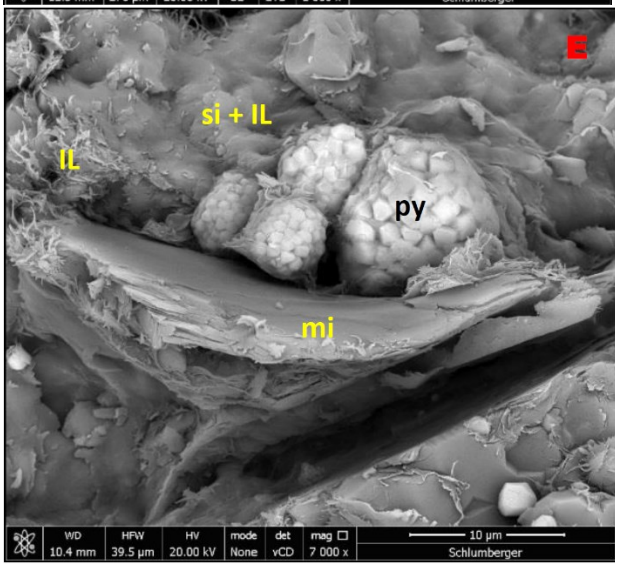
E
si + IL
IL
py
mi
WD 10.4 mm
HFW 39.5 µm
HV 20.00 kV
mode None
det vCD
mag 7 000 x
10 µm
Schlumberger

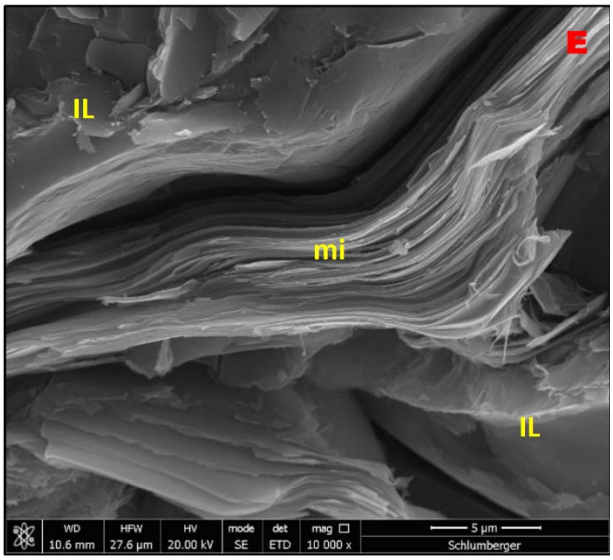
E
IL
mi
IL
WD 10.6 mm
HFW 27.6 µm
HV 20.00 kV
mode SE
det ETD
mag 10 000 x
5 µm
Schlumberger

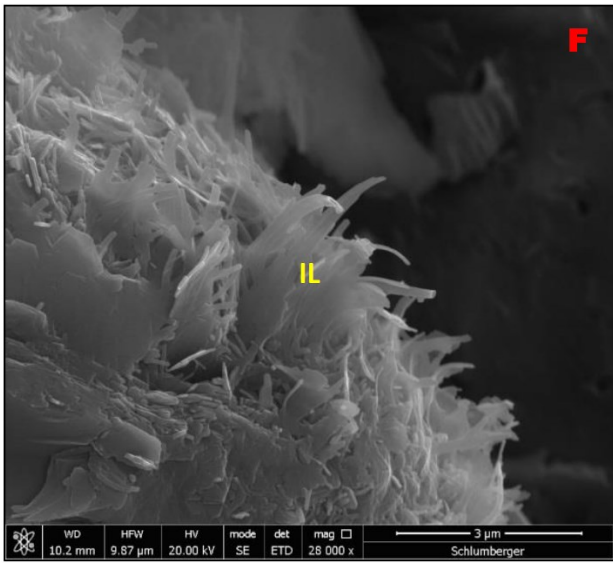
F
IL
WD
10.2 mm
HFW
9.87 µm
HV
20.00 kV
mode
SE
det
ETD
mag
28 000 x
3 µm
Schlumberger

C. MICP profile

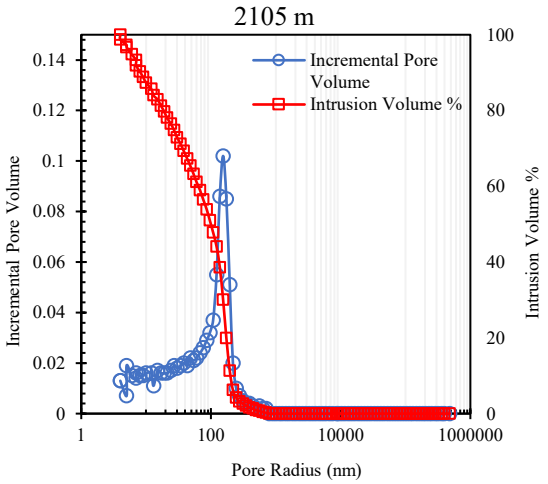
2105 m
Incremental Pore Volume
Intrusion Volume %
Incremental Pore Volume
Intrusion Volume %
Pore Radius (nm)
0
0.02
0.04
0.06
0.08
0.1
0.12
0.14
0
20
40
60
80
100
1
100
10000
1000000

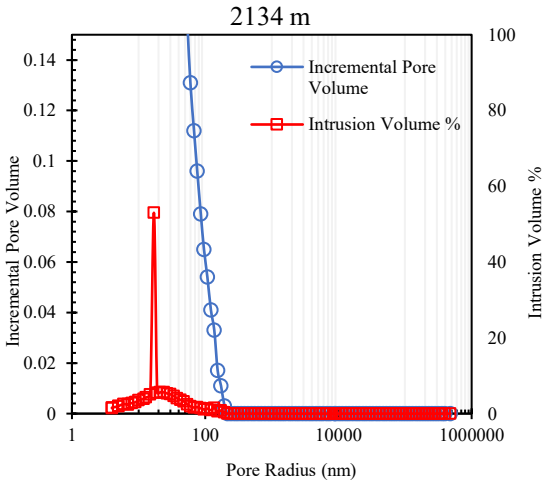
2134 m
Incremental Pore Volume
Intrusion Volume %
Incremental Pore Volume
Intrusion Volume %
Pore Radius (nm)
0
0.02
0.04
0.06
0.08
0.1
0.12
0.14
0
20
40
60
80
100
1
100
10000
1000000

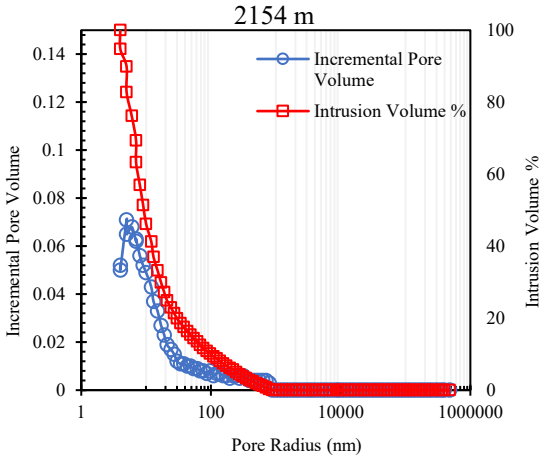
2154 m
Incremental Pore Volume
Intrusion Volume %
Incremental Pore Volume
Intrusion Volume %
Pore Radius (nm)
0
0.02
0.04
0.06
0.08
0.1
0.12
0.14
0
20
40
60
80
100
1
100
10000
1000000

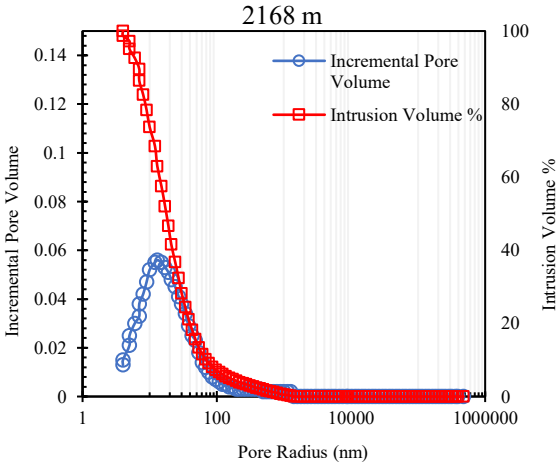
2168 m
Incremental Pore Volume
Intrusion Volume %
Incremental Pore Volume
Intrusion Volume %
Pore Radius (nm)
0
0.02
0.04
0.06
0.08
0.1
0.12
0.14
0
20
40
60
80
100
1
100
10000
1000000

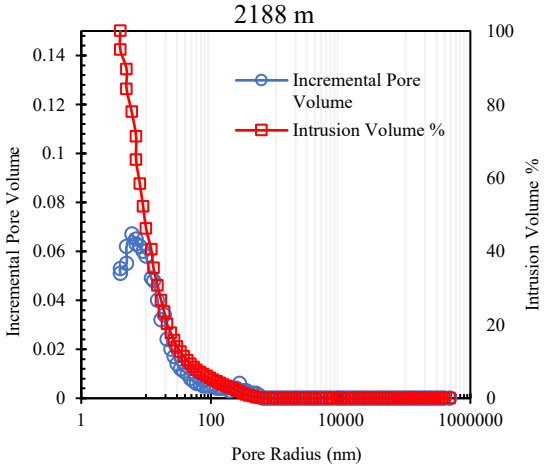
2188 m
Incremental Pore Volume
Intrusion Volume %
Incremental Pore Volume
Intrusion Volume %
Pore Radius (nm)
0
0.02
0.04
0.06
0.08
0.1
0.12
0.14
0
20
40
60
80
100
1
100
10000
1000000

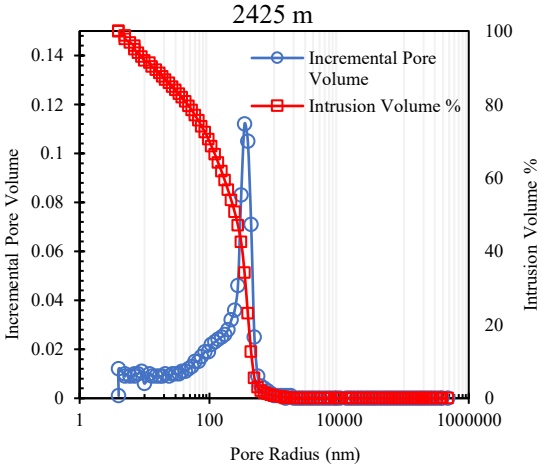
2425 m
Incremental Pore Volume
Intrusion Volume %
Incremental Pore Volume
Intrusion Volume %
Pore Radius (nm)
0
0.02
0.04
0.06
0.08
0.1
0.12
0.14
0
20
40
60
80
100
1
100
10000
1000000

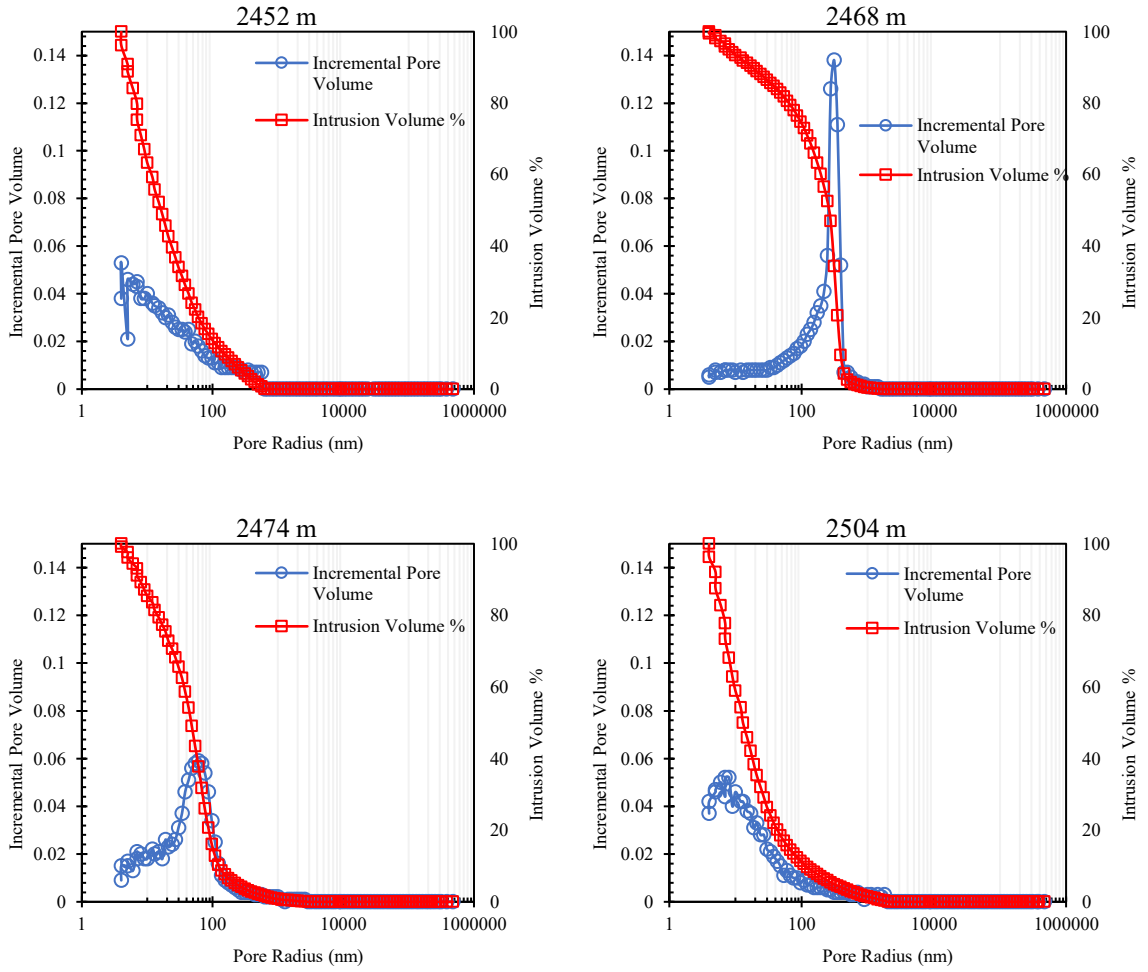

D. Liquid-liquid contact angles of ND solutions.

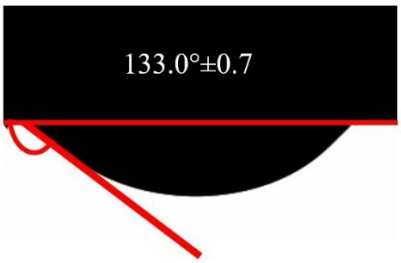

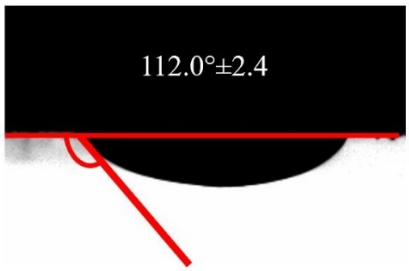

CnF-01+brine

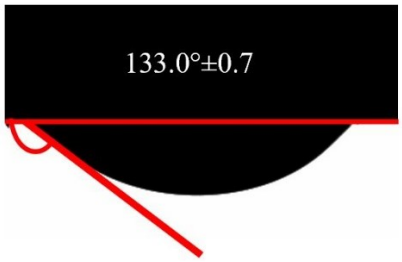	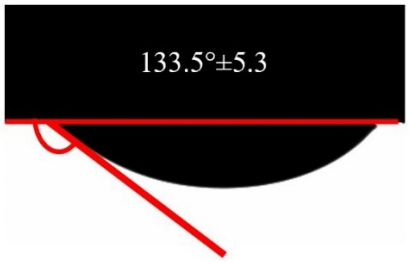	CnF-03+brine
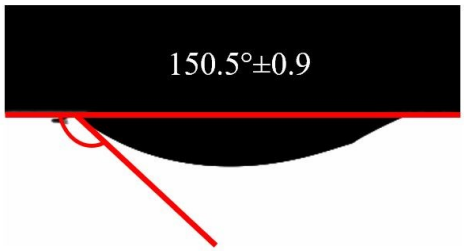	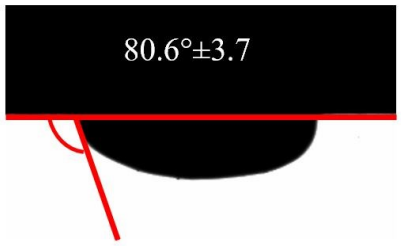	CnF-01+TW
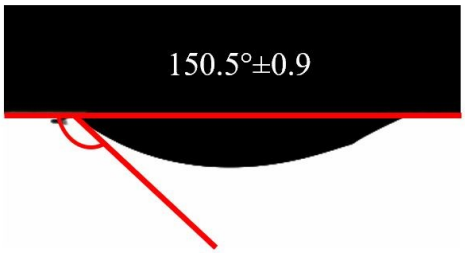	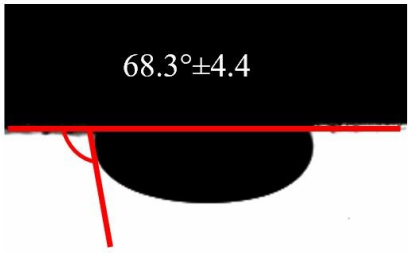	CnF-02+TW
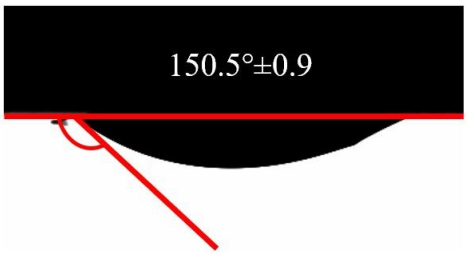	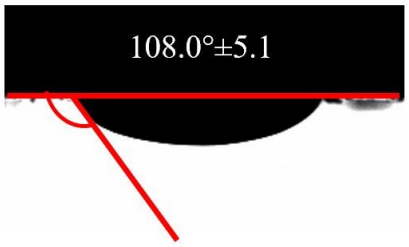	CnF-03+TW